APPLICATION SPECIFIC MULTILAYER OPTICAL STRUCTURES

Ph. D. THESIS

by

BABITA

DEPARTMENT OF PHYSICS
INDIAN INSTITUTE OF TECHNOLOGY ROORKEE
ROORKEE- 247 667 (INDIA)
JULY, 2014

APPLICATION SPECIFIC MULTILAYER OPTICAL STRUCTURES

A THESIS

Submitted in partial fulfilment of the requirements for the award of the degree of

DOCTOR OF PHILOSOPHY in

PHYSICS

by

BABITA

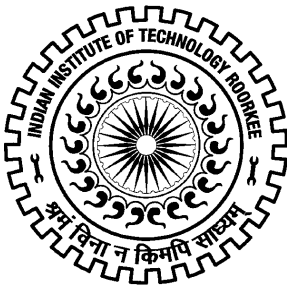

DEPARTMENT OF PHYSICS
INDIAN INSTITUTE OF TECHNOLOGY ROORKEE
ROORKEE- 247 667 (INDIA)
JULY, 2014

INDIAN INSTITUTE OF TECHNOLOGY ROORKEE

ROORKEE

CANDIDATE'S DECLARATION

I hereby certify that the work which is being presented in the thesis entitled **"APPLICATION SPECIFIC MULTI-LAYER OPTICAL STRUCTURES"** in partial fulfilment of the requirements for the award of the Degree of Doctor of Philosophy and submitted in the Department of Physics of the Indian Institute of Technology Roorkee, Roorkee is an authentic record of my own work carried out during a period from July, 2009 to July, 2014 under the supervision of **Dr**. **Vipul Rastogi**, Associate Professor, Department of Physics, Indian Institute of Technology Roorkee, Roorkee.

The matter presented in this thesis has not been submitted by me for the award of any other degree of this or any other Institute.

(Babita)

This is to certify that the above statement made by the candidate is correct to the best of our knowledge.

(……..)
Supervisor

(Vipul Rastogi)
Supervisor

Date:……

ABSTRACT

The contemporary physics revolution based on discovery of electromagnetic waves has led science and technology into new era. Development of modern technologies like wireless communication systems, high energy particle accelerators, electron microscopy, high precision devices and systems, active and passive microwave and optical devices, high speed internet, sensing systems and telecommunication infrastructure have great impact on modern society. This has been possible because of discovery of electromagnetic waves. Electromagnetic waves in open space can propagate in all the directions. The efficient transfer of optical energy from one point to another can be performed using a specially designed electromagnetic structure called optical waveguide. On the basis of geometry of the structure, waveguides one can be divided into following two main categories.

1. Integrated optic waveguide
2. Cylindrical waveguide (Optical Fiber)

Optical waveguides are used in many applications in integrated optics, fiber optics and biomedical optics. Integrated optics mainly consists of planar waveguide and rectangular waveguide and is used in optical-integrated circuits while optical fiber is basically used in optical communication for data transmission at high bit rate over long distances. In integrated optics rectangular waveguides have used for applications in optical modulator, optical amplifier, optical switches, wavelength filters, laser, and refractive index sensors. Optical fibers are used for applications which include optical telecommunication, optical amplifiers, fiber sensors, fiber lasers, delivery of high power laser pulses, refractive index sensors and fiber optic devices and components such as directional coupler, wavelength filter, dispersion compensating fibers and dispersion flattened fibers. All these applications require designing waveguide in some specific geometry and refractive index profile. The structures used in general have several layers of materials of different refractive indices and specific thicknesses. This thesis presents various multilayer novel designs in cylindrical and rectangular geometries for specific applications. In particular we present multilayer designs for dispersion management, refractive index sensing and improving light extraction in organic light emitting diodes. All these waveguide structures have been designed by tailoring refractive index of

waveguides in core and cladding regions to achieve specific characteristics according to the requirement of application.

Segmented core fibers having non-zero positive, non-zero negative and near-zero ultra-flattened dispersion with small dispersion slope and ultra-large effective area over a wide spectral range has been presented. Transfer matrix method has been used to analyze the structure. The designs consist of a concentric multilayer segmented core followed by a trench assisted cladding and a thin secondary core. The central segmented core helps in maintaining desired dispersion over a wide range of wavelength. The second core of the fiber helps in achieving ultra-large effective area and trench assisted cladding reduces the bending loss. Designed fibers show very small bending loss. We report breakthrough in the mode area of the single mode optical fiber with ultra flattened dispersion and low dispersion slope. These characteristics of the fiber make it an attractive candidate for DWDM optical communication system.

The idea of multilayer structure is also extended to design fibers for delivery of ultrashort laser pulses. Three layered fiber structure and segmented cladding fiber have been designed for delivery of femtosecond laser pulses. Effective index and field profile of modes of the fibers have been calculated using transfer matrix method. Pulse propagation through the fibers has been studied using split-step Fourier method. Distortion-free propagation of the pulse has been achieved by keeping ratio of dispersion to nonlinear length close to 1 in both the fibers. The modal purity in the fiber structures have been maintained by leaking out HOM except LP_{11}. Mode stability has been ensured by sufficient mode spacing between LP_{01} and LP_{11} modes ensure mode stability. Design of the fibers ensures no intermodal coupling, low bending loss, and high fabrication tolerances while maintaining large-mode-area. Fibers can be fabricated using modified chemical vapor deposition technique. Whereas for fabrication of segmented cladding fiber in silica glass a technique has been developed and is presented in thesis. We have optimized design of large mode area segmented cladding fiber with effective single mode operation. Fiber has been fabricated using modified chemical vapor deposition technique at CGCRI Kolkata. Fiber has been fabricated with 45 μm core diameter and 125 μm as the outer diameter. Characterization of the fiber at IIT Roorkee has shown mode filtering effect.

Another application of multilayer design as a refractive index sensor in cylindrical geometry has been presented. The design of a refractive index sensor is based on depressed index clad fiber. We utilize variation of leakage loss with variation

in refractive index of outermost layer of waveguide (analyte) to design a simple, compact, low cost and ultra high sensitive refractive index sensor. Different regions of leakage loss curve to have been used to design sensors in different ranges, with different index resolutions, and for specific applications. The practical realization of the sensor requires etching of some portion of the cladding of the fiber and does not require any costly methods of wavelength or polarization interrogation. Fiber can be easily fabricated using standard modified chemical vapor deposition technique. However, fiber is too fragile to handle and the quantity of analyte to sense refractive index is also larger.

We extended the idea to design a miniaturized sensor using planar geometry of the waveguide. We have presented a simple, compact, low cost and highly sensitive refractive index sensor based on single mode leaky planar waveguide. An optical waveguide deposited on glass substrate has been proposed to construct the sensor. In this structure cytop works as guiding layer while teflon forms the cladding layers. Propagation of light in cytop layer is strongly affected by the refractive index of external medium placed on top of teflon layer. If the refractive index of the medium is close to or greater than that of cytop then there is leakage of power from cytop layer to external medium which affects the transmittance of the waveguide. The structure can be designed to have strong variation in transmittance with the refractive index of external medium, and thus, can be utilized as highly sensitive refractive index sensor for biomedical applications. In this chapter we have carried out the design strategies of such a refractive index sensor for various biological and chemical applications. We have designed a sensor with index resolution of the order of 10^{-5}. Fabrication of the sensor can be carried out by using cost effective spin coating technique. Long range, high sensitivity, simple manufacturing process and compactness make the sensor attractive for diverse applications.

We have extended the applications of multilayer structures to organic light emitting diode to increase its efficiency. Extraction efficiency of conventional organic light emitting diode structure has been increased by inserting a low index layer of polymer Teflon between glass substrate and ITO. This low refractive index layer helps in breaking wave guidance of modes. Such a structure helps in leaking out more power into the glass substrate from organic and ITO layer. We show around 15% increment in extracted power at 442-nm wavelength and 29% increment at 539-nm wavelength, and

3 % at 620-nm wavelength. Fabrication of the structure can be done using very cost effective spin-coating technique.

Future work coming out of this thesis is also discussed in brief.

LIST OF RESEARCH PUBLICATIONS

Journal articles:

1. **Babita**, Vipul Rastogi and Ajeet Kumar,"Design of large-mode-area three layered fiber structure for femtosecond laser pulse delivery,"***Optics Communications*** , vol. 293, pp. 108-112, 2013.
2. **Babita Hooda** and Vipul Rastogi,"Ultra-large effective area dispersion flattened fiber for DWDM applications,"***Progress In Electromagnetic Research B***, vol. 51, pp. 157-175, 2013.
3. **Babita** and Vipul Rastogi,"Design of segmented cladding fiber for ultra-short pulse delivery at 1064 nm and 1550 nm wavelengths,"***Optical and Quantum Electronics***, vol. 46, pp. 397-408, 2014.
4. **Babita** and Vipul Rastogi,"Low cost highly sensitive miniaturized refractive index sensor based on planar waveguide,"***Biophotonics*** (submitted).
5. **Babita** and Vipul Rastogi,"W-type fiber as a low cost highly sensitive refractive index sensor," ***Optical Fiber Technology*** (submitted).
6. **Babita**, Atasi Pal, Vipul rastogi, Ranjan Sen, Jimit Gandhi, and J. Kobelke," Development of fabrication technology for segmented cladding fiber in silica-based glass,"***Optical Fiber Technology*** (submitted).

Conference contributions:

1. **Babita** and Vipul Rastogi,"Design and Analysis of Multi-ring Large Mode Area Optical Fiber,**"** International conference on optics and optoelectronics (ICOL-2014), IRDE Dehradun, India, 5-8 march, 2014.
2. **Babita** and Vipul Rastogi, "Large effective area dispersion flattened fiber for DWDM optical communication system," Frontier in optics/ laser science XXIX (FIO/LS-2013), doi.org/10.1364/FIO.2013.FM4B.2, Orlando Florida, USA, 6-10 October, 2013.

3. **Babita** and Vipul rastogi, "Design and analysis of a low cost highly sensitive refractive index sensor," The XXIth International Workshop on Optical Wave & Waveguide Theory and Numerical Modelling, Enschede, The Netherlands, April 19-20, 2013.
4. **Babita Hooda** and Vipul Rastogi, "Ultra-large-effective-area dispersion-flattened segmented-core optical fiber," International Conference on Communication and Electronics System Design (ICCESD), Proc. SPIE 8760, doi: 10.1117/12.2012119, MNIT Jaipur, India, January 28-30, 2013,**.**
5. **Babita** and Vipul Rastogi,"Dispersion flattened single mode optical fiber with large effective area," Recent trends in applied physics and materials science , AIP Conf. Proc. **1536**, 729, http://dx.doi.org/10.1063/1.4810434 Bikaner, India, Feb. 1-2, 2013.
6. **Babita**, Vipul Rastogi and A. Kumar, "Segmented cladding fiber design for femtosecond laser pulse delivery at 1550-nm and 1064-nm wavelengths," Opto-Electronics and Communications Conference (OECC), pp.359-360, 2-6 July 2012.
7. **Babita**, Rajnish Kumar and Vipul rastogi,"Dual core Segmented cladding fiber as a dispersion compensator," International Conference and Exhibition on Lasers, Optics & Photonics" (Optics-2013), Hilton San Antonio Airport, USA, October 7-9, 2013.
8. **Babita** and Vipul Rastogi, "Long-period grating in segmented cladding fiber," International Conference on Specialty Glass and Optical fiber: Materials, Technology and Device (ICGF-2011), CGCRI Kolkata, Aug. 4-6, 2011.
9. **Babita** and Vipul Rastogi "Segmented cladding fiber based highly sensitive refractive index sensor," International Conference on Specialty Glass and Optical fiber: Materials, Technology and Devices (ICGF-2011), CGCRI Kolkata, Aug. 4-6, 2011.
10. **Babita** and Vipul Rastogi**,"**Design of segmented cladding fiber for femtosecond-pulse laser beam delivery," XXXVI OSI Symposium on Frontier in Optics and Photonics, IIT-Delhi, Delhi, India, Dec 3-5, 2011.
11. Neha Gupta, **Babita** and Vipul Rastogi "Surface plasmon resonance based glucose sensor using a cd-r," XXXVI OSI Symposium on Frontier in Optics and Photonics, IIT-Delhi, Delhi, India , Dec 3-5, 2011.

12. **Babita**, Vipul Rastogi and Ajeet Kumar,"Dual shape large mode area optical fiber for femtosecond laser pulse delivery," NCAP, IITR, Roorkee, India, 24-25 Feb., 2012.
13. **Babita**, Vipul Rastogi and A. Kumar "W-type fiber for femtosecond laser pulse delivery," International OSA Network of Students-11 (IONS-11), École Polytechnique, the Insti, Paris, Feb. 22-25, 2012.
14. **Babita** and Vipul Rastogi "Depressed index clad fiber as a highly-sensitive low-cost refractive index Sensor," International conference on Fiber Optics and Photonics, IIT Guwahati, Dec. 11-15, 2010**.**

DEDICATED TO

MY PARENTS AND MY LOVING BROTHERS

ACKNOWLEDGEMENTS

Persuing Ph.D. is both enjoyable and painful experience. It's like climbing a mountain slowly accompanied with encouragement, hard work, trust, bitterness and frustration. Now when I found myself on mountain, I realize that it's a team work that helped me in being here. Although the cover of thesis states that I, Babita has written this thesis but there are many people behind the scene in completing this thesis. It is a pleasant aspect that now I have the opportunity to express my sincere gratitude to all of them.

First and foremost, I want to thank Dr. Vipul Rastogi for taking a chance on me and providing me the opportunity to work at IIT Roorkee. With great pleasure I would like to express appreciation and sincere gratitude for his advice, guidance, assistance, numerous suggestions, constructive criticism, and encouragement throughout the period of my research. I have learnt a lot from him. I am grateful to have benefitted from the supervision of such an acknowledged person. He consistently gave me the freedom to pursue projects of my own choice without any objection. I am also very much thankful to his wife Mrs. Kopal Rastogi for her blessings and his kids Ishi and Diwesh for their love which never made me feel homesick.

I would also like to thank committee members Professor Rajesh srivastava (Internal expert and DRC chairman) and Professor Dharmendra Singh (External expert) for their time, valuable suggestions and support. I am also thankful to Professor B.D. Indu and Professor A.K. Jain for providing me basic infrastructural facilities to carry out my research work.

I would like to give my special gratitude to Dr. Anirban Mitra for having discussions on OLED project and guiding me to buy many chemicals to carry out my research work. I also give my special thank to Mrs. Meena Kothari for having fun with us inspite of having busy schedule which made my time more enjoyable here.

I also thank present and past members of Photonics Lab.: Dr. Ajeet Kumar for sharing the knowledge, having insightful discussions about research and giving valuable suggestions. I could always ask him for advice and opinions on lab related issues. I would like to give my sincere thanks to him for his generous help. Dr. Kamakshi Koppole for having discussions related to personal and academic life. Dr. Ashok Nandam for being such a nice and supportive labmate. Mr. Girish Semwal for being always a supportive labmate. I can't forget his kind help when we visited DRDO for a conference. Ankita Gaur

and Vidhi Mann for being so friendly, wish you both good luck and happy stay at IITR. I am glad to have all of them as my lab mates.

I would also like to thank all M.Tech, M.Sc. and B. Tech. students (Anil Bhaiya, Rajiv, Shivam, Seema, Neha, Ragni, Kajari, Prince, Debjyoti, Rajnish, Jimit, Vikraman, Rahul, Hemant Kumar, and Ashwin Philip) who have completed their projects in Photonics Lab and have contributed for the Lab.

I am in dearth of proper words to express my feeling towards my respected mother and father for their immutable encouragement, moral support, blessings and for being there always with me during all up and down in my life. My mother's phone conversation for hours at crucial time strengthened me to continue my work here.

I am greatly indebted to my loving brothers Jayant and Vidur who are backbone of my happiness. Their love and support at every step enabled me to complete this thesis successfully.

I would also like to give my sincere gratitude to my devoted husband Dr. Naresh Kumar and my in-laws for their affection and support during the last days of my Ph.D.

I would also like to thank all my friends who made my time more enjoyable here. The humor, support and cooperation which I have received from my friends are beyond the scope of any acknowledgement, yet I would like to express my heartfelt gratitude to them. The list of friends is long but I must accolade the company of Neha Gupta, Rakhi Bhardwaj, Monika Dhariwal, Darshana, Swati Modi, Ankita, Manjusha, Neha, Manu Chaudhary, Meera, Sudesh, Tapasi, Mahima and Gurpreet. I also express my sincere thanks to all the research scholar of the department for their support and understanding.

My special thanks to my previous teacher Dr. Praveen Aghamkar who inspired me to persue Ph.D. I would also like to thank my school and college friends Reena, Rajni and Sangeeta who still haven't grown apart even if we don't talk everyday and are always there to discuss during hard times.

I owe a debt of gratitude to all the persons who have gone unnamed and helped me directly or indirectly in completing this thesis.

I gratefully acknowledge the financial assistance provided by Department of Science and Technology (DST) and Ministry of Information Technology (MIT).

Finally, I would like to thank God, the almighty for his shower of blessings throughout my research work and who led me to go through difficult times.

(Babita)

CONTENTS

LIST OF FIGURES

LIST OF TABLES

CHAPTER-1

Introduction

An optical waveguide is a physical device that guides electromagnetic waves in optical spectrum. In 1864, a Scottish physicist J.C. Maxwell for the first time predicted theoretically the electro dynamical formulation of wave propagation through space in his mathematical derivation of electromagnetic field.

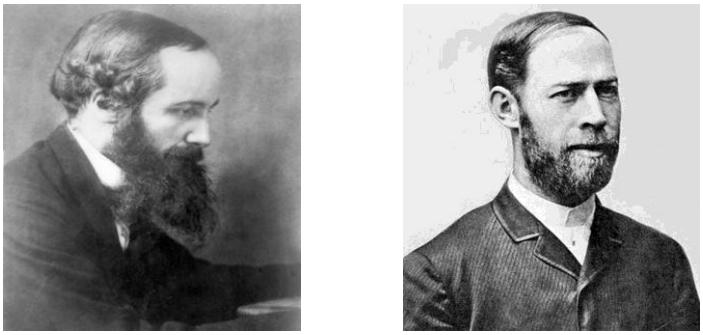

Figure 1.1 *Portraits of Scottish Physicist J.C. Maxwell (left) source: http://www.clerkmaxwellfoundation.org/html/picture_viewer_10.html and German Physicist H.R. Hertz source: http://www.nndb.com/people/419/000072203/*

In 1888, an experiment was performed by a German Physicist H. R. Hertz, using a spark gap oscillator and proved Maxwell’s theory to be correct. Electromagnetic waves are the

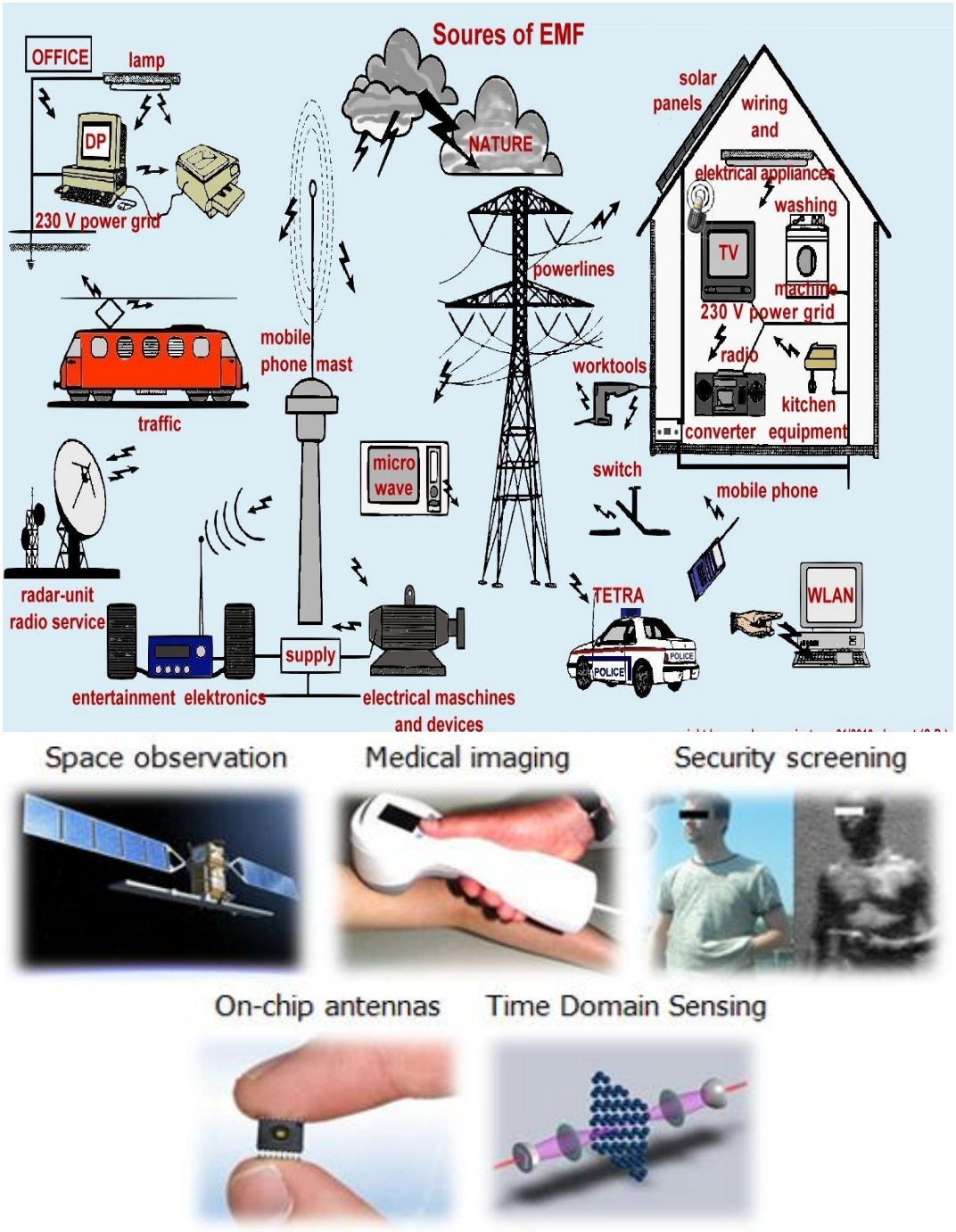

Figure1.2 *Artistic drawings of applications of electromagnetic waves. Source: ;* http://www.hese-project.org/hese-uk/en/niemr/

http://www.tudelft.nl/uploads/RTEmagicC_applied-electromagnetics.png.png

wave which are created by vibration of electric charge and consists of transverse electric and magnetic components which are perpendicular to each other. Electromagnetic waves propagate in a direction perpendicular to electric and magnetic field and can carry their energy and information from one point to other.

The contemporary physics revolution based on discovery of electromagnetic waves, has led science and technology into new era. Development of modern technologies like wireless communication systems, high energy particle accelerators, electron microscopy, high precision devices and systems, active and passive microwave and optical devices, high speed internet, sensing systems and telecommunication infrastructure have great impact on modern society as shown in Fig. 1.2. This has been possible because of discovery of electromagnetic waves. Waves in open space propagate in all direction as spherical waves and hence they loose their energy. The efficient transfer of energy from one point to another can be performed using a specially designed electromagnetic structure called optical waveguide. Waveguide was first referred to as light piping in 1880 by Wheeler, which is now known as optical fiber [1]. Initially waveguides were made of metal only however later it was realized that electromagnetic waves can be guided through dielectric material also. Active study in propagation of electromagnetic wave in metal and dielectric guiding medium came out as a fundamental branch of electromagnetism. Waveguides can be broadly classified as close waveguide and open waveguide. In case of closed waveguide, field is confined in the inner region. In closed waveguide inner and outer regions are well defined and are isolated from surrounding. These waveguides have metallic shielding and electromagnetic field is therefore sharply confined within the core of the waveguide. These waveguides have metallic boundary with the surrounding so no field goes out to the surrounding. The wave is guided by the phenomenon of total internal reflection within the waveguide. A physical structure having longitudinal axial symmetry and unbounded cross-section and is able to guide electromagnetic waves is called an open waveguide. In an open waveguide electromagnetic field in cross-section is not confined to a limited region of space but it extends upto infinity. Both types of electromagnetic waveguides can be analysed by solving Maxwell's equation by applying suitable boundary conditions which are determined by materials of obtained which are defined as eigenfunctions of the system [2]. These multiple solutions of the equation are called modes of the waveguide and these modes have their own propagation constant. Each

mode has its own cutoff frequency below which it ceases to exist. The modes in closed waveguides have purely real propagation constant which are called guided modes. Whereas open waveguides have guided modes and leaky modes, leaky modes are the modes which have complex propagation constant. So when an electromagnetic wave propagates through any waveguide either it will be leaky or purely guided. Mathematically, leaky waves are improper as radiation condition at infinity is violated. We have studied the behavior of electromagnetic wave within very simple geometry. If we change the geometry of the film or add more slabs of different materials in the device then waveguide is termed as multilayer waveguide as it is made of different media. Incident waves may be totally guided or leaky, which depends on the refractive index and geometry of various layers of multilayer waveguide [2]. Analysis of these waveguides can be carried out using Maxwell's equations [3]. Waveguides with many slabs or we can say with many refractive index layers are useful in various applications because of unusual behavior in terms of dispersion characteristics, transmission characteristic, cut off wavelengths etc. The basic structure of multilayer planar waveguide is shown in Fig. 1.3. The waveguide consists of five layers having different refractive index in each layer. Light propagation in the waveguide is in z direction and variation in refractive index is in *x* direction. These waveguides can be used for many applications like optical modulator, optical amplifier, optical switches, wavelength filters, laser, refractive index sensors etc.

Multilayer cylindrical waveguide in cylindrical coordinate is depicted in Fig. 1.4. The structure of this fiber is different from that of conventional fiber but analysis of the fiber can be done with the same method as that of conventional fiber by solving Maxwell's eqn. and applying suitable boundary conditions at each layer. But complexity of the design increases if variation in refractive index in structure is in angular direction also. The analysis of these types of structures can be done by generating effective refractive index profile and then solving Maxwell's equations for effective refractive index profile by employing appropriate boundary conditions. Numbers of layers as well as other parameters of the fiber are chosen according to application. There are many kinds of multi-layer fibers; these fibers give flexibility in refractive index to achieve desired unusual characteristics for specific applications. Multilayer fiber structures have been used for many applications which include large mode area fiber, fibers for delivery of

high power pulses, dispersion compensating fibers, dispersion flattened fiber, refractive index sensor and many more other applications [4].

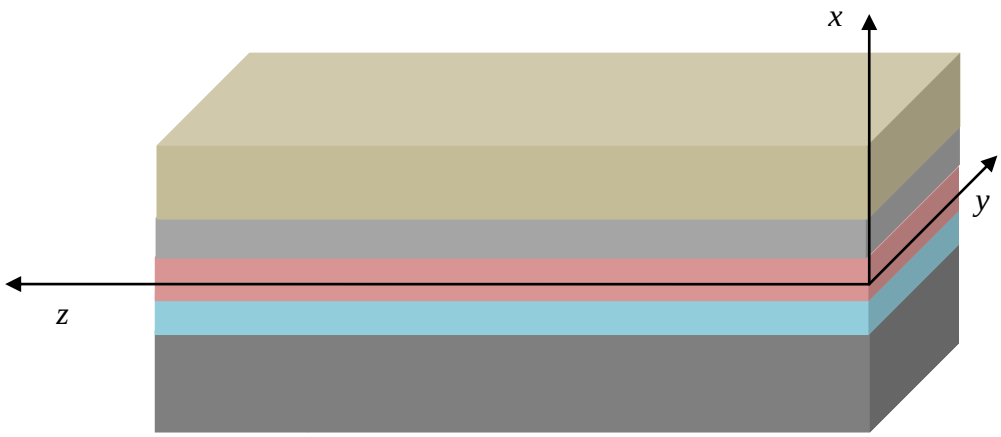

Figure 1.3 *A schematic representation of multilayer planar waveguide.*

1.1 Applications of multilayer *cylindrical* waveguides

1.1.1 *Dispersion flattened fibers*

In communication system dense wavelength division multiplexing (DWDM) has come into existence to increase transport of data over long or metro distances. Standard silica fibers have some limitations while employing this technique. The main two drawbacks of standard silica fiber are basically related to dispersion and nonlinear effects. In a conventional silica optical fiber value of dispersion increases with wavelength therefore different channels suffer from different amount of pulse

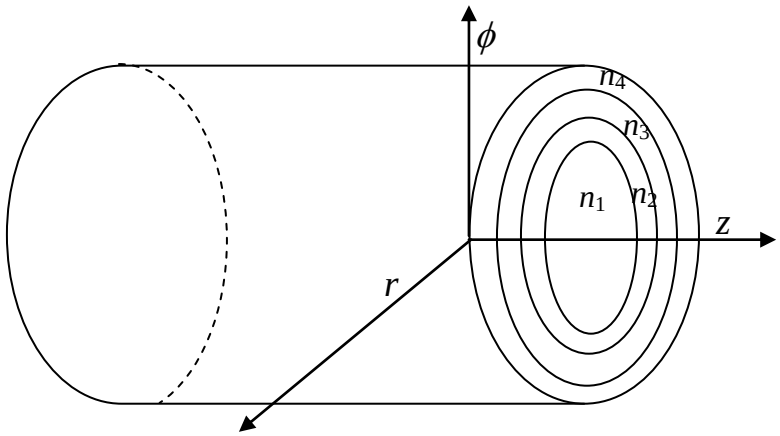

Figure 1.4 *Geometry of multi-layer optical fiber*

broadening. Different alternatives to conventional fiber have been proposed to overcome the problem [5-11]. One of the alternatives is multi-layer fiber structures. Varshney et al. have proposed a fiber structure having flat modal field accompanied with positive dispersion and small dispersion slope in spectral range 1.53-1.61 μm. In this fiber they have reported effective area of 56.1 μm^2 at 1.55 μm wavelength. They have shown dispersion of the fiber ranging from 2.7 to 3.4 ps/km/nm in the wavelength range 1.53-1.61 μm [5]. However, the mentioned wavelength range of the fiber does not cover the entire S+C+L band. Tian et al. have proposed ring index profiles represented as RI and RII triple-clad optical fibers with effective area varying from 95 to 118 μm^2 in wavelength range 1.54-1.62 μm. The reported maximum total dispersion and dispersion slope in the aforementioned wavelength range are 4.5 ps/km/nm and 0.006 ps/km/nm^2 respectively [6]. Okuno et al. have reported a fiber having negative dispersion of about –8ps/km/nm over the entire S+C+L band [7]. However, the reported mode area is small. Recently Rostami et al. have proposed a modified W-type single mode optical fiber with ultra low dispersion, dispersion slope and ultra high effective area. They show very small dispersion varying from 0.1741 to 0.9282 ps/km/nm within the spectral range of 1.460-1.625 μm. Dispersion slope and mode area reported by them in the aforementioned wavelength range are [(–0.011)-(0.0035)] ps/km/nm^2 and [103.56-232.26] μm^2 respectively. In their structure they have achieved all these features by introducing extra depressed cladding layers in W-type fiber [8]. In present thesis we have presented a segmented core dispersion flattened fiber which is capable to be designed as (i) small positive-non-zero dispersion flattened fiber, (ii) small negative-non-zero dispersion flattened fiber, and (iii) near-zero dispersion flattened fiber. The designed fibers show ultra low dispersion slope, ultra large mode effective area and small bending sensitivity over the S+C+L band.

1.1.2 *Delivery of ultrashort laser pulses*

Ultrashort pulses (USPs) are now used in variety of applications in science and technology such such as femtochemistry, frequency combs, multiphoton fluorescence microscopy. Therefore, it is required to transport these pulses with some suitable medium while retaining their basic properties like pulse duration and peak power. An optical fiber can be the best choice to realize this task. However, propagation of USPs

through small core standard silica fiber leads to significant nonlinear effects and dispersion which lead to deformation of pulses. To circumvent this problem researchers have used specialty fibers such as photonic crystal fibers (PCFs) or photonic band gap fibers (PBGs) [12-17], OmniGuide fibers [18], multi-mode high dispersion fibers [19], rigid glass rod type fibers [20] and higher-order mode fibers [21, 22]. Glass rod type fibers have drawn much attention because of large mode area with low susceptibility to mode coupling. However, these structures are not suitable for long length devices because of difficulty in compact packaging. PCFs can be designed with a large differential leakage loss between fundamental mode (LP_{01}) and LP_{11} mode, and therefore, can give higher modal purity at the output. However, modal coupling remains an issue with the PCFs [22]. The largest mode area reported in PCFs is approximately 1400 μm^2. Hollow core photonic bandgap fibers can be the promising choice because optical nonlinearities are reduced by a factor of 1000 compared with silica-core fibers. However, the guidance of the laser beam through the hollow core negates the possibility of constructing a distributed amplifier by incorporating rare earth dopants. Recently, the higher-order-mode (HOM) fibers with the very large mode area and low susceptibility to mode coupling emerged for USP delivery, however, they require selective higher-order-mode excitation using a long-period grating [21, 22]. In this thesis we have presented a design of three layered fiber structure and segmented cladding fiber (SCF) for delivery of high energy fs-pulses through the fundamental mode of the fiber. Three layered fiber structure has been designed to deliver USPs at 1.55 μm wavelength whereas SCF has been designed to deliver USPs at more than one wavelength. Development of technology for fabrication of SCF has also been reported.

1.1.3 *Refractive index sensors*

Measurement of refractive index of various biological and chemical samples is important for detecting several physical and biological parameters. An optical fiber refractive index sensor provides a good alternative for a compact lightweight and highly sensitive refractive index sensor. An optical fiber refractometer is also suitable for remote sensing and in otherwise inaccessible places. In addition, it can be employed to sense polymer or liquid composites [22-46]. The quantity of sample required to carry out the measurement can also be very small. Currently, fibers having metal coating [25, 26] and fiber Bragg grating (FBG) are being widely studied as highly sensitive

refractive index sensing devices for biological and chemical samples [29-31]. Tapered fibers and fibers employing stripped-off cladding have also been used as another alternative for refractive index sensors [33, 44]. Long period grating (LPG) and untapered fibers having thin films coating over full cladding of fiber are also used as refractive index sensors [34-42]. Villatoro et al. have reported core diameter mismatch based low cost refractive index sensor [44]. The sensor has been formed by splicing a small section of single mode fiber (SMF) to a multimode fiber. Recently, a low cost core diameter mismatch based fiber sensor has been reported [45]. The choice of technique employed is a tradeoff between fabrication cost, practicality, robustness, simple manufacturing processes, sensitivity, and sensing range. Here we present an optical fiber sensor that combines simplicity, compactness, high resolution, low cost and competitive sensing range. The sensor is based on a depressed index cladding (DIC) type leaky fiber. Leakage loss in such fibers can be highly sensitive to the variations in refractive index of the outermost leaky layer.

1.2 Applications of multilayer planar waveguides

1.2.1 *Refractive index sensors*

Refractive index sensors based on conventional optical fiber are difficult to handle because of fragile nature of the fiber. Fiber structures specially designed for the purpose with special geometry can be the solution of the problem however fabrication process of the complex designs is not so simple and cost effective. To overcome the problem various types of integrated optical sensor have been described including interferometric, refractrometric, evanescent field, fluorescent or absorbance based sensors, and surface-plasmon resonance based sensors [47-52]. The choice of technique employed is a tradeoff between fabrication cost, practicality, robustness and simple manufacturing processes. Although some of the refractometric biosensing systems have been commercially successful but their use has been mostly limited to research laboratories due to their cost and complexity. We have designed a leaky planar waveguide based refractive index sensor which is simple, compact and cost effective.

1.2.2 *Extraction of light in Organic light emitting diodes*

Another important area where multilayer planar structures can find applications is light emitting diode (LED) lighting. Organic light-emitting diodes (OLED) have drawn much attention because of their advantages such as low power consumption, high contrast, high brightness, low cost and their promising applications in flat panel displays, illumination, domestic solid state lighting etc. Radiative decay of molecular excited state is responsible for light generation mechanism in OLED. But a most of the l light is lost inside the device because of different mechanisms. A major issue in OLED is its poor light extraction efficiency which is defined as defined as the number of generated photons coming out of the device per number of photons generated in the device. A large fraction of generated light approximately 40% is coupled to surface Plasmon polaritons generated at metal/organic interface and is lost [53]. Due to total internal reflection at glass/ITO interface 15% of the light is lost in guided modes. Approximately 23% of generated photons are lost at substrate/air interface by total internal reflection. Roughly 20% of generated photon in organic layer is extracted out from the device [53]. However approximately 80 % of light is lost due to poor extraction efficiency. Many approaches have been described in literature to increase performance of OLED. The ratio of total number of generated photons in organic layer to the number of injected electrons defines the internal quantum efficiency of OLED which is only 25%. However by harvesting both singlet as well as triplet excitation states using electrophosphorescent materials the internal quantum efficiency of OLEDs can be achieved near 100%. Back texturing of the glass substrate can be an alternative to avoid light propagation in substrate modes and can lead to increase in extraction efficiency [54]. High index substrate can also be used to increase extraction efficiency [55]. However, high index substrate can lead to high index contrast between substrate and air. Micro lenses and periodic micro structures can also be inserted to couple the guided modes power to useful power radiation modes [56-62]. However the process to fabricate micro-lenses and periodic structures is cumbersome and expensive. Another important technique to out couple the guided mode power is the use of grating coupler, where a grating is employed to avoid refractive index mismatch between high index and low index layer which prevents coupling of radiation modes to guided modes [63]. Patterned ITO electrode coated with PEDOT: PSS (a low index polymer) also increases

the external quantum efficiency. The patterning of ITO can be done using photolithographic steps or micro-contact printing. Low index materials grids have also been used between ITO and organic layer interface [64, 65]. Standard photolithographic method can be used to embed these grids at ITO/organic layer interface. Insertion of aerogel layer between glass and ITO in conventional OLED structure can avoid coupling of power to substrate modes [66] and results in significant enhancement in external quantum efficiency. However, this method is accompanied by change in radiation pattern and exhibits an undesirable angle dependent emission spectrum and also involves complex processing methods. Silica aerogels are hydrophilic in nature and absorb moisture easily and suffer a structural change which results in degradation of the device. In this thesis we have proposed to enhance the efficiency of OLED by inserting low refractive index material between glass substrate and ITO. Such a structure can help in leaking out more light which is subsequently available for extraction from the organic and ITO layer.

The work of thesis has been divided into eight chapters. First chapter is introduction which describes the motivation for specialty multi-layer waveguide designs such as segmented core fiber, segmented cladding fiber, multi-ring large mode area fiber, three layered w-fiber, multi-layer planar waveguide and OLED structure. The chapter also includes the state of art of these structures or applications. This thesis presents various novel designs in planar and cylindrical geometry to achieve flattened dispersion with large mode area, very large mode area fiber for delivery of ultra-short laser pulses, highly sensitive refractive index sensor to sense biological and chemical samples. In addition multilayer OLED structure has been proposed to increase its efficiency. Proposed structures have been analyzed using established numerical methods such as transfer matrix method (TMM).

In chapter 2, we have discussed designs of segmented core fibers having small positive, small negative and near-zero ultra-flattened dispersion with small dispersion slope and ultra-large effective area over a wide spectral range. The designs consist of a concentric multilayer segmented core followed by a trench assisted cladding and a thin secondary core. The central segmented core helps in maintaining desired dispersion over a wide range of wavelength. The second core of the fiber helps in achieving ultra-large effective area and low index trench in the cladding reduces the bending loss. Designed fibers show very small bending loss. We report breakthrough in the mode area

of the single mode optical fiber with ultra flattened dispersion and low dispersion slope. These characteristics of the fiber make it an attractive candidate for DWDM optical communication system.

In chapter 3 we have presented large mode area fiber designs for delivery of ultra-short laser pulses. We have presented three layered fiber structure and segmented cladding fiber for delivery of femtosecond laser pulses. Pulse propagation through the fibers has been studied using split-step Fourier method. Distortion-free propagation of the pulse has been achieved by keeping ratio of dispersion to nonlinear length close to 1 in both the fibers. The modal purity in the fiber structures has been maintained by leaking out all the higher order mode (HOM) except LP_{11} mode. Mode stability has been ensured by sufficient mode spacing between LP_{01} and LP_{11} modes. Design of the fibers ensures no intermodal coupling, low bending loss, and high fabrication tolerances while maintaining large-mode-area. Fibers can be fabricated using modified chemical vapor deposition technique.

Chapter 4 contains fabrication of segmented cladding fiber in silica. We have optimized the design of SCF for large mode area application and has been fabricated using modified chemical vapor deposition technique at CGCRI Kolkata. Fiber has been fabricated with 45 μm core diameter and 125 μm as the outer diameter.

In chapter 5 we present the design of a refractive index sensor based on depressed index clad fiber. We utilize variation of leakage loss with variation in refractive index of outermost layer of waveguide to design a simple, compact, low cost and ultra high sensitive. We utilize different regions of leakage loss curve to design sensors in different ranges, with different index resolutions, and for specific applications. One of such designed sensors works in the range 1.457325 to 1.457350, which corresponds to the refractive index of jojoba oil. The resolution within this range is of the order of 4×10^{-7} which is the finest resolution of the sensor. The fabrication of the sensor requires etching of some portion of the cladding of the fiber and does not require costly methods of wavelength or polarization interrogation.

In chapter 6 we have proposed a simple, compact, low cost and highly sensitive refractive index sensor based on single mode leaky planar waveguide. An optical waveguide deposited on glass substrate has been proposed to construct the sensor. In this structure cytop works as guiding layer while teflon forms the cladding layers. Propagation of light in cytop layer is strongly affected by the refractive index of

external medium placed on top of teflon layer. If the refractive index of the medium is close to or greater than that of cytop then there is leakage of power from cytop layer to external medium which affects the transmittance of the waveguide. The structure can be designed to have strong variation in transmittance with the refractive index of external medium, and thus, can be utilized as highly sensitive refractive index sensor for biomedical applications. In this chapter we have carried out the design strategies of such an refractive index sensor for various biological and chemical applications. We have designed a sensor with index resolution of the order of 10^{-5}. Fabrication of the sensor can be carried out by using spin coating technique. Long range, high sensitivity, simple manufacturing process and compactness make the sensor attractive for diverse applications.

In chapter 7 we have extended the applications of leaky structure to organic light emitting diode to increase its efficiency. Extraction efficiency of conventional OLED structure has been increased by inserting a low index layer of polymer Teflon between glass substrate and ITO. This low refractive index layer helps in breaking wave guidance of modes. Such a structure helps in leaking out more power into the glass substrate from organic and ITO layer. We show 14% increment in extracted power at 0.442-μm wavelength and 27% increment at 0.539-μm wavelength, and 3 % at 0.633-μm wavelength is Fabrication of the structure can be done using very cost effective spin-coating technique.

In chapter 8 we have presented concluding remarks and scope for future work. In thesis we have presented multi-layer fiber and waveguide designs. Designs have been carried out for ultra-short laser pulse delivery, for sensing refractive index of biological and chemical samples, to enhance efficiency of organic light emitting diode. We have also presented multi-ring fiber designs for high power applications and for flattened dispersion. Fabrication and characterization of segmented cladding fiber in silica core has also been presented.

CHAPTER–2

Large Mode Area Dispersion Flattened Fiber*

2.1 Introduction

The communication system based on the dense wavelength division multiplexing (DWDM) has come into existence after the successful development of broadband erbium doped fiber amplifiers (EDFAs) [68-76]. Optical fiber is a medium to realize the task of DWDM and has two basic problems which must be addressed for having reliable data transmission. These drawbacks are basically related to dispersion and nonlinear effects. In a conventional silica optical fiber value of dispersion increases with wavelength therefore different channels suffer from different amount of pulse broadening. Dispersion compensators can be used alternative for periodic reshaping the signal after a suitable length of the fiber [77-84]. But in optical network the placement of dispersion compensating module increases the cost of the system. Furthermore, the loss added by dispersion compensating module increases effective noise figure of the system and different optical channels in a fiber undergo different amount of accumulated dispersion. To overcome this difficulty, fibers with small finite dispersion and dispersion slope have been proposed [5-11].

* A part of the results presented in this chapter have been reported in a research publication:
B. Hooda and V. Rastogi, "Segmented-Core Single Mode Optical Fiber with Ultra-Large-Effective-Area, Low Dispersion Slope And Flattened Dispersion For DWDM Optical Communication Systems", PIER B, vol. 51, pp. 157-175, 2013.

Another problem in conventional optical fibers is its small effective area, which leads to nonlinear effects like self phase modulation (SPM) and cross-phase modulation (XPM). XPM limits the number of different wavelength signals that can be transmitted through the fiber. Therefore, there is a need of suitable transmission medium for high data rate optical communication system employing DWDM. The maximum distance a signal can travel also depends on the choice of optical transmitter and its characteristics. Different types of optical transmitters like directly modulated distributed feedback lasers (DMLs), electro-absorption modulated distributed feedback lasers (EA-DFBs) or externally modulated lasers using Mach–Zehnder $LiNbO_3$ modulators (MZ) can be used. Recently, low-cost DMLs have attained much attention [7]. Negative dispersion fibers can balance the positive chirp characteristic of directly modulated laser (DML) transmitters and can enhance transmission distance. To achieve this, suitable refractive index profiles of the fibers which lead to small dispersion, dispersion slope and large effective area have been developed [5-11]. Here we review some of dispersion flattened designs. Hatayama et al. have reported dispersion flattened fiber with effective area more than 50 μm^2. However the bandwidth that could be achieved is small for DWDM applications [85]. Lundin has presented a design of single mode W fiber which shows flattened dispersion over the wavelength range 1.25-1.60 μm. The root mean square value of the chromatic dispersion over the aforementioned wavelength range in this design is less than 1 ps/km/nm. However the small core radius of the fiber results in small effective area and restricts its application in DWDM long-haul optical communication system [11]. Varshney et al. have proposed design of a flat modal field fiber with positive dispersion and small dispersion slope over the wavelength range of 1.53-1.61μm. In this fiber they have reported effective area of 56.1 μm^2 at 1.55 μm wavelength. They have shown dispersion of the proposed fiber as 2.7-3.4 ps/km/nm within the wavelength range of 1.53-1.61 μm. The dispersion slope of the designed fiber at 1.55 μm wavelength is 0.01 $ps/km/nm^2$ [5]. However, the wavelength range of the fiber does not cover the entire S+C+L band. Tian et al. have proposed ring index profiles named RI and RII triple-clad optical fibers with effective area ranging from 95-118 μm^2 in the spectral range of 1.54-1.62 μm. The reported total dispersion in the aforementioned wavelength range are 4.5 ps/km/nm and 0.006 $ps/km/nm^2$ respectively [6]. The wavelength range reported by them also does not cover the entire S+C+L band. Okuno et al. have reported a fiber having negative dispersion of about –8ps/km/nm over the entire telecommunication

band [7]. However, the reported mode area is small. Recently Rostami et al. have proposed a modified W-type single mode optical fiber with ultra low dispersion, dispersion slope and ultra high effective area. They show very small dispersion varying from 0.1741-0.9282 ps/km/nm in the spectral range of 1.460-1.625 μm. Dispersion slope and mode area reported by them in the aforementioned wavelength range are [(–0.011)-(0.0035)] ps/km/nm^2 and [103.56-232.26] μm^2 respectively. In their structure they have achieved all these features by introducing extra depressed cladding layers in W-type fiber [8].

In this chapter we present a segmented core dispersion flattened fiber which is capable to be designed as (i) small positive-non-zero dispersion flattened fiber, (ii) small negative-non-zero dispersion flattened fiber, and (iii) near-zero dispersion flattened fiber. The designed fibers show ultra low dispersion slope, ultra large mode effective area and small bending sensitivity over the S+C+L band. We have organized the chapter as follows:

Theory to calculate modes, dispersion, bending loss and splice loss has been discussed in section 2.2. Fiber design has been discussed in section 2.3 The designs of the proposed fiber and performances of the fiber through our simulation results are discussed in Section 2.3. Feasibility of fiber fabrication has been discussed in section 2.3. Compatibility of the designed fiber with other optical fiber based components has been discussed in section 2.4. Sensitivity analysis of the structural disorders on the performance of the fiber has been presented in section 2.5. Concluding remarks are presented in section 2.6.

2.2 Theory

2.2.1 *Transfer matrix method*:

We have used transfer matrix method (TMM) for modal analysis of the designed fiber [86]. TMM is a very powerful technique for solving any arbitrary refractive-index profile of the fiber and is easy to implement. In TMM arbitrary refractive index profile of the fiber is divided into homogeneous layers using stair-case approximation. A radially symmetric refractive-index profile having N layers of refractive indices n_1, n_2, n_3……n_N is shown in Fig. 2.1. Radial part of mode field in i^{th} layer can be described by the following equation using scalar approximation:

$$r^2\frac{d^2\psi}{dr^2}+r\frac{d\psi}{dr}+[(k_0{}^2n_i{}^2-\beta^2)r^2-l^2]\psi=0 \tag{2.1}$$

and the total modal field is represented by

$$R(r,\phi,z,t)=\psi(r)\left[\frac{\cos l\phi}{\sin l\phi}\right]\exp i(\omega t-\beta z);\qquad l=1,2,3,\ldots \tag{2.2}$$

Where l represents azimuthal mode number and β represents propagation constant of the mode. Here we will discuss in detail the solution for $l = 0$, however the procedure is same for $l \neq 0$ modes also. For $l = 0$ Eq. (2.1) becomes:

$$r^2\frac{d^2\psi}{dr^2}+r\frac{d\psi}{dr}+[(k_0{}^2n_i{}^2-\beta^2)r^2]\psi=0 \tag{2.3}$$

The solution of the above equation can be given by Bessel functions. In guiding region, where $\beta^2 < k_0{}^2n_i{}^2$ solution of above mentioned equation is given by:

$$\psi(r)=A_iJ_0(k_ir)+B_iY_0(k_ir) \tag{2.4}$$

Where A_i and B_i are field coefficient in i^{th} layer. For $\beta^2 > k_0{}^2n_q{}^2$, the general solution of Eq.(2.3) in qth region is given by

$$\psi(r)=A_qK_0(\gamma_qr)+B_qI_0(\gamma_qr) \tag{2.5}$$

where

$$k_i{}^2=k_0n_i{}^2-\beta^2;\qquad \gamma_q{}^2=\beta^2-k_0{}^2n_q{}^2.$$

By applying appropriate boundary conditions which require ψ and $d\psi/dr$ must be continuous at each interface. Field coefficients of $(i+1)^{th}$ layer and its preceding (i^{th}) layer can be related by a 2×2 matrix as given below:

$$\begin{bmatrix}A_{i+1}\\B_{i+1}\end{bmatrix}=\begin{bmatrix}a_i & b_i\\c_i & d_i\end{bmatrix}\begin{bmatrix}A_i\\B_i\end{bmatrix} \tag{2.6}$$

Where a_i, b_i, c_i and d_i can be easily calculated by multiplication of two 2×2 matrices involving Bessel and modified Bessel function [87]. The field coefficients of the first and the last layer (N) of the structure can be easily connected by simply multiplying the transfer matrices of all the intermediate layers.

$$\begin{bmatrix}A_N\\B_N\end{bmatrix}=\begin{bmatrix}S_{11} & S_{12}\\S_{21} & S_{22}\end{bmatrix}\begin{bmatrix}A_1\\B_1\end{bmatrix} \tag{2.7}$$

Where S_{11}, $S_{12,}$ S_{21} and S_{22} are elements of transfer matrix which is the product of various 2×2 matrices. For guided modes $\beta > k_0 n_1$ as the field has finite value at $r = 0$ and $r = \infty$, therefore $B_1 = 0$, and $B_N = 0$ which implies $S_{21} = 0$, which is eigen value equation. Therefore, by scanning $S_{21}(\beta)$ on the β-axis, propagation constant of the mode can be obtained. If refractive index of inner cladding of the fiber is smaller than that of outermost cladding then in that case fundamental mode of the fiber becomes leaky. For

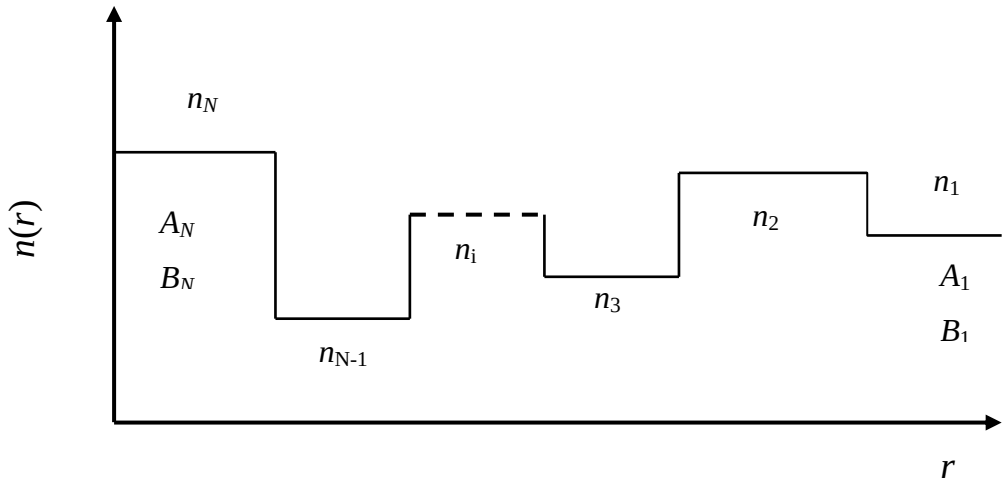

Figure 2.1 *Stair case representation of a radially symmetric arbitrarily shaped fiber*

a leaky mode, $\beta < k_0 n_1$ and represents a purely outgoing wave where n_1 is the refractive index of outermost cladding. Therefore, a linear combination of $J_0(k.r)$ and $Y_0(k.r)$ should be chosen in such a way that it describes an outgoing wave. In that case

$$A_1 = iB_1 \tag{2.8}$$

Therefore, from the Eq. (2.8) we have

$$A_N = A_1 (S_{11} + iS_{12}) \tag{2.9}$$

$$B_N = A_1 (S_{21} + iS_{22}) \tag{2.10}$$

In the innermost region, the boundary condition that the field should be finite at $r = 0$ gives a complex eigenvalue equation $B_N(\beta) = 0$. Scanning of $\left|1/B_N(\beta)\right|^2$ along the real β axis gives several peaks that are Lorentzian in shape. The position of Lorentzian peak corresponds to real part of β of modes and corresponding full widths at half maxima (FWHM) gives imaginary part of modes. Real part of propagation constant gives the

information about the effective indices of modes while leakage losses can be calculated from the imaginary part. Leakage loss can be calculated by using the following formula:

Leakage loss = 20*0.4343*neffim*k

Where neffim = imaginary part of effective index.

2.2.2 *Dispersion*

Material response to interaction of electromagnetic waves with bound electrons of dielectric depends on optical frequency ω. This property is referred to as chromatic dispersion. The cause of chromatic dispersion is characteristic resonance frequencies at which medium absorb electromagnetic radiation. In propagation of short optical pulses fiber dispersion plays a critical role as spectral components of the pulse travel with different speeds. A temporal pulse propagates with group velocity v_g given by following equation [88]:

$$v_g = \frac{1}{\left(dk/d\omega\right)} \tag{2.11}$$

Where

$$k(\omega) = \frac{\omega}{c} n(\omega) \tag{2.12}$$

Mathematically, effect of fiber dispersion is taken into account by expanding propagation constant β in Taylor series about central frequency (ω_0) of pulse spectrum.

$$\beta(\omega) = n(\omega)\frac{\omega}{c} = \beta_0 + \beta_1(\omega - \omega_0) + \frac{1}{2}\beta_2(\omega - \omega_0)^2 + ... \tag{2.13}$$

Where

$$\beta_m = \left(\frac{d^m \beta}{d\omega^m}\right) \qquad (m = 0,1,2.....) \tag{2.14}$$

Parameters β_1 and β_2 are related to $n(\omega)$ and using Eq.(2.11) and Eq.(2.12) are given as:

$$\beta_1 = \frac{1}{v_g} = \frac{1}{c}\left(n + \omega\frac{dn}{d\omega}\right) \tag{2.15}$$

β_1 represents group velocity and β_2 represents group velocity dispersion. Light transmission through the single mode fiber undergoes material and waveguide dispersion. Total induced dispersion (D) in ps/km/nm is defined as:

$$D = \frac{d\beta_1}{d\lambda} = -\frac{\lambda}{c}\frac{d^2 n_{eff}}{d\lambda^2} \tag{2.16}$$

Where c is the velocity of light in free space and λ is the free space wavelength.

2.2.3 *Effective area*

Another optical property of the fiber which describes the power density within the fiber is mode effective area (A_{eff}). Nonlinear effects in the fiber strongly depend on A_{eff}. We have calculated A_{eff} of the fiber by using the following relation [89].

$$A_{eff} = \frac{2\pi\left[\int_0^\infty |\psi(r)|^2 \, r dr\right]^2}{\int_0^\infty |\psi(r)|^4 \, r dr} \tag{2.17}$$

The mode field diameter (MFD) of the fiber has been calculated using the Peterman II method using MFD = $2w_1$ [89] where

$$w_1^2 = \frac{2\left[\int_0^\infty |\psi(r)|^2 \, r dr\right]}{\int_0^\infty [\frac{d\psi(r)}{dr}]^2 r dr} \tag{2.18}$$

2.2.4 *Bending loss*:

The radiative loss caused by bend when bending radius is much larger than the diameter of the fiber is defined by macrobending loss and has been computed using the following relation[90]:

$$\alpha_{macro} = \frac{10}{\log_e 10}\left(\frac{\pi V^8}{16aR_bW^3}\right)^{1/2}\exp\left(-\frac{4R_bW^3\Delta_1}{3aV^2}\right)\frac{\left[\int_0^\infty (1-g)\psi r dr\right]^2}{\int_0^\infty \psi^2 r dr} \tag{2.19}$$

Where R_b is bending radius and a is core radius of the fiber. Other parameters appearing in Eq. (2.19) are given as:

$$V = k_0 a\sqrt{n_1^2 - n_2^2} \tag{2.20}$$

$$W = a\sqrt{\beta^2 - k_0^2 n_2^2} \tag{2.21}$$

$$g = \frac{n(r)^2 - n_{\min}^2}{n_{\max}^2 - n_{\min}^2} \tag{2.22}$$

$$\Delta = \frac{n_{\max}^2 - n_{\min}^2}{2n_{\max}^2} \tag{2.23}$$

Where $n_{\max}$ and $n_{\min}$ are the maximum and minimum values of refractive index respectively. β is the propagation constant of the mode.

2.2.5 *Splice loss*

When we splice conventional fiber with designed fiber then some loss occurs because all power can not be coupled from one fiber to another. Splice loss can also be caused because of longitudinal fiber separation, tilted splicing and splices with fiber offset. Power transmission coefficient for splice shown in Fig. 2.2 (a) is given as [91]:

$$T = \frac{4\left[4Z^2 + \frac{w_1^2}{w_2^2}\right]}{\left[4Z^2 + \frac{w_2^2 + w_1^2}{w_2^2}\right]^2 + 4Z^2\frac{w_2^2}{w_1^2}} \tag{2.24}$$

Where $2w_2$ is the MFD of conventional fiber and the separation distance L is defined as:

$$Z = \frac{L}{n_2 k w_1 w_2} \tag{2.25}$$

At $L = 0$,

$$T_0 = \left(\frac{2w_1 w_2}{w_1^2 + w_2^2} \right)^2 \tag{2.26}$$

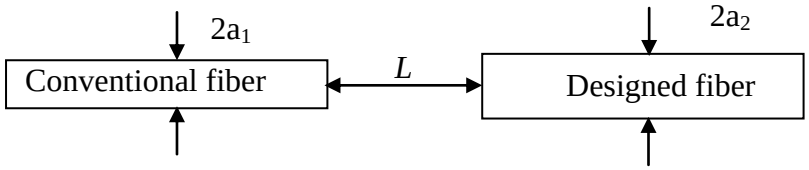

(a)

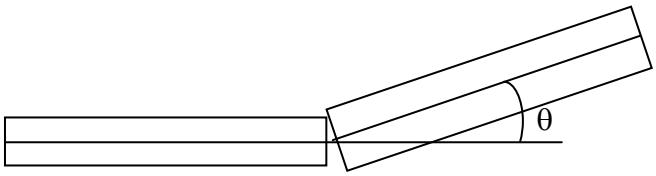

(b)

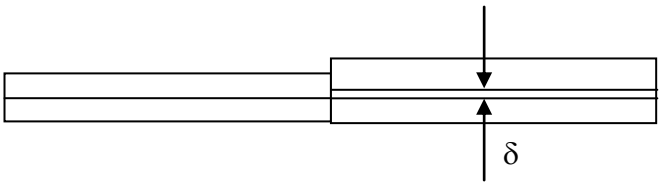

(c)

Figure 2.2 *(a) Splice imperfections due to longitudinal separations, (b) due to tilted alignment, (c) due to fiber offset*

At $L = \infty$

$$T_\infty = \left(\frac{n_2 k w_1 w_2}{L} \right)^2 \tag{2.27}$$

For the splices with tilt shown in Fig. 2.2 (b) the power transmission coefficient is given as:

$$T_1 = \left(\frac{2w_1 w_2}{w_1^2 + w_2^2} \right) \exp\left[-\frac{2\left(\pi n_2 w_1 w_2 \theta\right)^2}{\left(w_1^2 + w_2^2\right)\lambda^2} \right] \tag{2.28}$$

For smaller angles $\theta \approx \sin(\theta)$

The above equation therefore can be written as:

$$T_1 = \left(\frac{2w_1 w_2}{w_1^2 + w_2^2} \right) \exp\left[-\frac{2\left(\pi n_2 w_1 w_2 \sin\theta\right)^2}{\left(w_1^2 + w_2^2\right)\lambda^2} \right] \tag{2.29}$$

When the fibers are spliced with fiber offset as shown in Fig. 2.2 (c) then power transmission is given as:

$$T_2 = \left(\frac{2w_1 w_2}{w_1^2 + w_2^2} \right) \exp\left[-\frac{2\delta^2}{w_1^2 + w_2^2} \right] \tag{2.30}$$

Total transmittance is given as $T = T_1 + T_2 + T_3$

Splice loss of the fiber can be given as:

$$\alpha = -10 Log_{10}(T) \tag{2.31}$$

Which can be written as [e.g. neumanns fundamental of single mode):

$$\alpha(dB) = -10 Log_{10}\left[\frac{2w_1 w_2}{w_1^2 + w_2^2} \right]^2 + 4.343 \frac{2\delta^2}{w_1^2 + w_2^2} + 4.343 \left(\frac{2\pi n}{\lambda} \right)^2 \frac{\left(w_1 w_2\right)}{2(w_1^2 + w_2^2)} \sin^2(\theta) \tag{2.32}$$

δ represents radial offset between the cores of the fiber and θ represents angular misalignment of the two fibers. n is the refractive index of the medium between the fiber ends. In Eq. (2.32) first term represents the splice loss from mode field mismatch, second term calculates the splice loss due to radial offset between the cores of the fibers and the last term constitutes the loss due to fiber angular misalignment.

2.3 Fiber Design

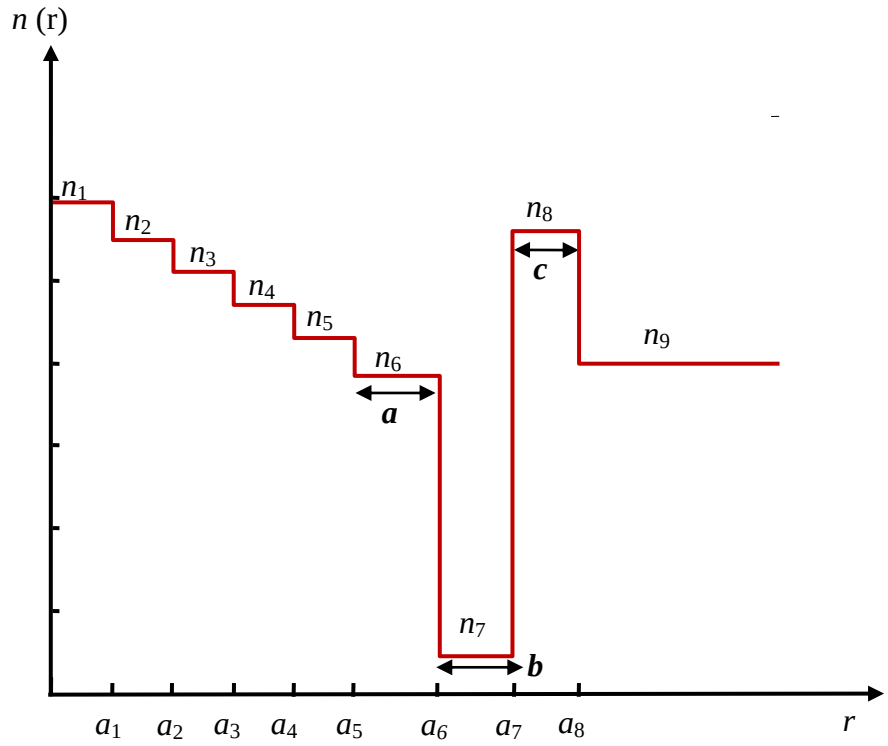

Figure 2.3 *The refractive index profile of the proposed structure*.

We have considered the fiber profile as shown in Fig. 2.3. Refractive index of the proposed structure is defined as follows.

$$n(r)=\begin{cases} n_1, & 0<r<a_1 \\ n_2, & a_1<r<a_2 \\ n_3, & a_2<r<a_3 \\ n_4, & a_3<r<a_4 \\ n_5, & a_4<r<a_5 \\ n_6, & a_5<r<a_6 \\ n_7, & a_6<r<a_7 \\ n_8, & a_7<r<a_8 \\ n_9, & a_8<r \end{cases} \tag{2.33}$$

$$\Delta_1=\frac{n_1^2-n_9^2}{2n_1^2},\quad \Delta_2=\frac{n_9^2-n_7^2}{2n_9^2},\ \Delta_3=\frac{n_8^2-n_9^2}{2n_8^2} \tag{2.34}$$

Where *r* is the radial position. Outermost layer is formed by fused silica. Δ_1 and Δ_3 represents the level of up-doping with respect to the outer most layer. Δ_2 represents the level of down-doping of low index trench with respect to outer most layer. Parameters of the fiber have been optimized in such a way as to achieve flattened dispersion with large effective area. The segmented core of the fiber is formed by six layers having monotonically decreasing refractive index. First five layers of the central core have equal widths while the width of the sixth layer is slightly larger. The cladding of the fiber is formed by a thin low-index trench which is followed by thin second core and a thick uniform outer cladding. Low-index trench in the cladding helps in reducing the bending loss of the fiber and segmented core helps in maintaining flattened dispersion. The second core of the fiber helps in achieving large A_{eff} as it taps some power from the central core. The fiber is a dual-core structure where resonance can lead to a high negative dispersion. We have optimized the parameters of the fiber in such a way that the resonance wavelength does not fall in the desired spectral range and the dispersion curve remain flat. By optimizing parameters of the fiber desired dispersion characteristics, large-effective-area and low bending loss can be obtained. Dispersion of the fiber can be controlled mainly by waveguide dispersion which is caused by wavelength dependence of distribution of energy for fundamental mode in the fiber. In case of single mode fiber, tailoring of dispersion is easier in comparison to multimode fiber as more energy penetrates in cladding in case of single mode fiber. Cladding index is lower thus faster will be the propagation in that region. Thus for a particular spectral width time delay differences develops. Therefore parameters of the core of the fiber can be selected in such a way as to achieve desired dispersion characteristics. As wavelength increases penetration of mode energy in cladding increases as shown in Fig. 2.4. Where *a* is the core diameter of fiber structure and Fig. 2.4 (b) indicates more field spread in the cladding at wavelength λ_2 than that of the field spread at wavelength λ_1. Fiber having parabolic type core has higher field spread in comparison to triangular fiber and step index fiber. Therefore parabolic core fiber has higher mode area and better dispersion characteristics according to the application. Proposed fiber can work as

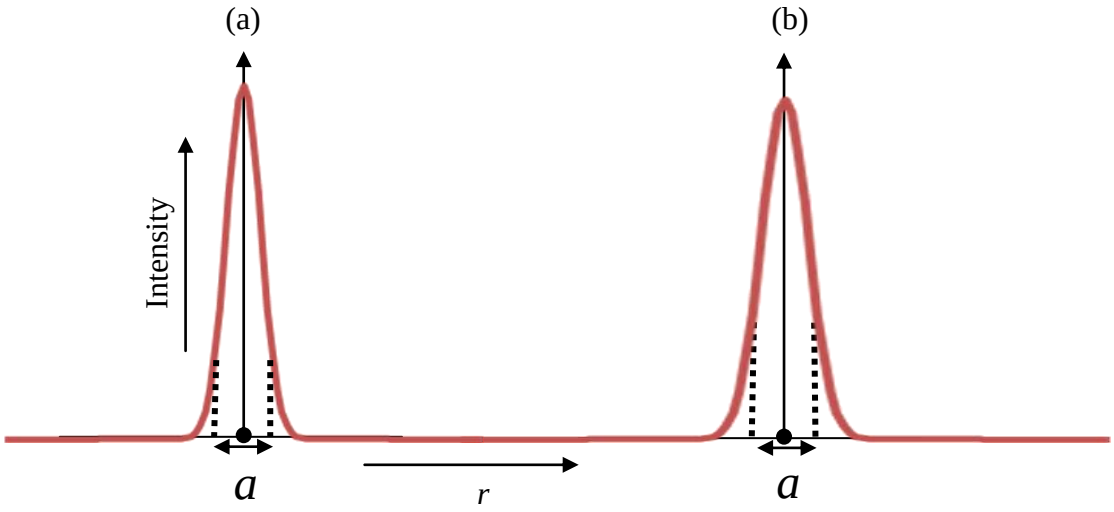

Figure 2.4 (a) *Intensity distribution of fundamental mode at* λ_1, (b) *Intensity distribution of fundamental mode at* $\lambda_2 > \lambda_1$

positive non-zero dispersion flattened fiber, negative non-zero dispersion flattened fiber and near-zero dispersion fiber in the wide band of wavelengths.

(i) Design of near-zero dispersion flattened fiber:

To achieve successfully near-zero total chromatic dispersion, we need to design fiber in such a way that waveguide dispersion of the fiber is balanced by material dispersion. The optimized parameters of the designed fiber having near zero flattened dispersion are listed in Table 2.1 and refractive index profile is shown in Fig. 2.3.

Table 2.1.

Proposed near-zero dispersion flattened fiber design parameters.

$n_1 - n_2 = n_2 - n_3 = n_3 - n_4 = n_4 - n_5 = n_5 - n_6 = 8 \times 10^{-4}$
$a_2 - a_1 = a_3 - a_2 = a_4 - a_3 = a_5 - a_4 = 1$ μm
$a = 1.68$ μm, $b = 1.2$ μm, $c = 1.1$ μm, $\lambda = 1.55$ μm, $n_9 = 1.4444$
$\Delta_1 = 0.22\%$, $\Delta_2 = 0.49\%$, $\Delta_3 = 0.27\%$

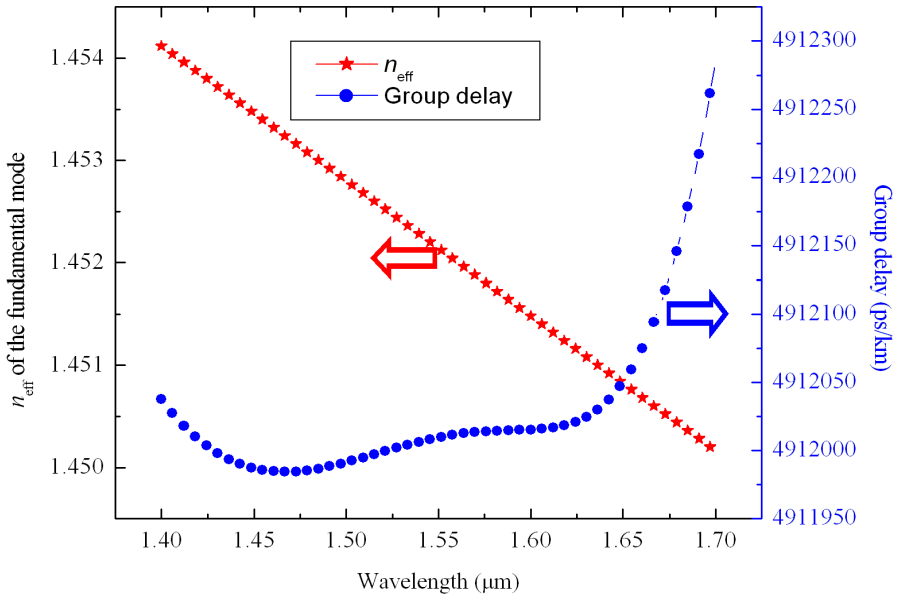

Figure 2.5 *Spectral variations of effective refractive index and group velocity of near zero dispersion flattened fiber for the parameters given in Table 2.1.*

The effective refractive index of the fundamental mode and group delay are important parameters for obtaining dispersion. In order to achieve flattened dispersion we have

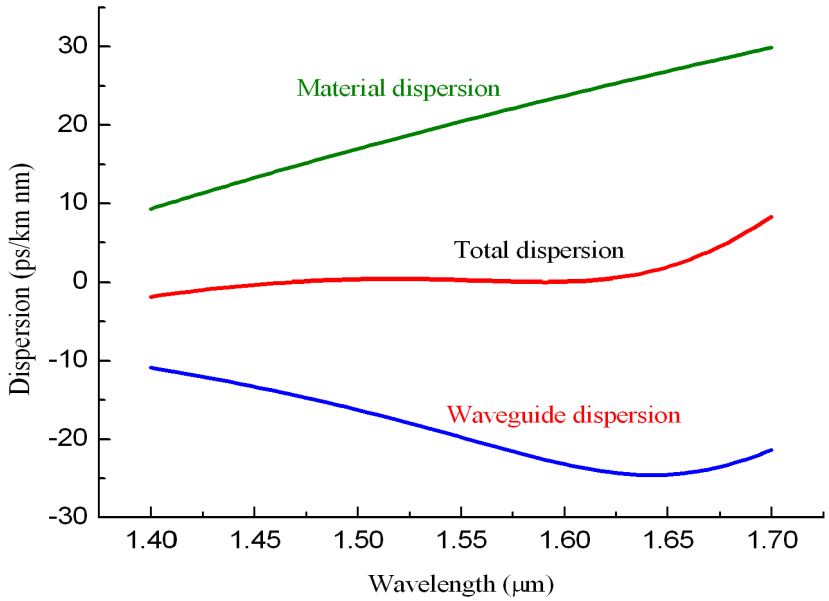

Figure 2.6 *Spectral variations of material, waveguide and total dispersion of near zero dispersion flattened fiber for the parameters given in Table 2.1.*

first studied the spectral variations of the effective index and group delay of the fiber as shown in Fig. 2.5. We can see that group delay does not vary significantly over the wavelength range 1.460-1.625 μm. n_{eff} of the fundamental mode of the fiber varies linearly with wavelength which shows that there is no resonance point in the considered wavelength range. Spectral variation of the dispersion of the fiber has been calculated using Eq. (2.16) and results are shown in Fig. 2.6. One can observe from Fig. 2.6 that the dispersion is nearly flat and varies from 0.0039 ps/km/nm to 0.520 ps/km/nm in the spectral range 1.460-1.625 μm, which covers S+C+L band completely. Spectral variation of dispersion slope of the designed fiber is plotted in Fig. 2.7. We observe from Fig. 2.7 that the value of dispersion slope is very small in the aforementioned wavelength range. The maximum value of dispersion slope in the considered wavelength range is 0.0365 ps/km/nm^2. We have compared various characteristics of the designed fiber with the already existing design reported in Ref. [8]. Dispersion and dispersion slope of the proposed design and the design reported in Ref. [8] in various bands are shown in Table 2.2.

Table 2.2.

Comparison of characteristics of proposed near zero dispersion flattened fiber design with already existing design reported in Ref. [8].

Wavelength band →	S-band (1.460-1.530) μm		C-band (1.530-1.565) μm		L-band (1.565-1.625) μm	
	Proposed design	Ref. [19]	Proposed design	Ref. [8]	Proposed design	Ref. [8]
Average dispersion (ps/km/nm)	0.259	0.8179	0.269	0.3621	0.140	0.0832
Average dispersion slope (ps/km/nm^2)	0.0069	–0.0057	–0.0035	–0.0109	0.0059	0.0073

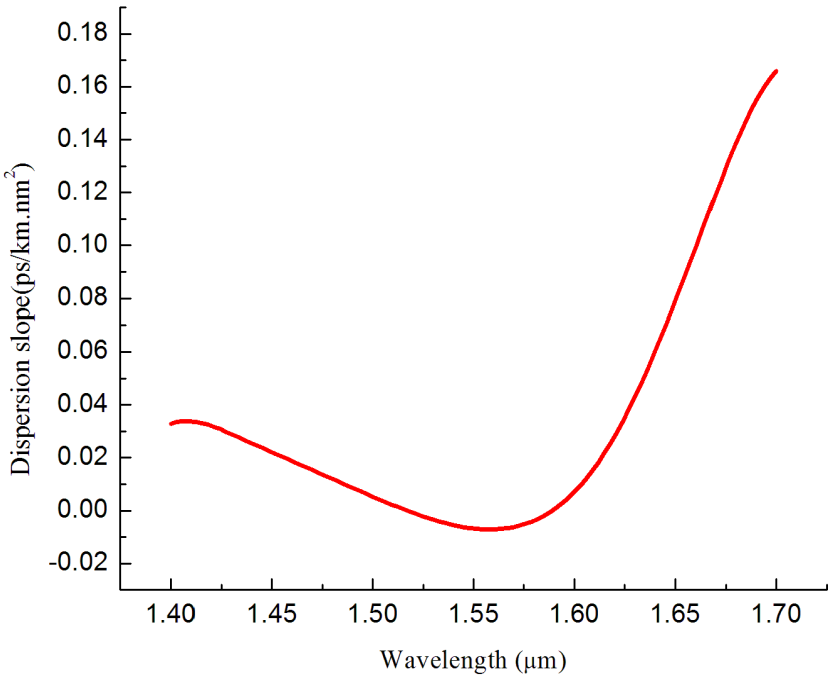

Figure 2.7 *Spectral variations of dispersion slope of near zero dispersion flattened fiber for the parameters given in Table 2.1.*

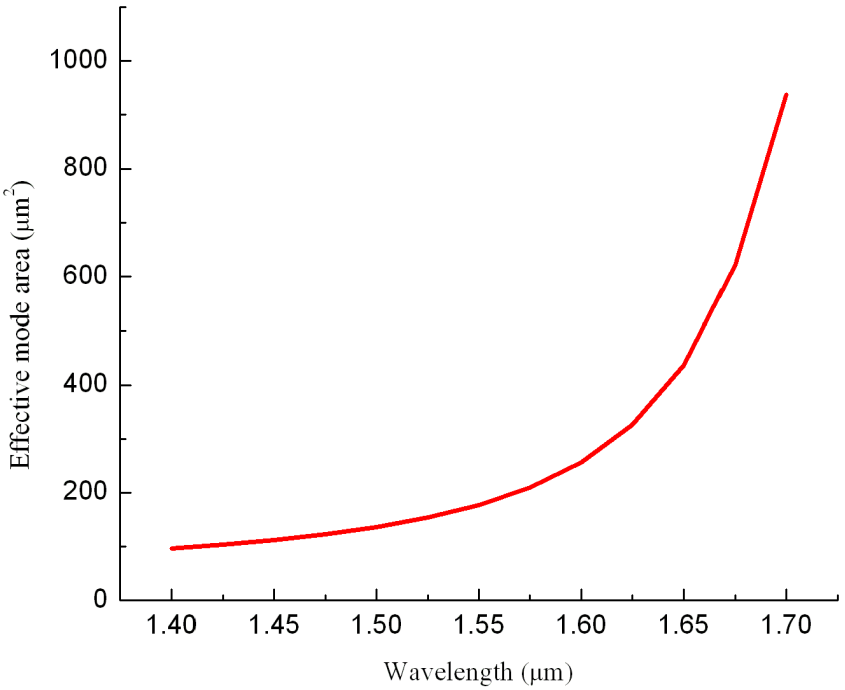

Figure 2.8 *Spectral variations of effective mode area of fundamental mode of near zero dispersion flattened fiber for the parameters given in Table 2.1.*

Another important factor which limits the bit rate is the nonlinear effects in single mode fiber. To overcome this difficulty one needs to design a fiber with large effective area while maintaining small dispersion and dispersion slope. We have calculated the effective area of the near zero dispersion flattened fiber using Eq. (2.17) and have plotted its spectral variation in Fig. 2.8. Minimum value of A_{eff} in the wavelength range 1.460-1.625 μm is 114 μm^2 and maximum value of mode area in the above mentioned wavelength range is 325.95 μm^2. The effective area of the fiber reported in [8] for ultra low dispersion fiber varies from 103.56 μm^2 to 232.26 μm^2 within the aforementioned wavelength range. Thus we show a significant improvement in the mode area of the proposed fiber.

(ii) Design of positive non-zero dispersion flattened fiber:

It is found that in a large effective area fiber (LEAF) positive dispersion of approximately +4 ps/km-nm at 1.55-μm wavelength is able to avoid four wave mixing (FWM) effect and enhance the performance of wavelength division multiplexed optical communication system. Therefore we have designed the fiber having dispersion around +4.5 ps/km/nm with large effective area, low dispersion slope and large bandwidth. The designed parameters of the positive non-zero dispersion flattened fiber are given in Table 3.

Table 2.3.

Proposed positive-non-zero dispersion flattened fiber structure parameters.

$n_1-n_2 = n_2-n_3 = n_3-n_4 = n_4-n_5 = n_5-n_6 = 8 \times 10^{-4}$
$a_2-a_1 = a_3-a_2 = a_4-a_3 = a_5-a_4 = 1$ μm
$a = 2.5$ μm, $b = 1.2$ μm, $c = 1.1$ μm, $n_9 = 1.4444$
$\Delta_1 = 0.22\%,\ \Delta_2 = 0.49\%,\ \Delta_3 = 0.27\%$

To achieve the dispersion near +4.5 ps/km/nm we have increased the value of parameter *a* of near-zero dispersion flattened fiber to 2.5 μm and all other parameters are kept same. Spectral variation of the dispersion and dispersion slope of the proposed fiber is shown in Fig. 2.9. Designed fiber has dispersion and dispersion slope within [4.5±0.5] ps/km/nm and [(–0.00003)-(0.0303)] ps/km/nm^2 respectively in the spectral

range of 1.460-1.650 μm. Table 4 shows characteristics of the designed fiber which are compared with the already existing fiber design reported in Ref. [5]. We see that the proposed design has nearly three times larger effective area at 1.55 μm. The absolute value of dispersion slope of the designed fiber is smaller over a larger bandwidth than that of fiber reported in Ref. [5]. Thus flattened dispersion with desired dispersion value and ultra-large effective area has been achieved with proposed design over a wide range of wavelength.

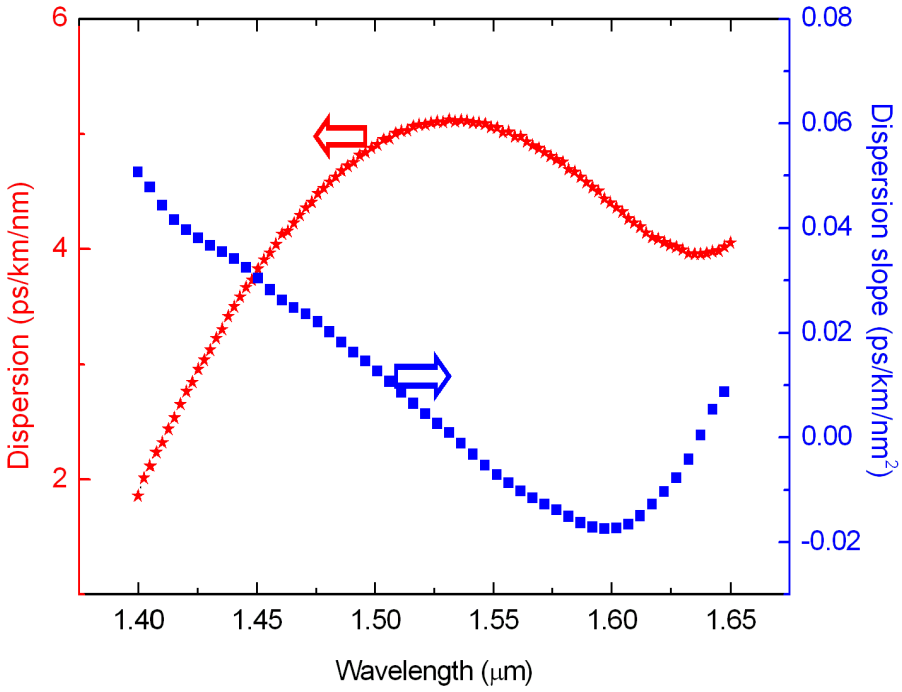

Figure 2.9 *Spectral variation of dispersion and dispersion slope of small +ve dispersion flattened fiber for the parameters given in Table 2.3.*

Table 2.4.

Comparison of characteristics of proposed positive-non-zero dispersion flattened fiber with the existing fiber design reported in Ref. [5].

Fiber	Bandwidth (μm)	Dispersion (ps/km/nm)	Dispersion slope at 1.55 μm wavelength (ps/km/nm^2)	A_{eff} at 1.55 μm wavelength (μm^2)
Ref. [5]	1.53-1.61	3.05±0.35	0.01	56.1
Proposed design	1.46-1.65	4.5 ±0.5	–0.007	155.71

(iii) Design of negative non-zero dispersion flattened fiber:

Recently a directly modulated laser (DML) has gained the attention for metropolitan networks. However, in DML carrier induced change in the mode effective index, leads to large chirp and small dispersion tolerance. This limits the transmission distance. Several techniques have been studied to improve the transmission distance. One of the techniques is to use negative dispersion fiber as transmission fiber. The negative dispersion can compensate the positive chirp of the DML. Here we propose a design of negative dispersion fiber having negative dispersion around 6 ps/km/nm. Parameters of the designed fiber used for calculation are given in Table 2.5.

Table 2.5.

Parameters of negative non-zero dispersion flattened fiber.

$n_1 - n_2 = n_2 - n_3 = n_3 - n_4 = n_4 - n_5 = 8 \times 10^{-4}$; $n_5 - n_6 = 1.3 \times 10^{-3}$

$a_2 - a_1 = a_3 - a_2 = a_4 - a_3 = a_5 - a_4 = 1$ μm

$a = 1.1$ μm, $b = 1.2$ μm, $c = 1.1$ μm, $\lambda = 1.55$ μm, $n_9 = 1.4444$

$\Delta_1 = 0.22\%$, $\Delta_2 = 0.49\%$, $\Delta_3 = 0.27\%$

To achieve negative dispersion we have decreased the value of parameter *a* of the near-zero dispersion flattened fiber from 1.68 μm to 1.1 μm. Difference between refractive index n_5 and n_6 of the near-zero dispersion flattened fiber has been increased from 8×10^{-4} to 1.3×10^{-3}. Dispersion and dispersion slope of the designed fiber are depicted in Fig. 2.10. We have compared characteristics of the proposed design with SMF-28 fiber and with the design reported in Ref. [7]. The comparison is shown in Table 2.6.

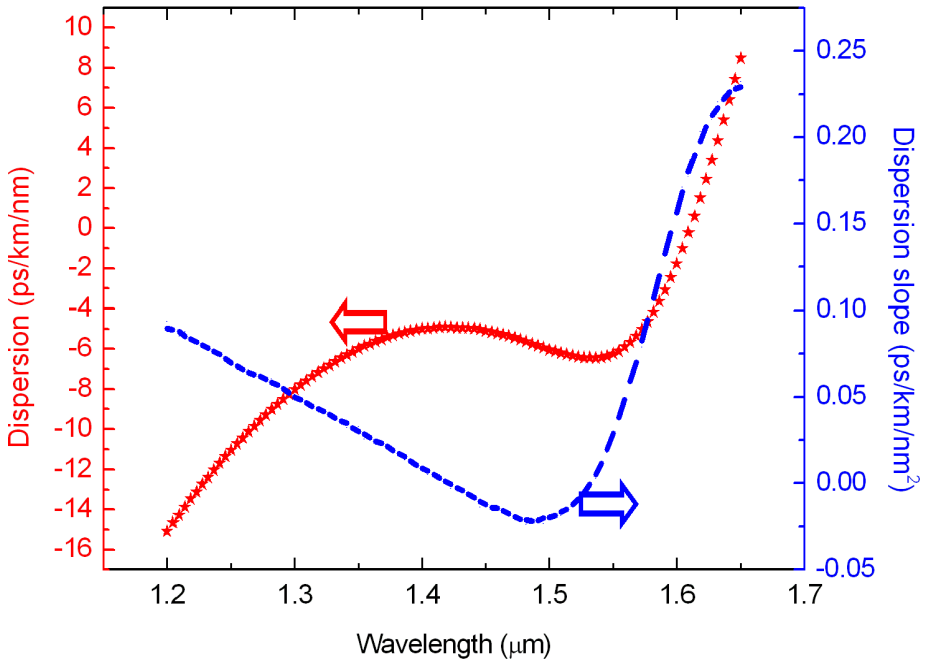

Figure 2.10 *Spectral variation of dispersion and dispersion slope of small –ve dispersion flattened fiber given in Table 2.5.*

We can observe from Table 6 that proposed design show smaller dispersion slope and ultra-large effective area while maintaining the required dispersion. A_{eff} of the SMF-28 is slightly greater than the double of the A_{eff} of the fiber structure reported in Ref. [7]. However, A_{eff} of the proposed design is nearly three times of the A_{eff} of the SMF-28.

Table 2.6.

Comparison of characteristics of proposed negative non-zero dispersion flattened fiber with SMF-28 and the design reported in Ref. [7].

Fiber	Dispersion at 1.33 μm wavelength ((ps/km/nm)	Dispersion at 1.55 μm wavelength (ps/km/nm)	Dispersion slope at 1.55 μm wavelength ($ps/km/nm^2$)	A_{eff} at 1.55 μm wavelength (μm^2)
Ref. [7]	–6.9	–6.7	0.043	36.1
SMF-28	–0.08	16.4	0.056	80
Proposed design	–6.6	–6.24	0.026	219

(iii) Feasibility of fabrication

In the proposed design the minimum width of the layer is typically 1 μm and the minimum refractive index required is 8×10^{-4}. Such values are achievable by modified chemical vapor deposition (MCVD) technology. For example, recently Messerly et al. have fabricated a design containing wave-guiding rings using MCVD technology having tolerance of 0.01μm on layer width and tolerance on refractive indices of the layer of the order of 1×10^{-4} [92]. There are also reports on fabrication of triangular-core dispersion shifted fiber, which requires a precise control in layer by layer deposition of the core material to achieve a smooth profile [93] and fabrication of multi-step core fiber by MCVD [92, 94]. The present design essentially consists of a triangular core with finite number of layers and should be easier to achieve by deposition of Ge-doped silica layers MCVD technology. Low-index trench of the structure can be achieved by depositing F-doped silica layers as demonstrated in Ref. [95].

2.4 Compatibility of the Proposed Fiber with Conventional Fiber

It is very important to examine the bending sensitivity and the compatibility of the proposed design with conventional SM fiber and fiber based components. A fiber with

large effective area usually has high bending loss. Double or triple core fibers show large bending losses. In our design we have introduced a low index trench between the two cores of the fiber to reduce bending loss. To study bending sensitivity and compatibility of the proposed fiber we have considered design of near-zero dispersion flattened fiber. We have calculated the bending loss of the fiber using Eq. (2.19). The macrobending loss of the fiber at 1.55 μm for bending radius 10 mm is 1.427×10^{-8} dB/km.

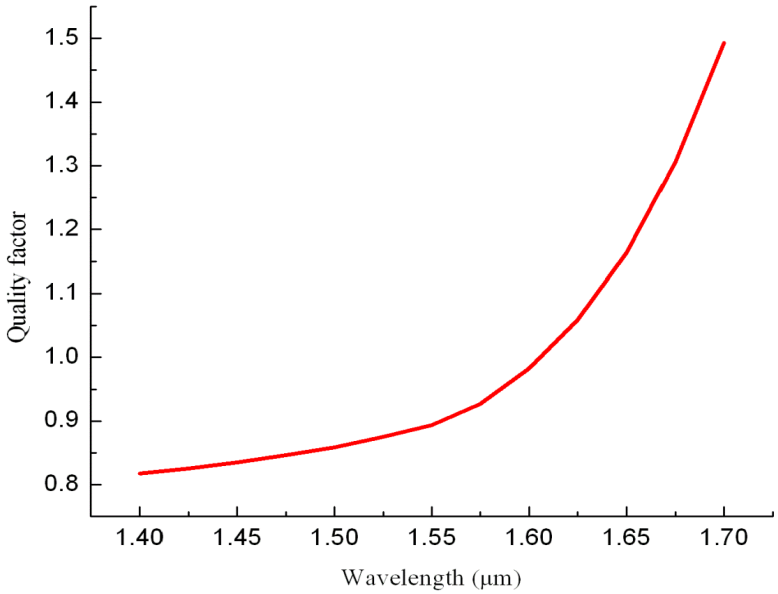

Figure 2.11 *Spectral variations of quality factor for the parameters given in Table 1*

We have used commercial fiber CAD software to calculate bending loss of the fiber. Effective MFD is an important parameter of the fiber while evaluating the performance of the fiber with regard to bending loss and splice loss. Long haul optical fiber communication link contains conventional single mode fiber (SMF) and fiber based components therefore the dispersion managed fiber is supposed to be spliced to the conventional SMF. To minimize splice loss MFD of the designed fiber should match with that of the conventional SMF. The effective MFD of the conventional single mode fiber at 1.55 μm is 10.4 ± 0.8 μm and that of the designed fiber is 14.0 μm, which matches quite well with that of the conventional single mode fiber. The splice loss of the fiber has been calculated by using Eq. (2.32) and has been found to be 0.059 dB at 1.55 μm by considering δ as 0.1 μm and θ as 0.2°. A parameter called quality factor has

been introduced to check the overall performance of the fiber and has been defined as the ratio of A_{eff} to the square of MFD. This is a dimensionless quantity and is used for assessing the overall performance of the fiber. Fiber having larger values of quality factor approaches towards the best design. Spectral variation of the quality factor of the designed fiber is shown in Fig. 2.11. The figure shows that the quality factor of the designed fiber varies from 0.8401 to 1.025 in the wavelength range 1.460-1.625 μm. The quality factor of the fiber reported in [20] varies from 0.8187-0.9957 in the same spectral range.

2.5 Sensitivity Analysis of the Structural Disorders on the Performance of the Fiber

In the previous sections we numerically demonstrated that the proposed fiber has exceptional chromatic dispersion flatness with low dispersion slope and large effective area in the S+C+L communication band. To evaluate the sensitivity of design parameters we have varied one of the parameters at a time while keeping all other parameters constant and calculated dispersion of near zero dispersion flattened fiber. Firstly, we varied n_6 by an amount δn_6 and the results are plotted in Fig. 2.12. One can observe that the maximum variation in dispersion value is at 1.6-μm wavelength. $\delta n_6 = -2\times10^{-4}$ results in 2.8 ps/km/nm deviation from the optimized dispersion at 1.6-μm wavelength. $\delta n_6 = +2\times10^{-4}$ results in 2.5 ps/km/nm deviation from the optimized value of dispersion. The analogous study has also been carried for variations in the values of parameter a and the results are plotted in Fig. 2.13. We see that positive deviation from the optimized value of a = 1.68 μm results in an increase in the value of dispersion where as negative deviation results in a decrease value of dispersion while maintaining the flatness. Variation of ±11.9% in the optimized value of parameter a results in approximately 1 ps/km/nm variation in the value of dispersion at 1.55 μm wavelength. The sensitivity of the design has also been examined against variations in value of n_7 and the results are plotted in Fig. 2.14. We observe that increase in value of n_7 results in an increase in value of dispersion however decrease in value of n_7 decreases the value of dispersion. Variations of $\delta n_7 = -2\times10^{-4}$ in values of n_7 result in nearly −1.48 ps/km/nm deviation in values of dispersion at 1.625 μm wavelength which is maximum deviation in considered spectral range.

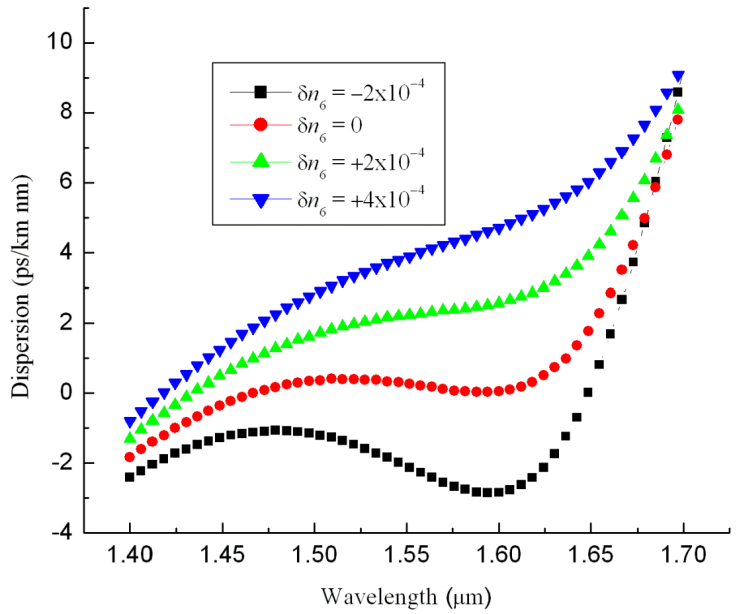

Figure 2.12 *Spectral variations of total dispersion of near zero dispersion flattened fiber with variations in n_6 for the parameters given in Table 1.*

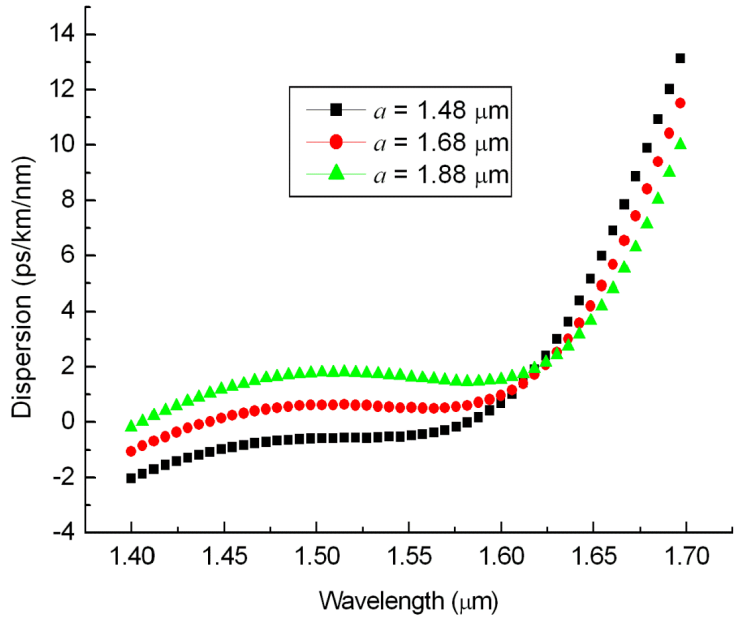

Figure 2.13 *Spectral variations of total dispersion of near zero dispersion flattened fiber with variations in a for the parameters given in Table 1.*

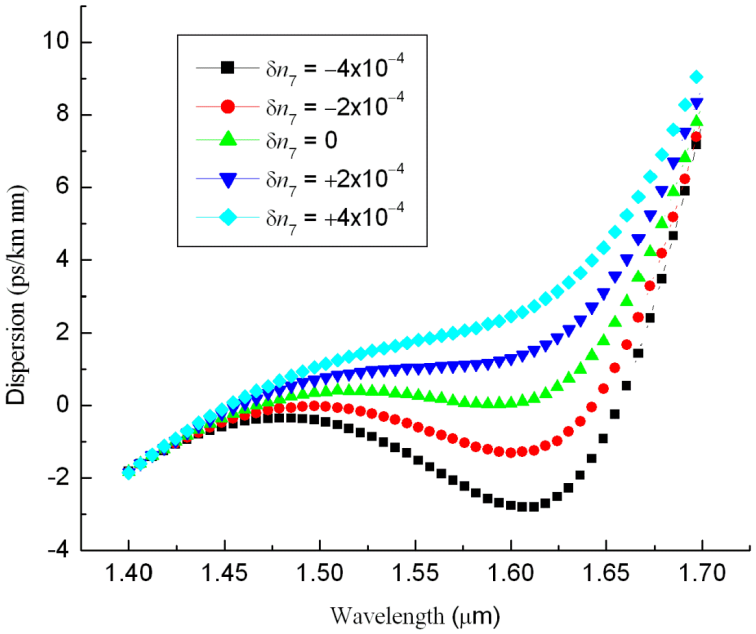

Figure 2.14 *Spectral variations of total dispersion of near zero dispersion flattened fiber with variations in n_7 for the parameters given in Table* 1.

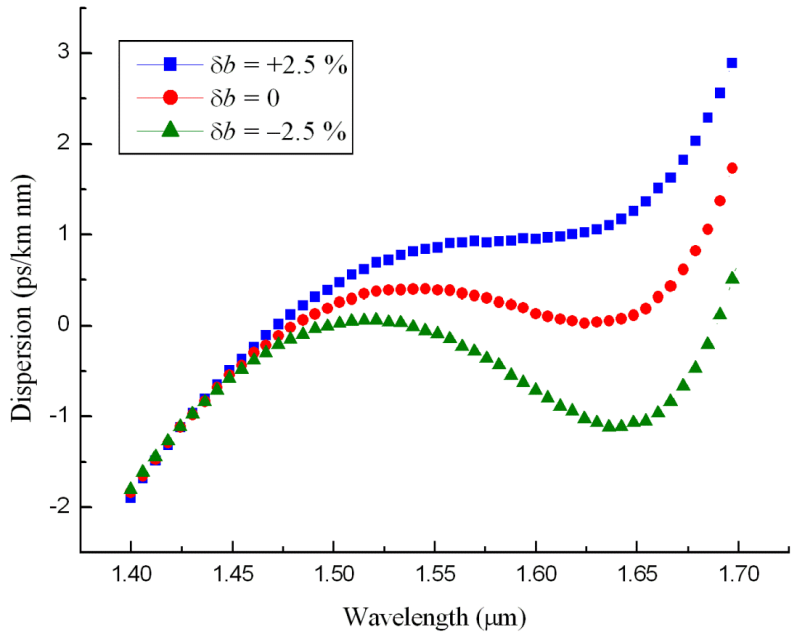

Figure 2.15 *Spectral variations of total dispersion of near zero dispersion flattened fiber with variations in b for the parameters given in Table* 1.

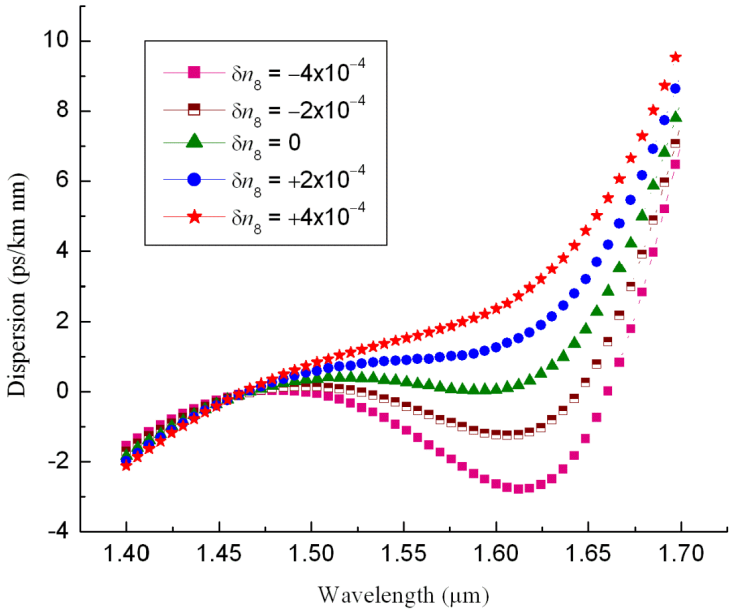

Figure 2.16 *Spectral variations of total dispersion of near zero dispersion flattened fiber with variations in n_8 for the parameters given in Table 1.*

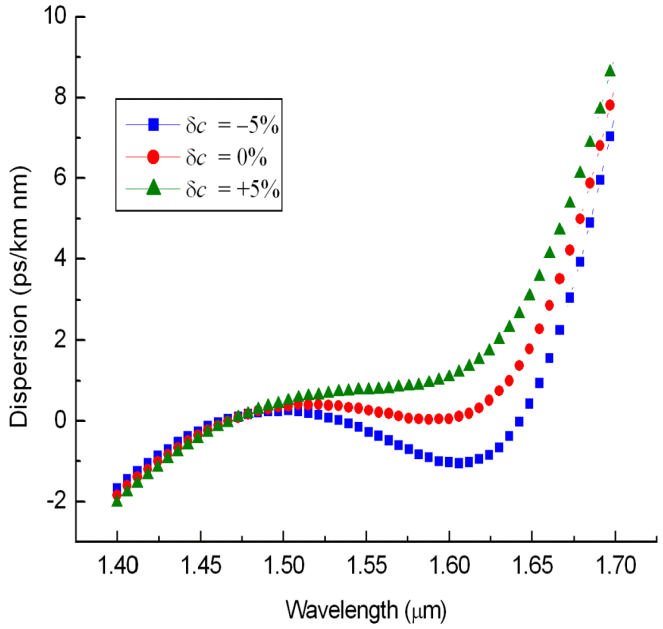

Figure 2.17 *Spectral variations of total dispersion of near zero dispersion flattened fiber with variations in c for the parameters given in Table 1.*

Variation of $\delta n_7 = +2\times10^{-4}$ results in maximum +1.40 ps/km/nm deviation from the optimized value at 1.633 μm wavelength. Sensitivity of the design has also been examined against ± 2.5% variations (δb) in b and the results are shown in Fig. 2.15. One can see clearly from Fig. 12 that δb = ±2.5% results in maximum variation of ±1.2 ps/km/nm in the values of optimized dispersion at 1.65 μm wavelength. Secondary core, which is an important parameter of the design plays a significant role in the design of the fiber. Spectral variations of the dispersion against variations (δn_8) in the refractive index of secondary core n_8 are presented in Fig. 2.16. Variation of $\delta n_8 = \pm\ 2\times10^{-4}$ causes maximum ± 1.5 ps/km/nm deviations in the values of optimized dispersion at 1.633 μm wavelength. We have also examined the effect of width of secondary core (c) and results are shown in Fig. 2.17. We can see that δc = ± 5.4% results in maximum ± 1.3 ps/km/nm variations in the value of dispersion at 1.633 μm wavelength. As a general discussion of this section, we have estimated the effect of structural imperfections in important parameters of the designed fiber. We showed that the dispersion of the fiber does not vary significantly with possible variations for the design parameters.

2.6 Conclusions

In this paper we have proposed a proposal for a segmented core fiber design having near-zero, small positive non-zero, and small negative non-zero flattened dispersion with small dispersion slope and ultra-large effective area. The segmented core of the fiber helps in maintaining desired dispersion and dispersion slope. We have introduced a low index trench to reduce bending loss of the fiber. A secondary core of the fiber helps in achieving ultra large effective area. For positive non-zero dispersion flattened fiber optimized dispersion is near +4.5 ps/km/nm in the wavelength range 1.46-1.65 μm. For non-zero negative dispersion flattened fiber, dispersion has been achieved near –6ps/km/nm in the spectral range 1.33-1.56 μm. In case of near zero dispersion flattened fiber effective area varies from 114-325.95 μm^2 within the wavelength range 1.460-1.625 μm which is the largest value reported for dispersion flattened fiber to the best of our knowledge.Dispersion and dispersion slope of the designed fiber are [0.0039-0.520] ps/km/nm and [0.0004-0.0365] ps/km/nm^2 respectively within the aforementioned wavelength range. The designed fiber also has appropriate quality factor, also which varies from 0.8401-1.025 over the entire S+C+L band. These

characteristics of the fiber make it an attractive candidate for DWDM optical communication system.

CHAPTER–3

Fibers for Delivery of Ultrashort Laser Pulses*

3.1 Introduction

Ultra-short pulse (USP) lasers find applications in micro-machining [96], laser ablation of solids [96,97], femtochemistry [98], multiphoton fluorescence microscopy [99], terahertz generation and detection [100], and frequency combs [101]. Advances in high-power fiber amplifiers and lasers, and specialty optical fibers have opened new doors for generation of ultra-short pulses (USPs) [102, 103]. Pulse energy and power from fiber laser system now compete in performance with conventional bulk-optic based USP systems. The inherently flexible nature of such lasers makes them attractive to fulfill the present laser

* A part of the results presented in this chapter have been reported in a research publications:

1. Babita, Vipul Rastogi and Ajeet Kumar, "Design of large-mode-area three layered fiber structure for femtosecond laser pulse delivery" Optics Communications , Vol. 293, pp. 108-112, 2013.

2. Babita and Vipul Rastogi, "Design of segmented cladding fiber for ultra-short pulse delivery at 1064 nm and 1550 nm wavelengths, Optical and Quantum Electronics , Vol. 46, pp. 397-408, 2014.

source requirements, and to scale in performance, form factor, and cost in order to keep pace with industrial growth. Apart from generation of USPs through fiber-based lasers, transport of high energy USPs through optical fibers has also found importance in various applications. Fiber delivery of USPs gives much flexibility for laser integration and allows easy access to otherwise inaccessible regions. In several applications it is advantageous to deliver ultra-short laser pulses (USPs) through an optical fiber over a distance of few meters to some specific location. One such example is biological basic research and clinical applications, which require miniaturized microscopes and multi-photon endoscopes to image living cells and intact tissues [96, 97]. Multi-photon imaging systems that use free space optics are cumbersome in design, non-compact and difficult to maintain. This limits the use of free space optics multi-photon systems in the medical field. An optical fiber which can deliver high peak power ultra-short pulses is attractive for aforementioned applications to develop flexible and miniaturized instruments. However, nonlinear effects, optical damage threshold and dispersion in a conventional optical fiber make distortion-free transport of high-peak-power ultra-short pulses difficult. Femtosecond pulses, which are usually used in these applications, have peak power in kW regime even with moderate energy. When these pulses pass through the small core of a conventional fiber, optical power density reaches up to GW/cm^2. At these high power densities optical damage can occur and nonlinearity can distort the pulse by self phase modulation (SPM). One way to avoid SPM is to reduce optical power density by using large-core fibers. In conventional large-core fibers intermodal dispersion significantly distorts ultra-short laser pulses. Moreover, the beam quality in a large core fiber is not good due to the presence of several modes. To preserve the pulse during propagation through the fiber, one needs to compensate for or minimize dispersive and nonlinear effects. Dispersion can be compensated by suitable frequency chirp on input pulses. One approach to reduce nonlinearity is to increase mode area by increasing the core size and correspondingly decreasing the numerical aperture (NA) while maintaining single-mode operation. While decrease in NA yields to extremely high bending loss because of weak mode confinement, increase in core radius leads to multimode cross-coupling and conflicts with single-mode operation, which is necessary for high resolution microscopy. To circumvent this

problem specialty optical fibers are used for the transport of such high-peak-power ultra-short pulses. Some of these fibers are photonic crystal fibers (PCFs) [98,99], rod-type fibers [100], and few-mode fibers [101-103]. PCF can show efficient single-mode operation and can maintain good beam quality in the output pulses. However, in PCFs because of large core, intermodal spacing is not large enough and mode coupling remains an issue. Rod type fiber has also been introduced for delivery of high-peak-power USPs [100]. These fibers maintain single mode operation with large mode area. However, inflexibility of the fiber remains an issue in compact packaging and in miniaturization. Recently, Ramachandran et al. have demonstrated delivery of high-peak-power ultra-short pulses using higher order mode fibers [101]. These fibers show very large-mode-area upto 3200 μm^2 by selective excitation of higher-order -mode. Enough intermodal spacing reduces the possibility of modal cross coupling [102]. But this technique uses long period grating for mode conversion which increases the complexity of the system.

In this chapter we present a design of three layered fiber structure for delivery of high energy fs-pulses through the fundamental mode of the fiber. The design is not susceptible to mode coupling and has sufficiently low bending loss. The modal purity at the output is maintained by stripping-off higher order modes. In the proposed structure LP_{01} and LP_{11} modes are guided whereas all the other modes are stripped-off owing to their high leakage loss. A sufficiently large index difference between the LP_{01} and LP_{11} modes ensured in the design prevents coupling between them. Apart from it we also present a design of segmented cladding fiber (SCF) which is capable to deliver ultra-short laser pulses at more than one wavelength. SCF is able to transport 100-fs, 53-kW peak power laser pulses over 4-m length of the fiber with mode area of about 1825 μm^2 at 1550-nm wavelength and 250-fs, 15-kW peak power laser pulses at 1064-nm wavelength with a mode area of 1793 μm^2.

3.2 Nonlinearities in fiber

Laser pulses when propagate through the fiber are affected by material dispersion and nonlinearities induced by their confinement to small core of the waveguide. Dispersion has already been discussed in previous chapter in section

[2.2.2]. Origin of non-linearities is related to aharmonic motion of electrons under the influence of an applied field. The total polarization *P* does not vary linearly with electric field *E* but satisfies the following relation[106-109]:

$$P = \varepsilon_0 \left(\chi^{(1)} E + \chi^{(2)} E^2 + \chi^{(3)} E^3 + ... \right) \tag{3.1}$$

Where ε_0 is vaccum permittivity and $\chi^{(j)}$ is *j*th order susceptibility. The main contribution to *P* is by term $\chi^{(1)}$. Higher order terms leads to nonlinear effects. Second-order susceptibility $\chi^{(2)}$ is responsible for second-harmonic generation and sum-frequency generation. $\chi^{(2)}$ is zero for media having inversion symmetry at molecular level. Silica (SiO_2) has molecular symmetry therefore $\chi^{(2)}$ is zero for SiO_2. Therefore fiber made of SiO_2 do not exhibit second-order nonlinear effects. The nonlinear effects in optical fiber made of silica originate from third order susceptibility $\chi^{(3)}$ and are elastic in nature. The elastic nature of non-linear effects means, there is no energy exchange between electromagnetic field and dielectric medium. Main nonlinear effects in fiber are originated from intensity dependence of refractive index. It can be expressed by the following equation [107]:

$$\hat{n}\left(\omega, |E|^2 \right) = \tilde{n}(\omega) + \tilde{n}_2 |E|^2 \tag{3.2}$$

Where $\tilde{n}(\omega)$ is linear part and $\tilde{n}_2$ is proportional to $\chi^{(3)}$ and is called nonlinear-index coefficient. For silica fiber $\tilde{n}_2$ has value lying between 2.2×10^{-20} and 3.4×10^{-20} m^2/W [88]. The intensity dependence of refractive index leads to self phase modulation (SPM) and cross-phase modulation (XPM). Self-induced phase shift experienced by optical field while its propagation through fiber is known SPM. When field *E* propagate through fiber having length *L* then induced phase shift is given as:

$$\phi = \hat{n} k_0 L = \left(\tilde{n} + \tilde{n}_2 |E|^2 \right) k_0 L \tag{3.3}$$

The second term in above equation is due to SPM. Where k_0 is free space wave number.

Another class of non-linear effects in which optical field transfers part of its energy to the nonlinear medium are due to stimulated inelastic scattering. These

nonlinear effects area known as stimulated Raman scattering (SRS) and stimulated Brillouin scattering (SBS). In SRS and SBS process, a photon of incident field is annihilated to create a photon of lower energy (belongs to Stokes wave) or higher energy (belong to anti-Stokes waves) depending on the energy and a phonon to conserve energy and momentum. Although both processes are same the two main differences between two processes are given as:

1. SBS in a single mode fiber occurs only in backward direction whereas SRS occurs in both directions.

2. Another main difference between SRS and SBS is that optical phonons participate in SRS while acoustic phonons participate in SBS [88].

Generation of Stokes wave can be expressed by the following relation:

$$\frac{dI_s}{dz} = g_R I_p I_s \tag{3.4}$$

Where g_R is Raman-gain coefficient, I_p is incident intensity and I_s is Stokes intensity. When pump intensity exceeds a certain value only then SRS and SBS phenomena occur and that certain value is called threshold value which is given as [110]:

$$I_p^{th} = 16\left(\frac{\alpha}{g_R}\right) \tag{3.5}$$

Where α is an attenuation coefficient and measure total fiber losses from all sources. g_R is Raman gain coefficient. Threshold for SBS is given as [110]:

$$I_p^{th} = 21\left(\frac{\alpha}{g_B}\right) \tag{3.6}$$

Where g_B is Brillouin gain coefficient. Because of dispersion and nonlinear effects studied above even a moderate peak power pulse gets distorted during propagation through the fiber because of nonlinearities and dispersion. Although $\tilde{n}_2$ is small in case of silica core fiber even then nonlinear effects can be observed at small power levels. Efficiency of non linear effects mainly depends on the spot size of the fiber, incident intensity and fiber length and to achieve high efficiency in case of bulk the beam has to be focused. Due to diffraction of beam this focusing requires a small length of interaction called effective length of interaction (L_{eff}). If w_0 is spot size of the fiber having core radius a then for a Guassian beam, L_{eff} is given as [111]:

$$L_{eff} = \frac{\pi w_0^2}{\lambda} \tag{3.7}$$

If P_0 is the optical power coupled to fiber then:

$$\left(I_0 L_{eff}\right) = \frac{P_0}{\pi w_0^2 \alpha}\left[1 - \exp(-\alpha L)\right] \tag{3.8}$$

$I_0 L_{\text{eff}}$ gives the efficiency of nonlinear process.

Therefore nonlinearities in a fiber depend on incident power, spot size and effective length. If we propagate a pulse of high energy through the fiber then it will be distorted because of nonlinearities. To have distortion-free propagation of USPs of high energy, a fiber requires a balance between pulse broadening due to dispersion and pulse distortion due to SPM. These effects are usually characterized by the two parameters called dispersion length L_D and nonlinear length L_{NL} and are given by the following equations [88]:

$$L_D = -\frac{2\pi c}{\lambda_0^2}\frac{\tau^2}{D} \text{ and } L_{NL} = \frac{A_{eff}\lambda}{2\pi nP} \tag{3.9}$$

where c is the speed of light in vacuum, τ is the pulse duration, λ_0 is the center wavelength, A_{eff} is the effective mode area, n is the nonlinear refractive index of the fiber material, and P is the peak power. D is the fiber dispersion coefficient and can be calculated using Eq.(2.16). In order to avoid nonlinear effects during propagation of high energy USPs, one requires very high values of A_{eff}. Scaling up the core dimensions of the fiber for high energy USP propagation requires lowering the numerical aperture (NA) of the fiber. This makes the fiber susceptible to mode instability due to mode-coupling and high bend loss. The mode coupling effects limit the mode area in a low NA fiber to 800 μm^2 [21]. It is preferred to have spacing between the adjacent modes, $\delta_{\text{neff}} = n_{\text{eff}}(\text{LP}_{01}) - n_{\text{eff}}(\text{LP}_{11})$, greater than 1.5×10^{-4} to avoid mode-coupling [112]. In PCF this spacing is 1×10^{-4} while in higher order mode (HOM) fibers this can go up to 5×10^{-4} [22]. In the aforementioned applications typical length of the fiber used is couple of meters and sensitivity to bends should not be large for bending radii larger than 20 cm [113]. Therefore, it is critical to design a fiber having single-

mode operation with large A_{eff}, low bend loss and sufficient mode spacing to avoid intermodal coupling.

3.3 Three layered fiber structure

3.3.1 *Fiber design*

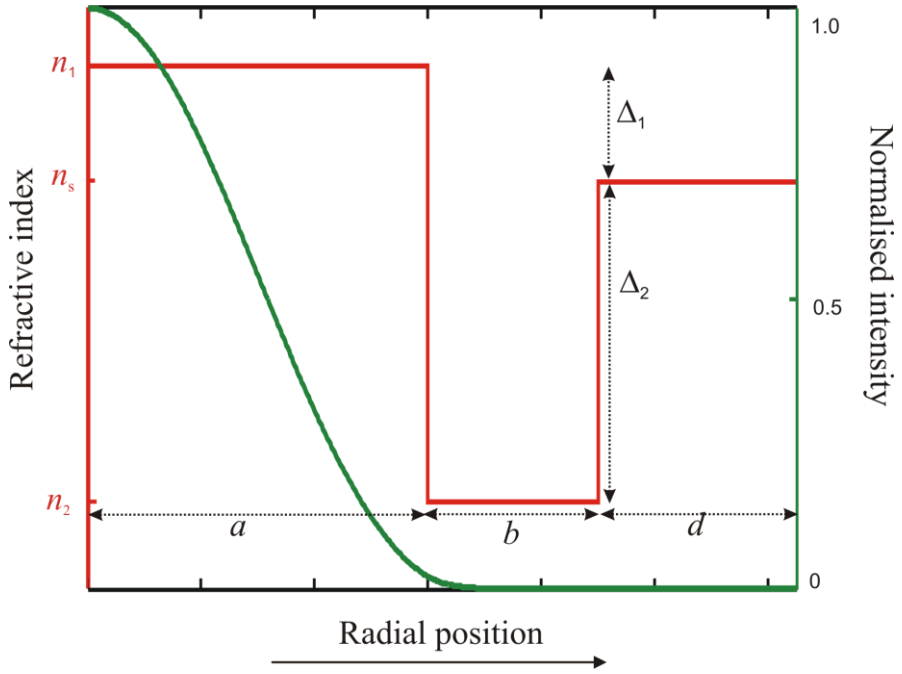

Figure 3.1 Refractive Index Profile of the fiber along with normalized intensity

To address the issues stated above we have designed a three layered fiber structure with core refractive index n_1, depressed cladding index n_2, and outer cladding index n_s. Where a is core radius of the fiber, b is width of the depressed cladding and d is the width of the outermost layer. The refractive index profile along with the mode intensity profile of the fiber is shown in Fig.3.1. The outer clad of the fiber can be realized by pure silica, the core can be realized by Ge up doping and the depressed cladding can be made by F down doping. Relative index difference of the core and the depressed cladding regions relative to pure silica (n_s), are defined as $\Delta_1 = (n_1^2 - n_s^2)/(2n_1^2)$ and $\Delta_2 = (n_s^2 - n_2^2)/(2n_s^2)$. The various parameters of the designed fiber are listed in Table 1.

Table 3.1.

Proposed fiber design parameters.

a = 30 μm, b = 15 μm, d = 17.5 μm, λ = 1550 nm, n_s = 1.4444
Δ_1 = 0.03%, Δ_2 = 0.08%

The fiber supports several modes owing to large value of the core radius. The values of Δ_1 and Δ_2 are so chosen as to make all the modes leaky except LP_{01} and LP_{11} modes. Such values of index difference can be realized by standard fabrication technique such as MCVD [115]. We have used transfer matrix method (TMM) described in previous chapter to analyze the modal properties of the fiber [86]. For the above mentioned designed parameters the fiber introduces 8.2 dB/m leakage loss to LP_{02} which is large enough to strip off the mode within 2.5 m length of the fiber by introducing 20 dB loss. The depressed cladding index and width are so chosen as to have sufficiently large A_{eff} while maintaining the mode stability. A_{eff} of the fiber has been calculated using Eq. (2.17). Variation in A_{eff} and mode stability with Δ_1 is shown in Fig.3.2. An increase in Δ_1 confines more power inside the core and also increases inter modal spacing that causes decrease in the A_{eff} and the increase in δ_{neff} of the designed fiber. Here δ_{neff} is mode spacing between LP_{01} and LP_{11} mode of the designed fiber. The value of Δ_1 is so chosen as to have value of A_{eff} as large as 1900 μm^2. We have also studied the effect of variation in Δ_2 on A_{eff} and δ_{neff} as shown in Fig. 3.3. When we increase Δ_2, the depressed cladding index decreases and confinement of the power in the core increases. This results in a decrease in A_{eff} whereas an increase in δ_{neff}. We see from Fig. 3.2 and 3.3 that by decreasing the values of Δ_1 and Δ_2 we could have achieved even larger A_{eff} than 1900 μm^2 with sufficient mode spacing. However we have chosen values of Δ_1 and Δ_2 in such a way that except LP_{01} and LP_{11} all the modes are leaky and index contrast can be achieved with standard fabrication technique. To achieve maximum A_{eff} with sufficiently large δ_{neff} we have also studied the effect of variations in b on A_{eff} and δ_{neff} as shown in Fig.3.4.

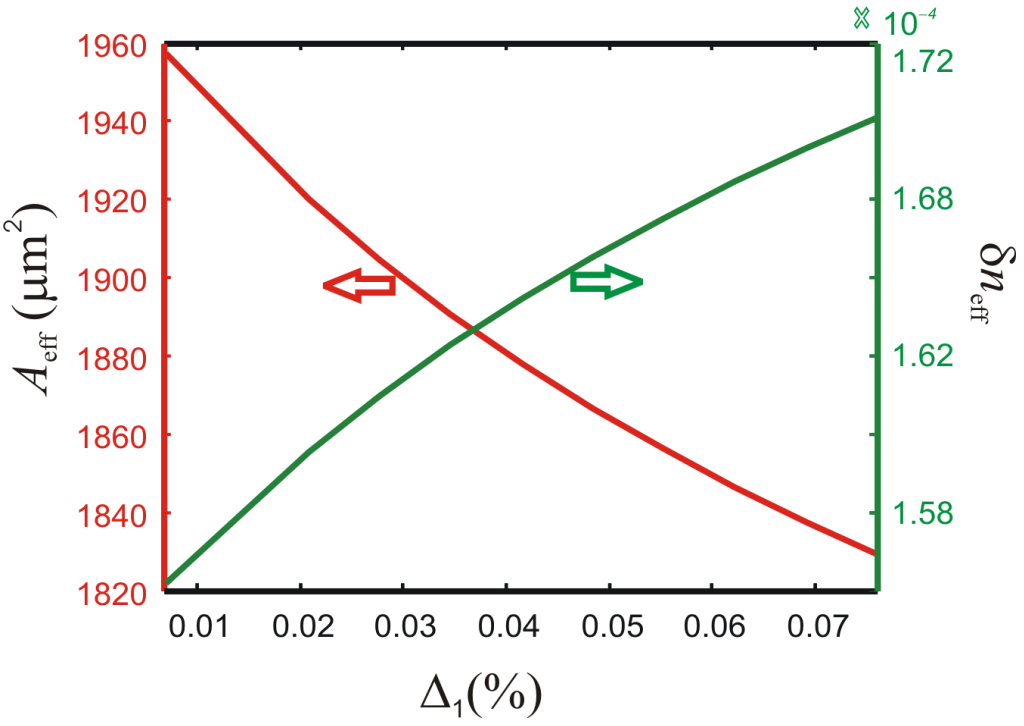

Figure 3.2 *Variation in A_{eff} and mode stability with Δ_1.*

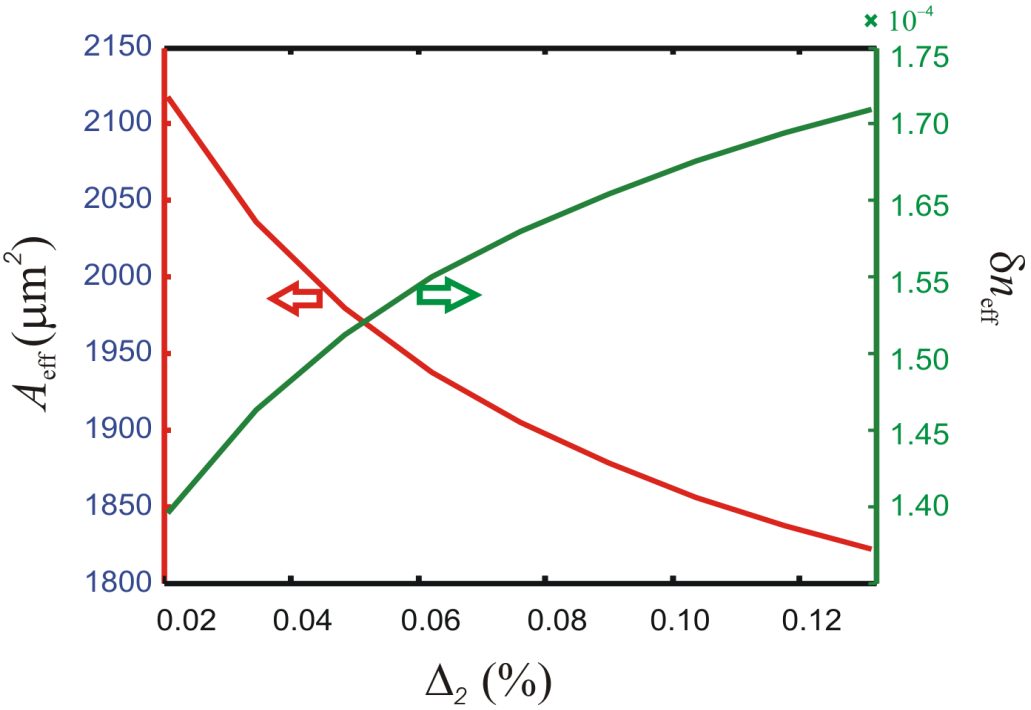

Figure 3.3 *Variation in A_{eff} and mode stability with Δ_2.*

One can see that variations in *b* do not cause significant change in A_{eff} and δ_{neff} and the fiber shows good tolerance towards variations in *b*. The effective area of

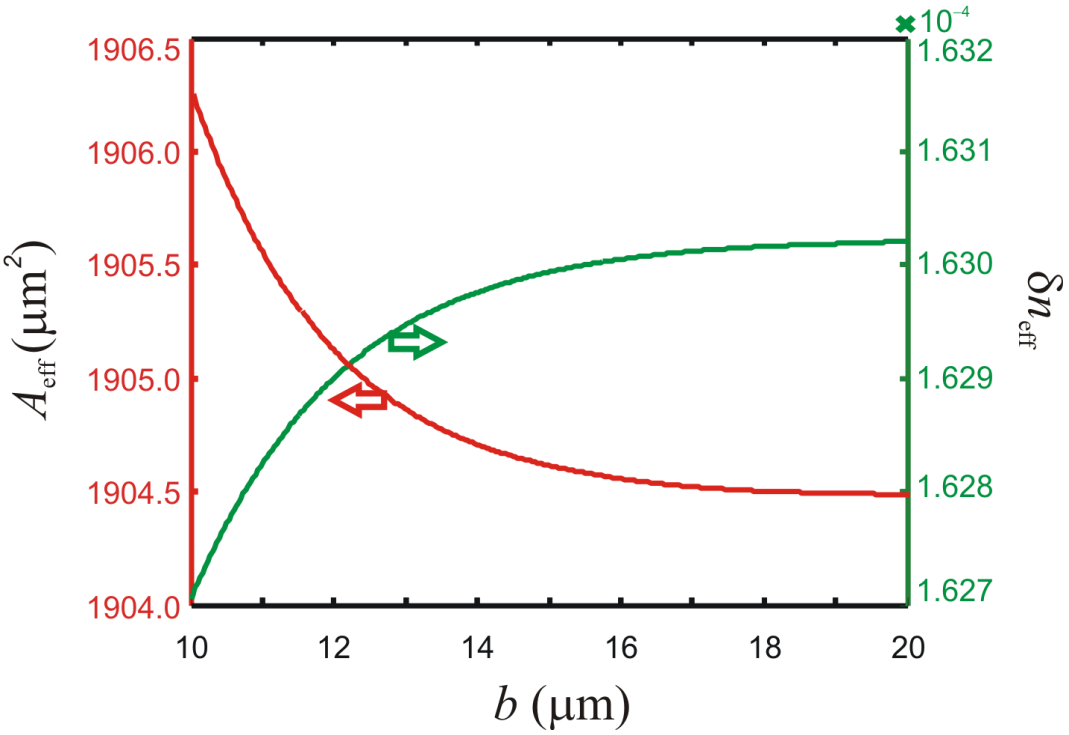

Figure 3.4 *Variation in A_{eff} and mode stability with b.*

the fundamental mode of the fiber, thus, designed and represented by fiber parameters given in Table 1 is 1900 μm^2 and δ_{neff} is 1.63×10^{-4}, which is higher than those shown by PCF [112] and ensures mode stability. Dispersion is also an important property of the fiber design as higher order dispersive effects can distort ultra-short optical pulses in both the linear and nonlinear regime. Nonlinear effects in fiber show different behavior depending on the sign of the dispersion coefficient. The dispersion parameter (*D*) of the fundamental mode of the fiber has been calculated by Eq. (2.16). Variation of *D* with wavelength is shown in Fig. 3.5. In view of ultra-short duration of the pulses, we have also calculated the third order dispersion (β_3) and is defined as $\beta_3 = \frac{\partial D}{\partial \lambda}$. The value of *D* at 1550-nm centre wavelength is +21.7 ps/(nm.km) which helps in balancing the nonlinear effects. β_3 is of the order of 10^{-4} and has insignificant effect for propagation over a few meters length of the fiber considered here. The macrobending loss of the fiber has been calculated by using the following formula given in Eq. (2.19) [90, 115]. The fiber shows bend loss of 0.008 dB/m at 5-cm

bend radius. The fiber has negligible loss for bending radii occurring in applications like multi-photon microscopy.

3.3.2. *Femtosecond pulse propagation*

Pulse propagation through the fiber can be characterized by parameter L_D / L_{NL}, where L_D and L_{NL} are defined by Eq. (3.9). When L_D / L_{NL} < 1, pulse evolution along the fiber is dominated by dispersion and pulse will be broadened in absence of any chirp otherwise it stretches or compresses in time, depending on the sign of initial chirp. However, if L_D / L_{NL} > 1 then nonlinearity dominates during the evolution of the pulse and the pulse suffers spectral narrowing or broadening and does not retain the original shape. In order to avoid nonlinearities, one needs to limit peak power to make L_{NL} larger than L_D. It makes sure that linear stretching happens in shorter time so that the nonlinear interactions do not build up. However, if L_D / L_{NL} ~ 1 dispersion D is balanced by the nonlinear effect of SPM, and fundamental soliton propagation can occur. If a hyperbolic secant pulse is launched inside an ideal lossless fiber, then the pulse having width τ and peak power P_0 propagates undistorted without change in shape for long distances. Quantitatively the peak power required for fundamental soliton propagation is given by [88]

$$P_0 = \frac{\lambda_0^3 D A_{eff}}{4\pi^2 c n \tau^2} \tag{3.10}$$

In the proposed fiber design, the dispersion at 1550-nm center wavelength is 21.7 ps/(nm.km), the peak power for soliton propagation of 100-fs pulse is 55.5 kW, where we have used $\tilde{n}_2 = 2.4 \times 10^{-20}$ m^2/W [88].

A typical soliton pulse is defined as a sech pulse given by the following equation [88].

$$A(z=0,t) = P_0^{1/2} \times \mathrm{sech}(t/\tau)^{1+iC} \tag{3.11}$$

Where, P_0 is the peak power, C is chirp parameter. To study pulse dynamics through the fiber we have launched a secant-hyperbolic un-chirped pulse into the

fiber and studied its propagation dynamics by solving the nonlinear Schrödinger equation given below[88]:

$$\frac{\partial A}{\partial z}+\frac{\alpha}{2}A+\frac{i\beta_2}{2}\frac{\partial^2 A}{\partial T^2}-\frac{\beta_3}{6}\frac{\partial^3 A}{\partial T^3}=i\Gamma(|A|^2 A+\frac{i}{\omega_0}\frac{\partial(|A|^2 A)}{\partial T}-T_R A\frac{\partial|A|^2}{\partial T} \quad (3.12)$$

A frame of reference moving with group velocity v_g is used by making transformation:

$$T = t - z/v_g = t - \beta_1 z \quad (3.13)$$

Where α is the fiber loss, Γ represents fiber nonlinearity coefficient and ω_0 is the central frequency of the pulse. T_R is Raman time constant and $A(t,z)$ represents amplitude of the pulse envelope in time t at the spatial position z. β_2 represent group velocity dispersion and can be calculated using following relation:

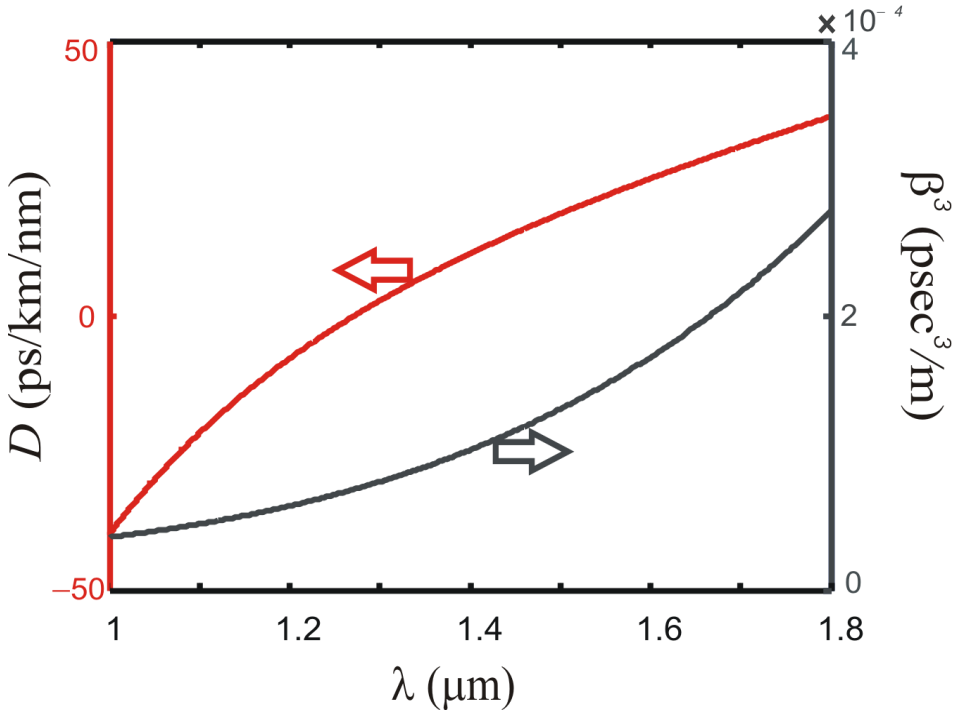

Figure 3.5 *Variation in dispersion and β_3 with wavelength.*

$$\beta_2 = -D\frac{\lambda^2}{2\pi c} \quad (3.14)$$

Nonlinear parameter Γ is defined as:

$$\Gamma(w_0) = \frac{\tilde{n}_2(\omega_0)\omega_0}{cA_{eff}} \quad (3.15)$$

Split-step Fourier method has been used to solve Eq. (3.12). In order to impliment split-step fourier method we write Eq. (3.12) as:

$$\frac{\partial A}{\partial z} = (\hat{\mathrm{D}} + \hat{\mathrm{N}})\,\mathrm{A} \tag{3.16}$$

Where $\hat{D}$ is a differential operator which takes into account dispersion and losses within linear medium and $\hat{N}$ is nonlinear operator which includes the effect of fiber nonlinearities on pulse propagation. $\hat{D}$ and $\hat{N}$ can be represented as [88]:

$$\hat{D} = -\frac{i\beta_2}{2}\frac{\partial^2}{\partial T^2} + \frac{\beta_3}{6}\frac{\partial^3}{\partial T^3} - \frac{\alpha}{2} \tag{3.17}$$

$$\hat{N} = i\Gamma\left(|A|^2 + \frac{i}{\omega_0}\frac{1}{A}\frac{\partial}{\partial T}(|A|^2 A) - T_R\frac{\partial |A|^2}{\partial T}\right) \tag{3.18}$$

In Eq. (3.16) dispersion and non-linearity act together along the length of the fiber. The solution of the equation is obtained by assuming that in propagating the optical field over a small distance *h* the dispersive and non-linear effects are assumed to act independently. Propagation from *z* to *z*+h is carried out in two steps, in first step we consider only non-linearity and effect of dispersion is neglected while in second step we consider only dispersion and non-linearity is neglected.

Mathematically, it can be expressed as:

$$A(\mathrm{z}+\mathrm{h},\mathrm{T}) \approx \exp(h\hat{D})\exp(h\hat{N})A(z,T) \tag{3.19}$$

$\exp(h\hat{D})$ can be expressed in fourier domain using the prescription:

$$\exp(h\hat{D})B(z,T) = F_T^{-1}\exp[h\hat{D}(-i\omega)]F_T B(z,T) \tag{3.20}$$

Where F_T denotes the Fourier-transform operation and $\hat{D}(-i\omega)$ is obtained using Eq. (3.17) by replacing operator $\partial/\partial T$ by $-\mathrm{i}\omega$, where ω is the frequency in Fourier domain. The use of fast Fourier-transform (FFT) algorithm makes the evaluation process faster and hence makes split-step Fourier method faster.

In the simulation of pulse propagation through the fiber, we have considered second order group velocity dispersion (GVD), third order dispersion, SPM and transmission loss of 0.2 dB/km. Since the pulses are of the order of 100-fs duration, we have also taken into account self-steepening and Raman scattering.

We have estimated Raman scattering by parameter τ_R which has value T_R/τ, T_R being Raman time constant. We have considered value of T_R as 3 fs at 1550-nm wavelength [88]. Self-steepening has been taken into account by parameter $s = 1/(\omega_0\tau)$, where ω_0 is central frequency of the pulse. Evolution of the sech pulse through 4-m length of the fiber is shown in Fig. 3.6(a) and the corresponding contour plot is shown in Fig. 3.6(b). Chirping due to nonlinearity and chirping due to dispersion cancel each other which results in a near distortion free propagation of the pulse through 4-m length of the fiber and can also be seen in Fig. 3.6(c)**.** Apart from the sech soliton solution, we have also studied the propagation of a Gaussian pulse through the fiber. A 100-fs Gaussian pulse has been propagated through the fiber and its peak power has been adjusted to 73.5 kW so as to obtain near distortion free propagation. The pulse evolution along with the contour plot is shown in Fig. 3.7(a) and Fig. 3.7(b), respectively. We can see that the pulse tries to attain balance between the nonlinearity and dispersion and fluctuates between the broadened state and the compressed state. The fluctuations**,** however, are not pronounced and the propagation is near distortion free over 2.5-m length of the fiber. The temporal profiles of the Gaussian-shaped pulses at the input and output end of the fiber are shown in Fig. 3.7(c) which shows that pulse of the shape is retained with slight compression. Thus, a three layered fiber design having mode area 1900 μm^2 has been proposed for the delivery of high power femtosecond laser pulses. The modal purity at the output has been maintained by leaking out HOM except LP_{11}. Mode stability has been ensured by sufficient mode spacing between LP_{01} and LP_{11}. We have numerically demonstrated the near distortion-free propagation of 100-fs, 55.5-kW peak power sech pulses and 73.5-kW peak power Gaussian pulses over 4.0-m and 2.5-m lengths of the fiber respectively. Therefore the fiber is a good candidate for ultra-short high peak delivery. However the fiber is able to transport USPs at one wavelength. We propose SCF design which is able to transport USPs at more than one wavelength.

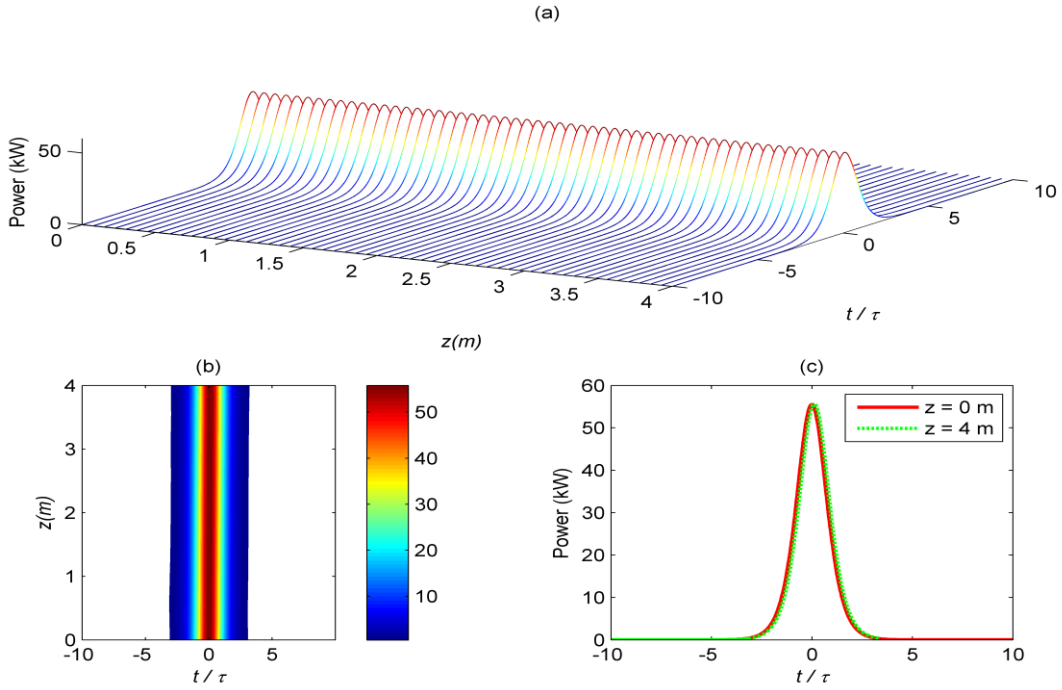

Figure 3.6 (a) *Propagation of a sech pulse in the fiber*, (b) *corresponding contour plot*, (c) *input and output temporal profiles of sech pulse.*

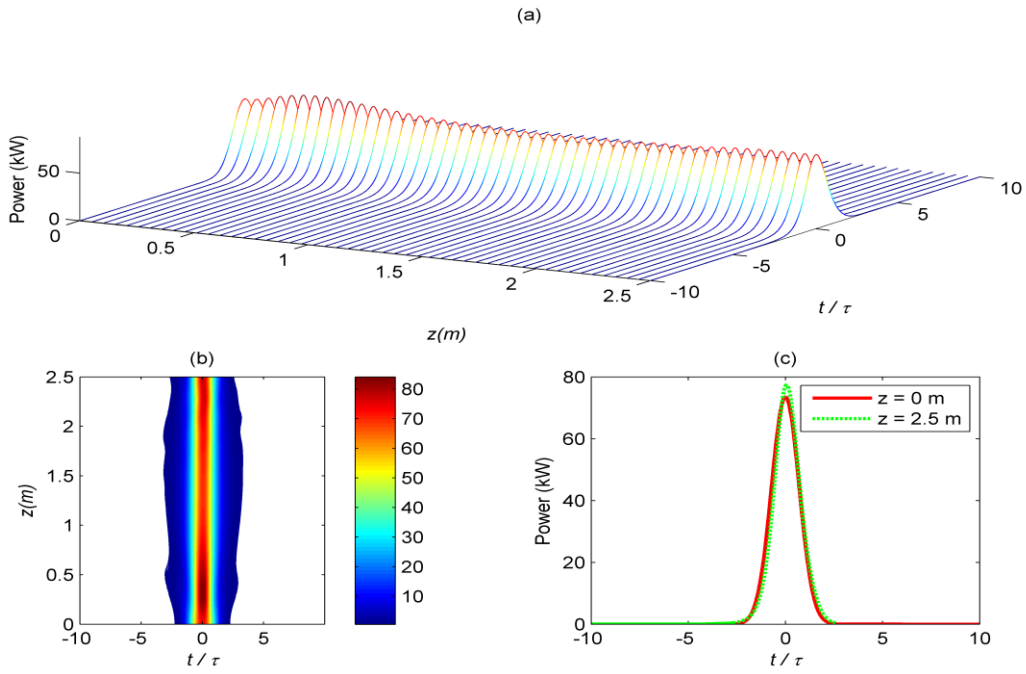

Figure 3.7 (a) *Propagation of a Gaussian pulse in the fiber*, (b) *corresponding contour plot*, (c) *input and output temporal profiles of sech pulse.*

3.3 Design of segmented cladding fiber

3.3.1 Fiber Design and method of analysis

We present a fiber design in which cladding is highly dispersive because of periodic arrangement of low and high index segments in angular direction. The transverse cross section of segmented cladding fiber SCF with field profile of LP_{01} mode is shown in Fig. 3.8. The fiber consists of a uniform core ($0 < r < a$) of refractive index n_1 and a segmented cladding ($a < r < b$) having alternate high

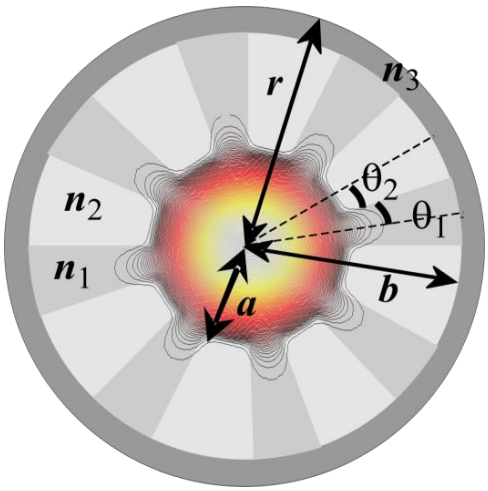

Figure 3.8 *Transverse cross-section of SCF with field profile of LP_{01} mode at 1550 nm wavelength.*

index medium (n_1) of angular width ($2\theta_1$) and low index medium (n_2) of angular width ($2\theta_2$). The relative index difference between the two regions is defined as $\Delta = \frac{(n_1^2 - n_2^2)}{(2n_1^2)}$ and has the value 0.9% in the proposed design. The period and the duty cycle of segmentation are given by $\Lambda = \theta_1 + \theta_2$ and $\gamma = \theta_2/\Lambda$ respectively. The outer jacket of the fiber having refractive index n_3 is of pure silica whereas n_1 and n_2 correspond to Ge-doped and F-doped silica respectively. We have considered a fiber with a = 29 μm and standard cladding diameter of 125 μm. The fiber is uniform in the axial direction which is the direction of wave propagation.

3.3.2 Method of analysis

3.3.2 (a) ***Radial-effective-index method*** **:**

Radial effective method has been developed for analysis of an arbitrary cross-section. In radial effective index method a non-circular fiber is approximated by an equivalent circular fiber and scalar wave equation is expressed in cylinderical coordinates. This method solves the refractive index profile of the fiber in angular direction to obtain radially varying effective index [116]. Therefore it can be used to calculate effective index profile of SCF. The scalar wave equation in cylindrical polar coordinate system can be written as [117]:

$$\frac{\partial^2\phi}{\partial r^2}+\frac{1}{r}\frac{\partial\phi}{\partial r}+\frac{1}{r^2}\frac{\partial^2\phi}{\partial\theta^2}+k^2[n^2(r,\theta)-n_{eff}^2]\phi=0 \qquad (3.21)$$

Where $\phi(r,\theta)$ is the field, $n(r,\theta)$ is the refractive-index distribution, n_{eff} is the effective index of mode, $k = 2\pi/\lambda$ is free-space wave number. The field of the mode can be expressed in the following form:

$$\phi(r,\theta)=\phi_r(r)\phi_{r\theta}(r,\theta) \qquad (3.22)$$

Substituting Eq. (3.22) into Eq. (3.21) gives

$$\phi_{r\theta}\frac{d^2\phi_r}{dr^2}+\frac{\phi_{r\theta}}{r}\frac{d\phi_r}{dr}+\frac{\phi_r}{r^2}\frac{\partial^2\phi_{r\theta}}{\partial\theta^2}+k^2[n^2(r,\theta)-n_{eff}^2]\phi_r\phi_{r\theta}=0 \qquad (3.23)$$

Now we make an assumption that $\phi_{r\theta}$ varies slowly with r in comparison to ϕ_r therefore $\partial\phi_{r\theta}/\partial r$ and $\partial^2\phi_{r\theta}/\partial r^2$ can be neglected. Therefore radially varying effective index profile satisfies $n_{effr}(r)$ satisfies the following equation [117]:

$$\frac{\partial^2\phi_{r\theta}}{\partial\theta^2}+k^2[n^2(r,\theta)-n_{effr}^2(r)]r^2\phi_{r\theta}=0 \qquad (3.24)$$

Eq. (3.23) can be written as

$$\frac{d^2\phi_r}{dr^2}+\frac{1}{r}\frac{d\phi_r}{dr}+k^2[\bar{n}_{effr}^2-\frac{l^2}{k^2r^2}-n_{eff}^2]\phi_r=0 \qquad (3.25)$$

Where $\bar{n}_{effr}^2(r) = n_{effr}^2(r) + \frac{l^2}{k^2 r^2}$; l=0,1,2.... (3.26)

There is no variation of refractive index in azimuthal direction in the core region of SCF, $0 < r < a$. Therefore, the effective index profile profile $\bar{n}_{effr}(r)$ from Eq. (3.24) can be written as:

$$\bar{n}_{effr}^2(r) = n^2(r) - \frac{l^2}{k^2 r^2} \tag{3.27}$$

However in cladding region of SCF refractive index varies in azimuthal direction i.e. $a \leq r \leq b$. In cladding region of SCF at a particular value of $r = r_i$, Eq. (3.24) can be written as:

$$\frac{\partial^2 \phi_{r\theta}(r_i,\theta)}{\partial \theta^2} + k^2[n^2(r_i,\theta) - n_{effr}^2(r_i)]r_i^2 \phi_{r\theta}(r_i,\theta) = 0 \tag{3.28}$$

$n(r_i,\theta)$ is a periodic function of θ and $\phi_{r\theta}(r_i, \theta)$ must satisfy the periodic boundary conditions. By applying suitable boundary conditions and solving Eq. (3.28) we get [117]:

$$\bar{u}\tan\bar{u} = \bar{w}\tanh(\bar{w}\frac{\theta_2}{\theta_1}) \tag{3.29}$$

for LP_{0m} mode and for LP_{1m} mode.

$$\cosh(2\bar{w}\frac{\theta_2}{\theta_1})\cos 2\bar{u} + \frac{\bar{w}^2 - \bar{u}^2}{2\bar{u}\bar{w}}\sinh(2\bar{w}\frac{\theta_2}{\theta_1})\sin 2\bar{u} = \cos\frac{2\pi}{N} \tag{3.30}$$

Where N is the number of segments, $\bar{u} = \theta r_i k(n_{effr}^2 - n_{effr}^2)^{1/2}$, $\bar{w} = \theta_1 r_i k(n_{effr}^2 - n_2^2)^{1/2}$. Using Eq. (3.29) and Eq. (3.30), one can calculate the effective-index profile $n_{effr}(r)$ of a particular mode. By using $n_{effr}(r)$ one can calculate effective-index profile $\bar{n}_{effr}(r)$ from Eq. (3.26). By solving Eq. (3.25) mode index n_{eff} as well as mode field can be calculated.

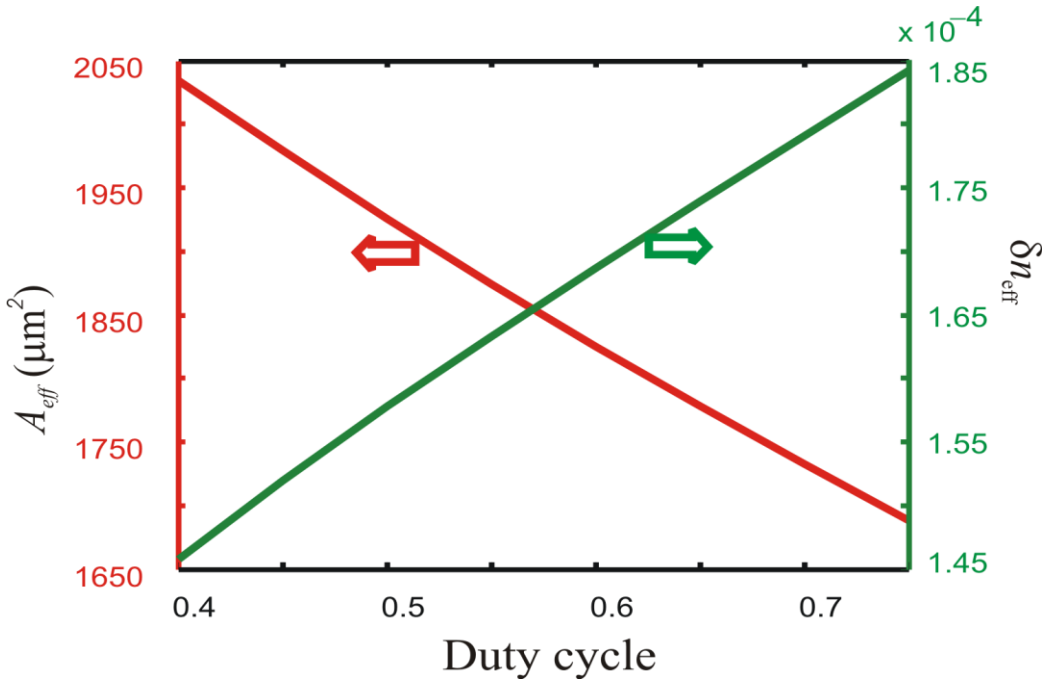

Figure 3.9 *Variation of* A_{eff} *and* δn_{eff} *with duty cycle.*

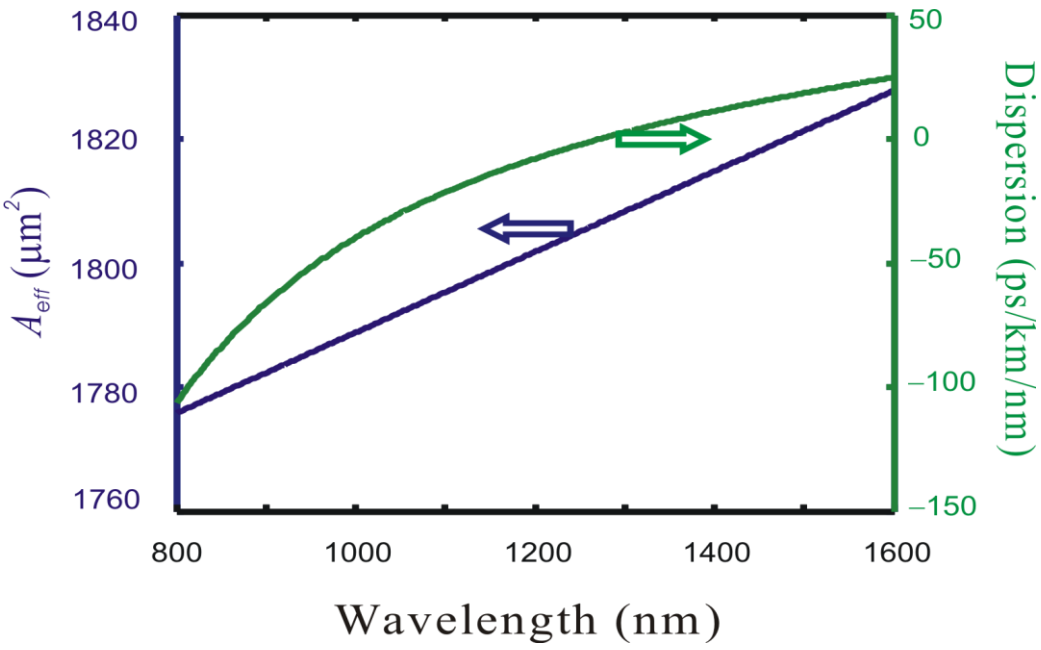

Figure 3.10 *Variation in* A_{eff} *and D with wavelength.*

A_{eff} and D of the fiber have been calculated using Eq. (2.17) and Eq. (2.16) respectively. A_{eff} and δ_{neff} of the fiber can be controlled by the duty cycle of segmentation as shown in Fig. 3.9. We have considered δ_{neff} for LP_{01} and LP_{11} modes. We can see that with duty cycle δ_{neff} increases whereas A_{eff} decreases and there is a tradeoff between A_{eff} and δ_{neff} while designing the fiber. We have chosen 60% duty cycle to achieve sufficiently high value of A_{eff} (1825μm^2) and δn_{eff} (1.68×10^{-4}) at 1550-nm wavelength which is higher than the limits observed in the 800 μm^2-mode area conventional large mode area fiber and in the PCF [22].

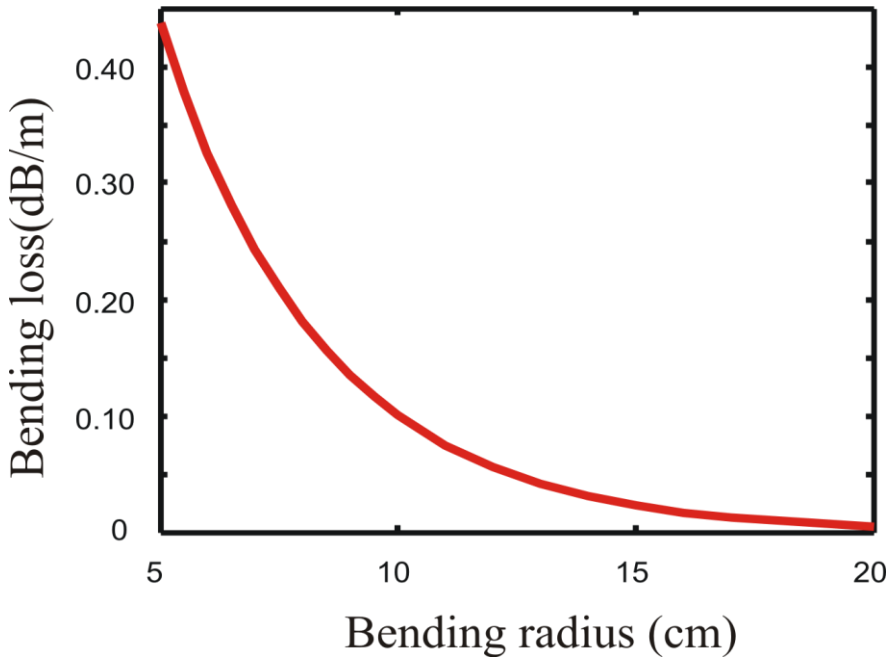

Figure 3.11 *Variation in bending loss with bending radii*.

The mode stability at 1064-nm wavelength, however, reduces to about 1×10^{-4} with mode area 1793 μm^2. A_{eff} and D of the fiber at different wavelengths for 60% duty cycle are plotted in Fig. 310. We can see that A_{eff} does not vary significantly over the entire wavelength range because of dispersive cladding of the fiber. Such a feature of the SCF makes it attractive for USP delivery at several wavelengths. A_{eff}, D and β_3 of the fiber is 1825 μm^2, 21.76 ps/nm/km and 1.495×10^{-4} ps^3/m respectively at 1550-nm wavelength, where β_3 is a third order dispersion coefficient.

The first higher-order mode (LP_{11}) of the fiber is guided, however, due to large modal spacing and its small overlap with LP_{01} mode, this will not affect the pulse propagation. The LP_{02} mode has 18-dB/m leakage loss at 1550 nm

wavelength and is not sustained over the length considered here. Mode spacing which plays a crucial role for mode stability is a function of wavelength and decreases with wavelength. While designing the fiber for USP the value of δn_{eff} larger than 1×10^{-4} is preferred [22]. The bend loss of the fiber has been calculated at different bending radii by using Eq. (2.5) [30] and is shown in Fig. 3.11. The fiber shows bend loss of 0.023 dB/m at 15-cm bend radius. At 1064-nm wavelength A_{eff}, D and β_3 of the fiber are 1793 μm^2, 27.4 ps/nm/km and 5.91×10^{-4} ps^3/m respectively. The leakage loss of LP_{02} mode is 0.002 dB/m and the mode spacing is close to 1×10^{-4}. Hence, the same fiber can be used for delivery of pulses at 1550-nm and 1064-nm wavelengths.

3.3.3 *Pulse propagation*

3.3.1 (a) *Pulse propagation at 1550-nm wavelength* :

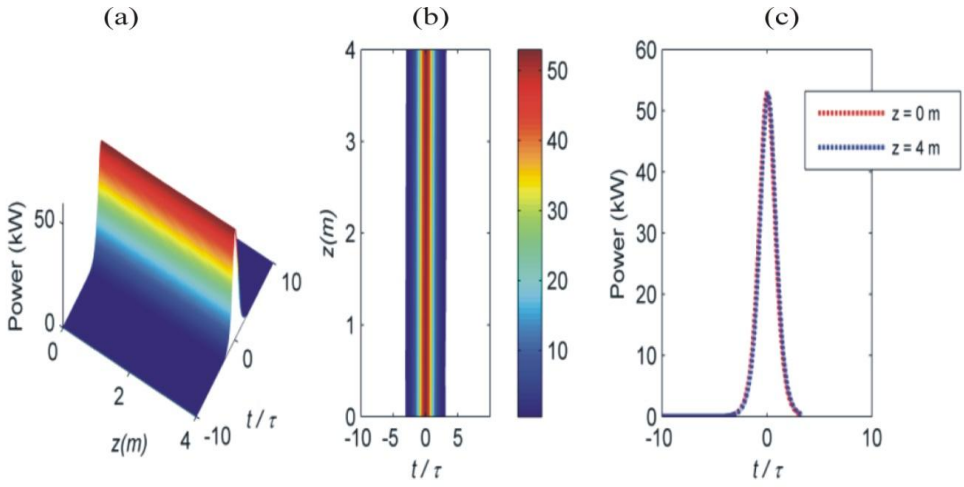

Figure 3.12 (a) *Propagation of a Gaussian pulse at 1550 nm wavelength*, (b) *Corresponding contour plot*, (c) *Input and output temporal profiles of the pulse*.

To study the propagation dynamics of sech pulse at 1550-nm center wavelength we have considered the pulse with C = 0. The peak power for soliton propagation of 100-fs pulse duration comes out to be 53 kW, where we have used N_2 = 2.36 $\times10^{-20}$ m^2/W. The transmission loss (α) of the fiber at 1550-nm wavelength has been considered as 0.2 dB/km. The value of Raman time constant ($\tau_R = T_R/\tau$) for

silica has been taken as 3 fs [88]. Evolution of pulse, corresponding contour plot and input-output profiles after 4-m propagation through the fiber are shown in Fig. 3.12. We can see distortion-free propagation of the pulse. Apart from the sech pulse we have also studied the propagation of a Gaussian pulse defined by the following equation through the fiber [88].

$$A(z=0,t) = P_0^{1/2} \times \exp(-t^2(1+iC)/(2\tau^2)) \tag{3.31}$$

For studying the propagation dynamics of 100-fs Gaussian pulse through the fiber and the peak power has been adjusted to 71 kW so as to obtain near distortion-free propagation. The pulse evolution along with the contour plot and input-output temporal profiles is shown in Fig. 3.13. Initially we can see compression of the pulse due to nonlinearity but as the pulse evolves nonlinearity and dispersion balance each other and we get near distortion-free propagation of the pulse through the fiber. The pulse shape is retained with only slight broadening. The near distortion-free propagation could be achieved for a 2-m long fiber.

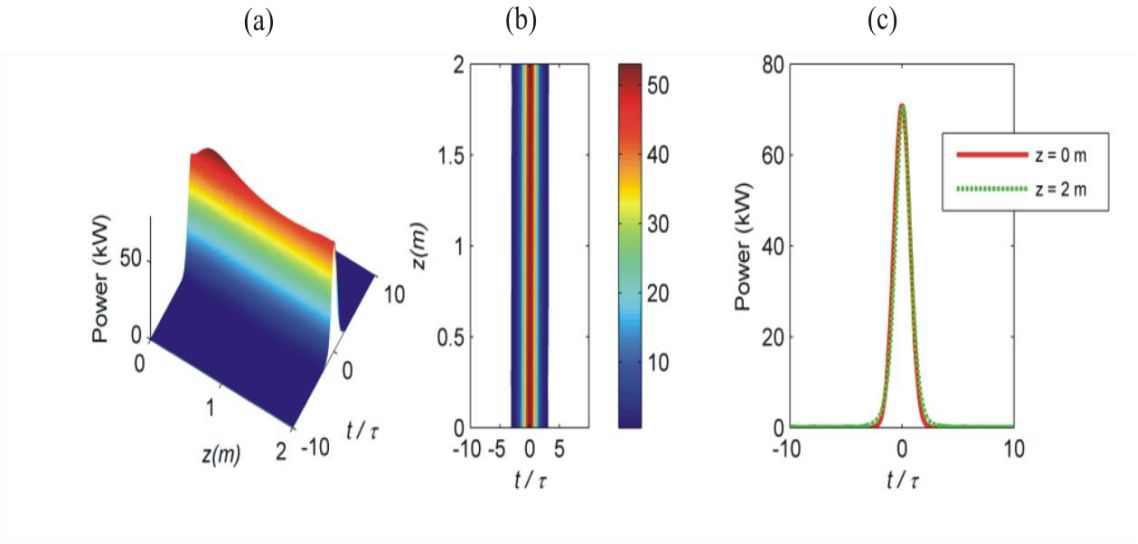

Figure 3.13 (a) *Propagation of a Gaussian pulse at 1550 nm wavelength, (b) Corresponding contour plot,*(c) *Input and output temporal profiles of the pulse*

3.3.2 (b) *Pulse Propagation at 1064-nm Wavelength*:

At 1064-nm wavelength, which falls into normal dispersion regime $D < 0$ and dispersion induced chirping is of the same sign as that of nonlinearity induced chirping. This leads to the chirping of output pulse and distortion-free propagation

of high power pulses becomes difficult. Segmented cladding fiber maintains a large mode area with small dispersion, therefore, the total chirping of the pulse is not significant and can be balanced by a slight negative chirping in the input pulse. We have studied propagation of 250-fs chirped sech and Gaussian pulses at 1064-nm wavelength with a peak power of 15 kW through the same fiber. We have considered an input pulse with $C = -1.1$, which is sufficient to counterbalance the total chirping induced due to dispersion and nonlinearity. The transmission loss of the fiber at 1064-nm wavelength has been taken as 0.76 dB/km and the Raman time constant as 5 fs. The evolution of the sech pulse through the fiber is shown in Fig. 3.14(a) with corresponding contour plot in Fig. 3.14(b). The input and output temporal profiles for a 1-m long fiber for $C = 0$ and $C = -1.1$ are shown in Fig. 3.14(c). Evolution of the pulse shows that the pulse is initially compressed due to nonlinearity and then broadens. Figure 3.14(c) shows that in case of chirped pulse dispersion and nonlinearity partially balance each other whereas in case of un-chirped pulse dispersion dominates and the pulse is broadened. The propagation of a Gaussian pulse is shown in Fig. 3.15(a) along with its contour plot in Fig.3.15 (b) and input and output pulse profiles in Fig.3.15(c). We can again see near distortion-free propagation for the case $C = -1.1$ and broadening in case of un-chirped pulse.

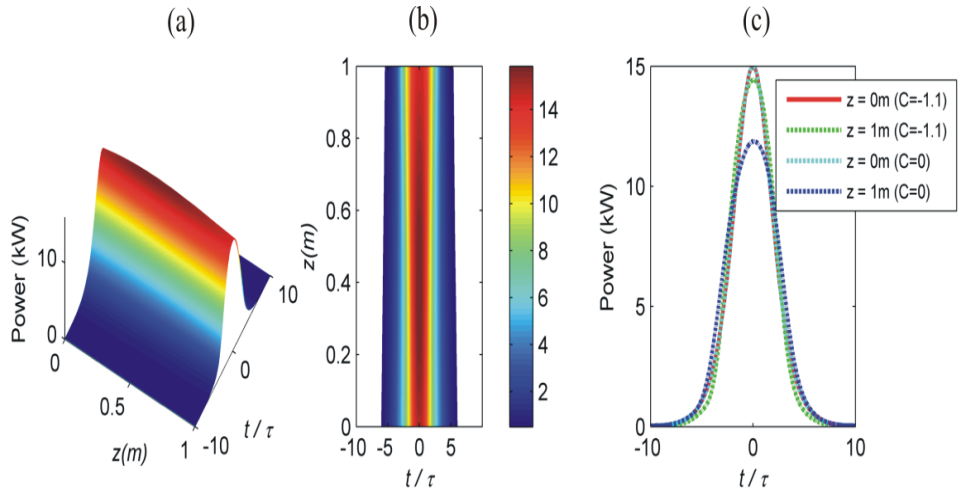

Figure 3.14 (a) *Propagation of a sech pulse in the SCF at 1064 nm wavelength,* (b) *Corresponding contour plot,* (c) *Input and output temporal profiles of the*

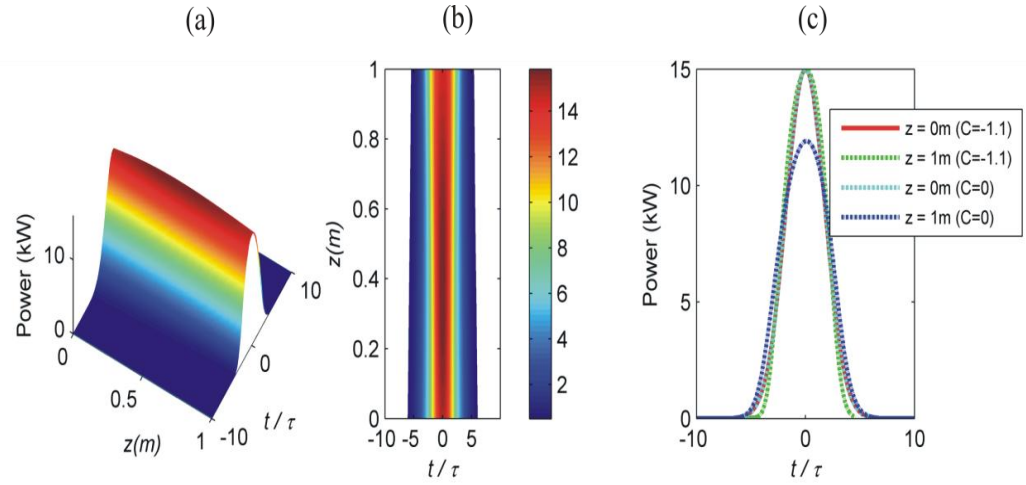

Figure 3.15 (a) *Propagation of a Gaussian pulse in the SCF at 1064 nm wavelength,* (b) *Corresponding contour plot,* (c) *Input and output temporal profiles of the chirped and unchirped pulses.*

3.4 Conclusions

A three layered fiber design and SCF design for delivery of USPs have been proposed in this chapter. Three layered fiber having mode area 1900 μm^2 has been proposed for delivery of 100-fs pulses at 1550 nm wavelength. Whereas SCF has been proposed for delivery of femtosecond pulses at 1064 nm and 1550 nm wavelengths. The modal purity at the output in three layered fiber has been maintained by leaking out HOM except LP_{11}. Mode stability has been ensured by sufficient mode spacing between LP_{01} and LP_{11} modes. In three layered fiber structure we have numerically demonstrated the near distortion-free propagation of 100-fs, 55.5-kW peak power sech pulses and 73.5-kW peak power Gaussian pulses over 4.0-m and 2.5-m lengths of the fiber respectively. It is shown that obtained design introduces so interesting features to be used for delivery of ultra short laser pulses. However this design is able to transport USPs at one wavelength only. Therefore SCF having mode area of 1825 μm^2 at 1550-nm wavelength and 1793μm^2 at 1064-nm wavelength has been proposed which is able to transport pulses at more than one wavelengths. SCF can deliver 100-fs sech and Gaussian pulses at 1550-nm wavelength and 250-fs pulses at 1064-nm wavelength without significant distortion.

The proposed designs should be useful in the area of multi-photon microscopy and biomedical applications for delivery of ultra-short laser pulses.

CHAPTER–4

Development of Fabrication Technology for Segmented Cladding Fiber in Silica-Based Glass

4.1. Introduction

Segmented cladding fiber (SCF) has been proposed for large-mode-area single-mode operation over an extended range of wavelengths [117-119]. Large-mode-area extended-single-mode operation of an SCF helps in suppressing unwanted nonlinear effects while accommodating large number of wavelengths in high data rate optical communication systems employing dense wavelength division multiplexing. An SCF is also attractive for high power fiber lasers and amplifiers as it can maintain single-mode operation with a large core and high numerical aperture (NA). The structure of the SCF, which contains alternate high- and low- index segments in the angular direction in the cladding, makes it difficult to fabricate with the conventional optical fiber fabrication technologies. Alternative technologies have been developed and the fabrication of the SCF has been demonstrated in soft materials like poly-methyl methacrylate (PMMA) and silver halide glass [120-123]. Yeung et al. experimentally demonstrated fabrication of polymer SCF. SCF preforms were fabricated using two methods. The first method was cladding-segment-in-tube technique. The prefabricated low index cladding segments of polymer were placed in glass tube to form desired segmented pattern. The high index monomer was then poured into tube. The second method was core-cladding-segment-in-tube technique. Prefabricated polymer low-index and high-index segments

were arranged in desired specific pattern and were placed in glass tube. Fabricated fibers were able to strip-off higher order modes but only little centimeter fiber could be obtained with uniformity [123]. Polymer optical fiber with segmented cladding cross section has also been fabricated by using bicomponent spinning technique [121]. SCF has also been fabricated from silver halide glass in middle infrared wavelength range [122]. The fabricated fiber however, suffers from high losses compared to fabricated step index fiber for mid-IR [120]. It is very difficult to fabricate the SCF in silica glass as it is comparatively hard material and not easy to shape it into segments of desired geometry. Here we present the fabrication technique of segmented cladding fiber in silica glass. SCFs with 45 μm and 30 μm core diameters, and 125 μm and 80 μm cladding diameters, respectively have been fabricated at central glass and ceramic research institute (CGCRI) Kolkata. The fibers have been characterized by near field imaging. The number of modes has been estimated from the near field images by neural network analysis. We show few-mode operation of SCF by efficient higher order mode filtering effect.

4.2. Fiber Design

Schematic of the transverse cross section of an SCF is shown in Fig. 4.1. The fiber consists of a uniform core ($0 < r < a$) formed by pure silica glass of refractive index n_1 and a segmented cladding ($a < r < b$) having alternate high index medium (pure silica glass) of angular width θ_1 and low index medium (F-doped silica glass) of refractive index n_2 and angular width θ_2. The relative index difference between the two regions is defined as $\Delta = \frac{(n_1^2 - n_2^2)}{(2n_1^2)}$. The structure is characterized by duty cycle of segmentation defined by $\gamma = \theta_2/(\theta_1+\theta_2)$. An SCF is essentially a leaky structure. High index regions of the fiber work as leakage channels and all the modes of the fiber suffer from finite leakage loss. It has been shown that the leakage loss of a mode increases with mode number [117]. Effective single mode operation of the fiber is ensured by high differential leakage loss between fundamental mode and first higher order mode. This differential leakage loss is a strong function of fiber parameters. It is therefore important to have an estimation of correct values of various fiber parameters prior to its fabrication. To have an idea of values of various fiber parameters, we have analyzed the fiber by radial effective index method (RIEM) in conjunction with transfer matrix

method [117,86]. For numerical calculations, we have considered a fiber with a = 15 μm, standard cladding diameter of 125 μm and Δ as 0.004. The value of Δ chosen is according to the availability of F-doped glass rods. A conventional step-index fiber with these parameters would support more than 20 modes at 630-nm wavelength. REIM converts the refractive index variation $n(r,\theta)$ of Fig.4.1(a) into an effective refractive index profile $n_{effr}(r)$ as shown in Fig. 4.1(b), which is independent of θ and can be solved by TMM to obtain the propagation constant and leakage loss of the modes. Fig. 4.2 shows the variation of leakage loss of fundamental mode (LP_{01}) and first higher order mode (LP_{11}) with core radius for different duty cycles. For pure silica core fiber, the Rayleigh scattering loss is small while Δ and γ are the critical parameters in SCF design to reduce the leakage loss in order to be suitable for long distance transmission. The operation of SCF is based on differential leakage loss of the fundamental mode and first higher order mode. If the fiber is long enough such that only the fundamental mode can survive then the fiber behaves like as effective single mode fiber. The length for effective single mode operation depends on the differential leakage loss between fundamental mode and first higher order mode.

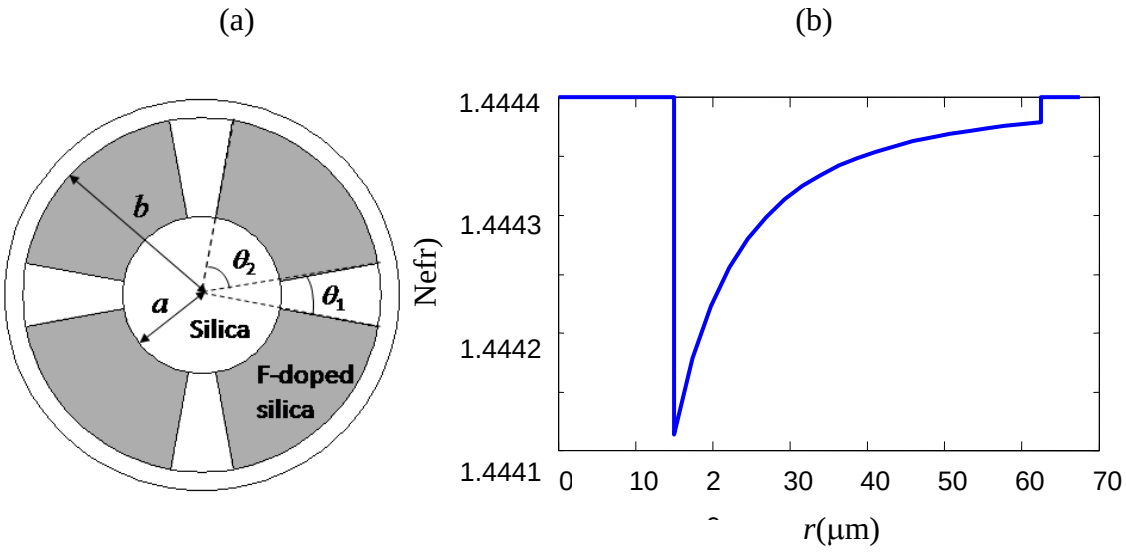

Figure 4.1(a) *: Schematic of the transverse cross section of an SCF. Pure silica glass regions are shown in white and F-doped silica glass regions are shown in gray,* **(b)** *Effective refractive index profile of the fiber for* γ = *60% at 630 nm wavelength wavelength obtained by REIM.*

The length for single mode operation is defined as the length at which the differential leakage loss between the fundamental mode and the first higher order mode is 20 dB and is defined as:

$$L_{SM} = \frac{20}{Loss(\mathrm{LP}_{11}) - Loss(LP_{01})} \tag{4.1}$$

Where $Loss(LP_{01})$ and $Loss(LP_{11})$ denote the leakage losses of the fundamental mode and the first higher order mode respectively in dB/m. We have studied the effect of various parameters to design a fiber feasible for fabrication. The effect of core radius at

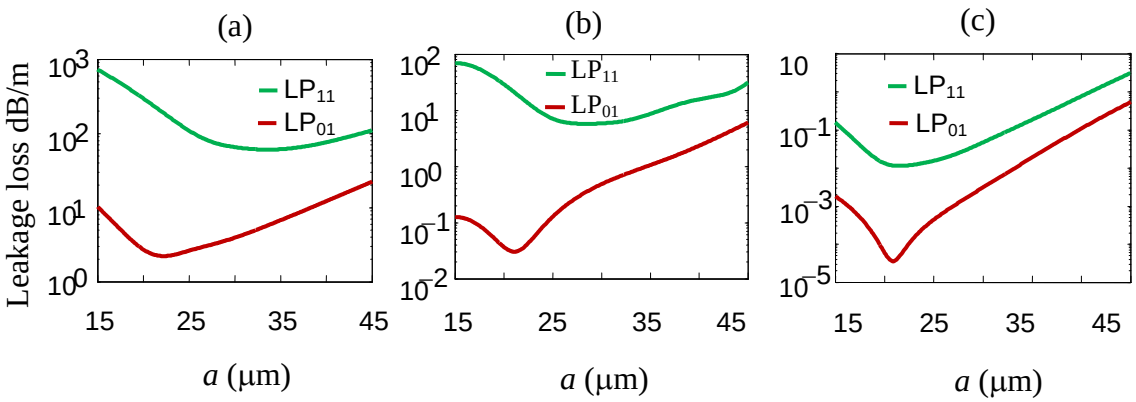

Figure 4.2 *Variation in leakage loss with core radius at 60% duty* (a), *70% duty cycle* (b), *80% duty cycle at for b = 125 μm at 630 nm wavelength.*

different duty cycles on the leakage loss of the first two modes is shown in Fig. 4.2. We have calculated leakage losses for 60%, 70% and 80% duty cycles for 4 numbers of segments. To avoid birefringence fiber should have four-fold symmetry and the minimum segment requirement for that is four. Fiber with number of segments (M = 4) is easy to fabricate also in comparison to large number of segments therefore M = 4 is the best choice for practical realization of the fiber. Fig 4.2 shows that the differential loss decreases with increase in a. However at shorter values of a leakage loss of the fundamental mode is also high at smaller values of γ. As we increase the value of γ effective index contrast between the core and the cladding increases which results in more confinement of modes. Therefore at higher values of γ, leakage loss of the modes decreases and single mode propagation length increases while enabling the fiber suitable for long distance transmission. Variation of single mode propagation length with core radius at different duty cycles is shown in Fig. 4.3. One can observe from Fig. 4.3 that single mode propagation length increases with increase in duty cycle.

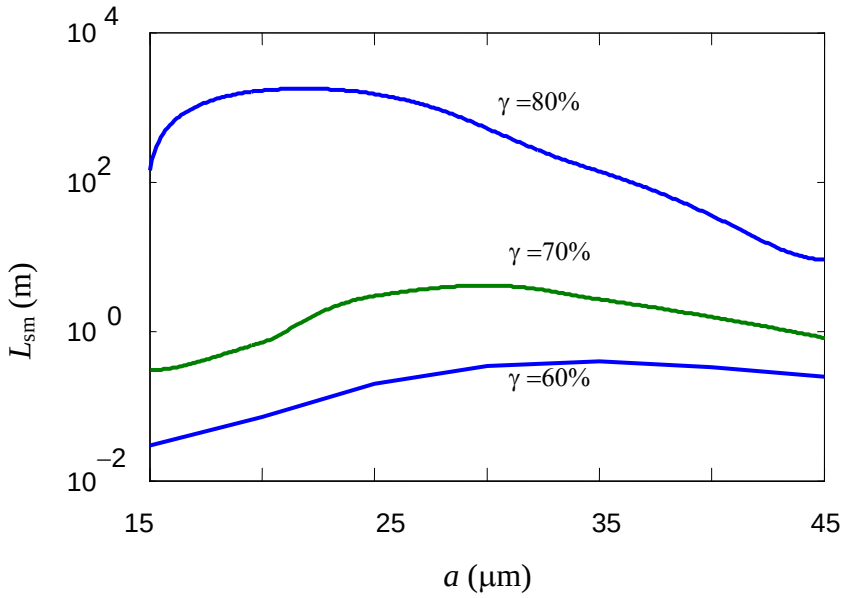

Figure 4.3 *Variation in L_{sm} with a for different duty cycles at 630 nm.*

For long distance transmission and to have small propagation loss of fundamental mode, 80 % duty cycle is good choice for filtering out the higher order modes.

4.3. Experimental

The segmented cladding fiber was prepared via Stack-and-Draw technique [124] from a stacked preform with central silica core surrounded by eight alternatively arranged F-doped and undoped silica rods. All undoped silica components (core with diameter 5 mm, four undoped cladding segments with diameter 3.1mm, jacketing tube: outer diameter 14.4 mm, inner diameter 11.5 mm) were made from Heraeus Suprasil F300. The four Fluorine doped segments were stretched from a 16mm thick preform to a diameter of 3.1 mm. The refractive index profile of the starting preform was measured in azimutal positions 0°, 90°, 135° and indicates circular homogeneity of the Fluorine concentration. Three performs were prepared with same circular homogeneity. The averaged Fluorine concentration corresponds to about 1.2 mol% SiF_4. The draw-technological consequence is a decrease of drawing viscosity around $\log \eta \approx 0.7$ compared to undoped silica F300. Furthermore this accords to a drawing temperature depression of about 100 K for the fluorinated segments. Affected by the Fluorine induced viscosity depression the segmented fiber was drawn at an effective temperature

of about 1810°C, which is 40 K below corresponding to undoped silica with similar preform dimension.

Table 4.1. Parameters of fabricated fiber (45/125) μm

(Sample I)

Fiber Diameter	125.0 μm
Core Diameter	45.0 μm
F-doped section Thickness	39.55 μm
Silica Segment-θ_1 (degree)	39.45
F Section-θ_2 (degree)	50.25
Δn for F-doping	6.3×10^{-3}

Table 4.2. Parameters of fabricated fiber (30/80) μm without jacket

(Sample II)

Fiber Diameter	80.0 μm
Core Diameter	30.0 μm
F-doped section Thickness	39.55 μm
Silica Segment-θ_1 (degree)	39.45
F Section-θ_2 (degree)	50.25
Δn for F-doping	6.3×10^{-3}

Table 4.3. Parameters of fabricated fiber (30/80) μm with jacket (Sample III)

Fiber Diameter	80.0 μm
Core Diameter	30.0 μm
F-doped section Thickness	39.55 μm
Outer Silica layer (c)	22.87 μm
Silica Segment-θ_1 (degree)	39.45
F Section-θ_2 (degree)	50.25
Δn for F-doping	6.3×10^{-3}

Two fibers were drawn with drawing speed of 8-10 m/min to diameter of 125 μm, 80 μm without jacket and one fiber with same drawing speed to a diameter of 80 μm and with jacket of 22.87 μm. Parameters of all the three fabricated fibers are given in Table 4.1, 4.2 and 4.3. A problem of drawing stacked preforms with higher Flourine doping is the high out-gassing tendency of SiF4. It generates bubbles at interface between the F-doped and undoped components during sintering in the neck down region. Such cavity disturbances can be minimized by pre-annealing the fluorinated rods. AFM image of one of the fiber sample (30/80 μm) is shown in Fig. 4.4. After fabrication of the fiber we launched light into few meters length of the fibers using He-Ne laser having wavelength 630 nm and observed intensity pattern at the output end of the fiber. We captured the image of the speckle pattern which is interference pattern of modes of fiber using camera. The output intensity patterns are shown in Fig. 4.5. We observe from Fig. 4.5 (a) that the fiber sample having core diameter 45 μm and is not jacketed with silica consists of large number of speckles. Whereas another unjacketed sample having core diameter 30 μm has bit clear near field intensity pattern as depicted in Fig. 4.5 (b) than that of previous one. This is because core diameter of sample II is less than that of

sample I which results in decrease in number of supported modes. The output intensity pattern of sample III which is jacketed with silica and is having core diameter 30 μm is more clear than that of sample I and II. The outer jacket of sample III make it leaky and some modes of the fiber stripped off and helps in reducing supported modes. Which improves the beam quality at the exit end of the fiber. To estimate the number of supported modes we have considered the fiber with jacket as it consists of minimum number of modes among three fabricated fibers. By visual inspection it is very difficult to estimate the number of modes so neural network model has been used to predicts the number of modes and is described in next section.

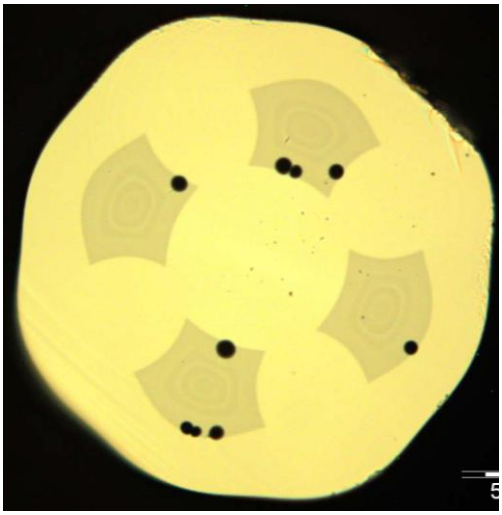

Figure 4.4 *AFM image of fabricated SCF sample*

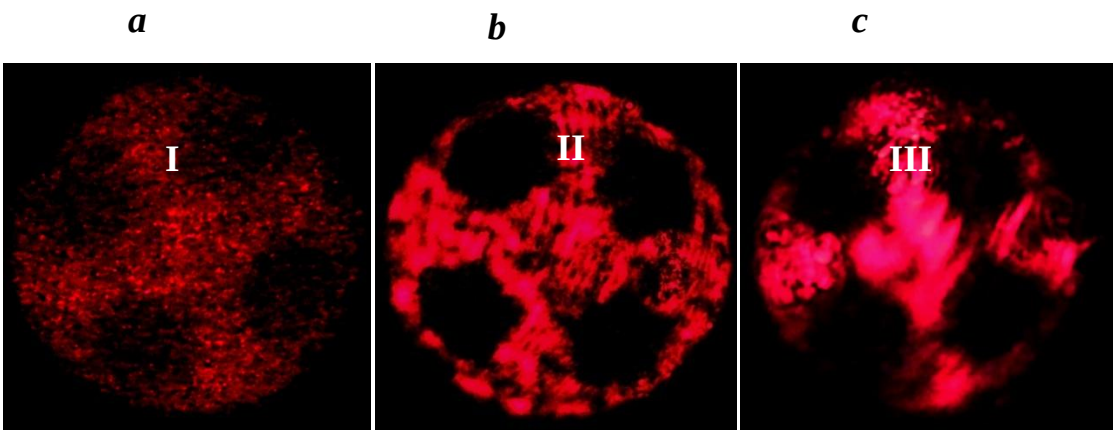

Figure 4.5 *Output intensity pattern for three different fabricated samples (a) 45/125 μm without jacket, (b) 30/80 μm without jacket, (c) 30/80 μm with jacket.*

4.4 Neural network implementation to estimate number of modes:

To estimate the number of modes in the pattern shown in Fig. 4.5 (c), we have implemented neural network algorithm. Neural computing has emerged as an efficient technology with many applications in various fields. Most of these applications are related to pattern recognition and use feed-forward network architectures [125]. Neural networks are basically family members of computational architectures inspired by biological brains and are called connectionist systems. These consist of interconnected and interacting components called nodes or neurons. A typical feed forward neural network is shown in Fig. 4.6 which indicated that network has links only in one direction and proceed from input nodes towards output nodes. In neural network each nodes take input data and emulate biological neurons then perform simple operations on data and selectively pass results to other neurons. Weight values area assigned with each node which determine how input data is related to output data. Weight values are established while training the network to identify a particular class by using input data characteristics [125]. Many issues related to neural network applications can be understood in simple context of polynomial curve fitting. If one has to fit a polynomial to a set of N data points by minimizing an error function. Consider a polynomial of M_{TH} order given as [125]:

$$y(x) = w_0 + w_1 x + ... + w_M x^M = \sum_{j=0}^{M} w_j x^j \tag{4.2}$$

This can be considered as nonlinear mapping in which input is x and produced output is y. w_0, w_1, w_2 .. are weights in neural network. The polynomial can be written as a functional mapping in the form $y = y(x;w)$. If x^n denote the input value corresponding to data nth data and the corresponding desired output values is denoted by t^n. If the corresponding predicted value by polynomial is given by $y(x^n; w)$ then to find the suitable coefficients of polynomial it is required to consider error between desired output (t^n) and the output predicted by polynomial $y(x^n; w)$. Basic curve fitting involve minimizing the square of this error for all data and is given as [125]:

$$E = \frac{1}{2}\sum_{n=1}^{N}\left(y(x^n; w) - t^n\right)^2 \tag{4.3}$$

From the above equation we observe that E is a function of w and the polynomial therefore can be fitted by choosing an value of w say w^* which minimizes E.

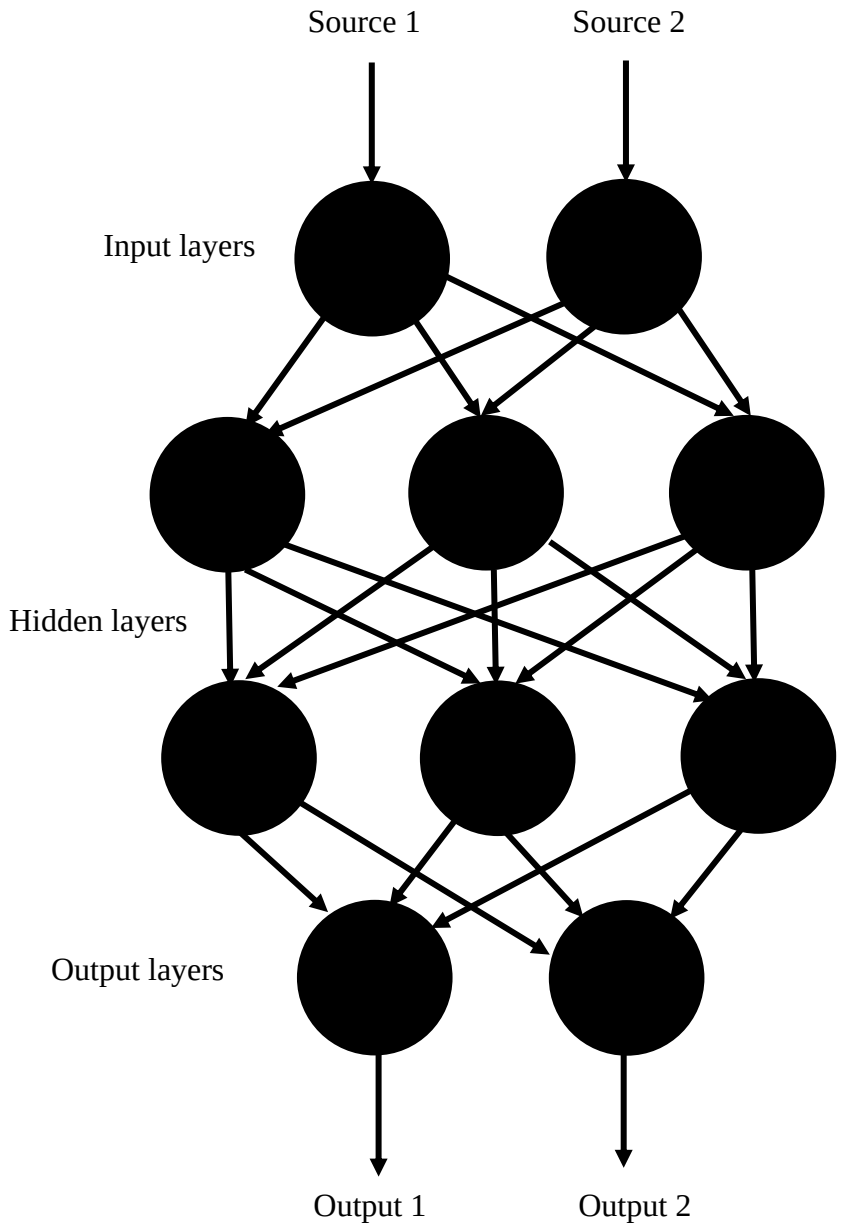

Figure 4.6 *A typical feedforward neural network.*

The best fitting is achieved when the complexity of the model say order of polynomial is neither too large nor too small. The same consideration is applied to neural network model and complexity of the model can be controlled by many adjustable parameters and by adding a penalty term Ω to error function and is represented as [125]:

$$\tilde{E} = E + R\Omega \tag{4.4}$$

Where Ω is called a regularization term and is used to control overfitting. We may choose value of Ω as:

$$\Omega = \frac{1}{2}\int\left(\frac{d^2y}{dx^2}\right)^2 dx \tag{4.5}$$

R is regularization coefficient and controls the extent up to which regularization term influences the complexity of model . Here we have applied these network architectures to train the network for computationally generated interference patterns of modes of fiber with random phases. To have benchmarking of the process, firstly we have applied the model to estimate the number of modes of well known results of polymer SCF [120]. Neural network was trained for computationally generated interference

(a) (b)

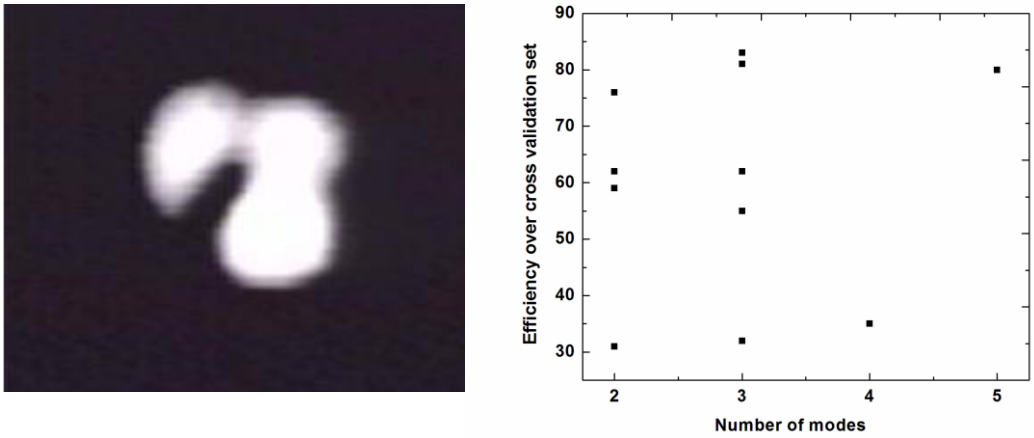

Figure 4.7 (a) *Experimentally observed pattern at the output end of the polymer SCF,* (b) *Variation in prediction distribution of modes with efficiency over cross validation set.*

pattern of 10 modes of an SCF with random phases. 10 number of modes. To process the image we have converted it into RGB pattern using Matlab. The input image is the intensity distribution at the fiber exit end as shown in Fig. 4.7 (a).Neural network was trained for 10 number of modes with optimized values of regularization coefficient (0.1), number of hidden layers (25) and 300 samples. Neural network testing shown in Fig.4.7 (b) predicts that the image consist of 2 or 3 modes. By visual inspection also one predicts that the image consists of interference pattern of 2 to 3 modes. Therefore mode prediction of neural network is reliable. Now we applied the model to estimate number of modes of intensity pattern shown in Fig. 4.5 (c). Firstly the output intensity pattern

was converted into RGB pattern using Matlab and is shown in Fig. 4.8. While applying the model to actual problem we have considered the factors which can affect performance of the network. In neural networking one is confronted with the problem of how complex to make a model. If the model is too simple it cannot capture the variability of the data. If model is too complex, coincidental complex relations will be found and no explanatory values will be predicted by model. Two commonly used terms regarding set of data are over-fitting and under-fitting. If the model is over-fitted then model has an excess of parameters. Over-fitted model gives improved accuracy on the training set while missing the overall message or pattern in the data. Whereas under-fitted model is incapable of capturing variability of the data. So we have to optimise the model to get good prediction. Quite important one important parameters to optimize the

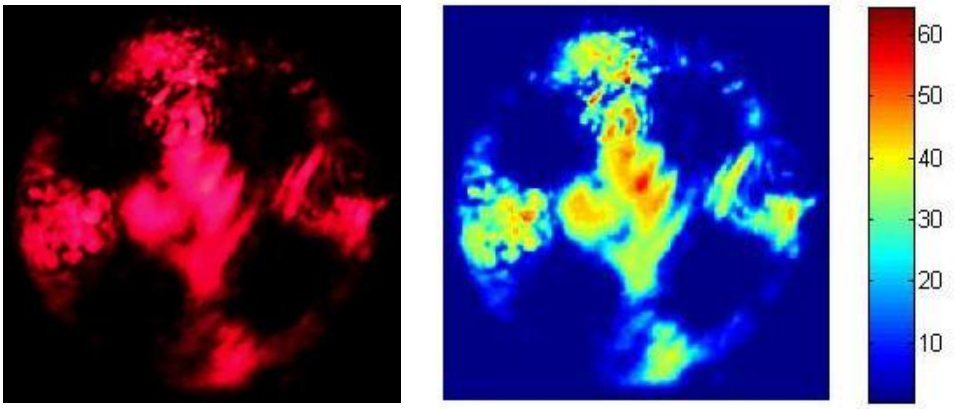

Figure 4.8 *Experimentally observed pattern at the output end of SCF* (a), (b) *Converted RGB image of the observed pattern.*

model are proportion of regularization, number of training samples, number of hidden layers.

(A) Regularization coefficient:

Regularization contains how well the training curve fits the data [125].

The prediction distribution of modes for different values of *R* is shown in Fig. 4.9. If *R* is low then the neural network tries to fit training data precisely. If the curve fits the neural network very accurately it fails to learn the trend and may not give predictions that are accurate. We need to optimize *R* to maintain balance of learning and predicting. It can be observed that when *R* is 0.01 the data gives high efficiency over cross validation set which is a mixture of images that neural network has seen and has not seen before. For *R* = 0.01 prediction of modes indicates a range of modes from 5 to 10

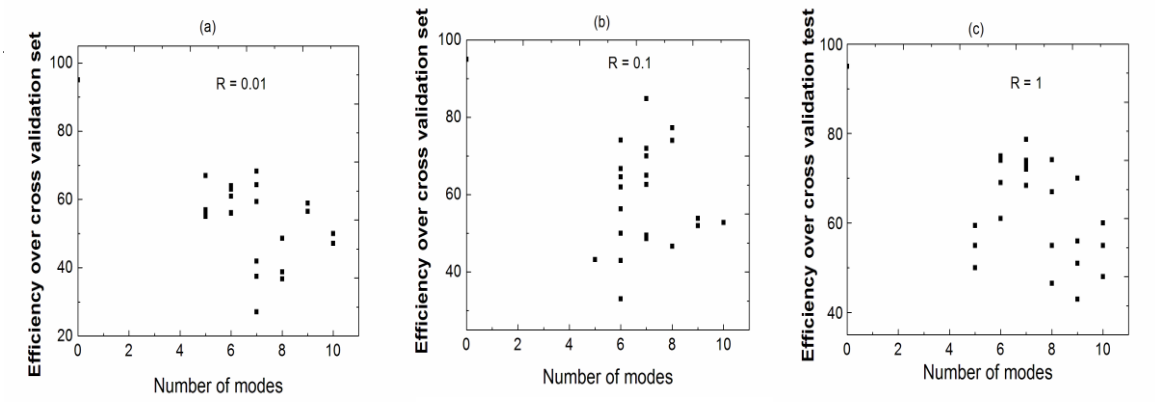

Figure 4.9 *Variation in prediction distribution of modes for (a) R = 0.01, (b) R = 0.1, (c) R = 1.0.*

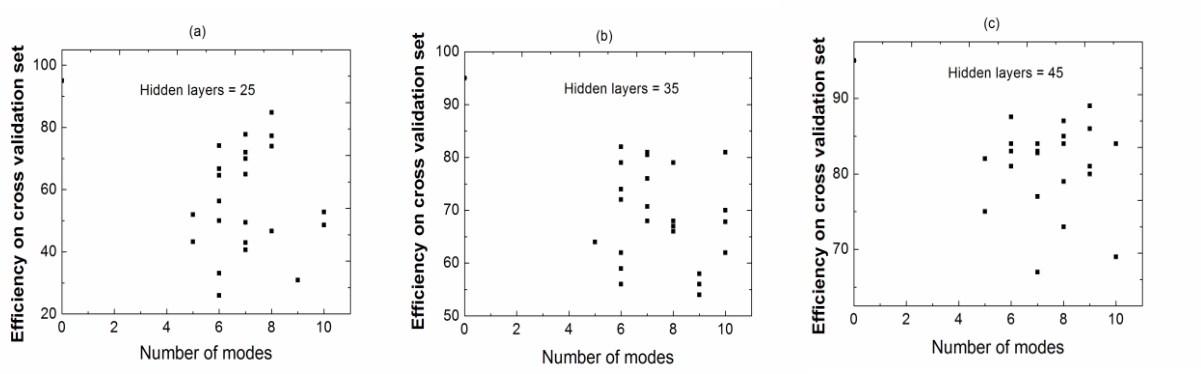

Figure 4.10 *Variation in prediction distribution of modes for (a) hidden layers = 25, (b) hidden layers = 35, (c) hidden layers = 45.*

and all with almost equal probability. When the coefficient is increased to 0.1 the efficiency over cross validation decreases by small amount but we can get predictions for 6 or 7 modes. Setting coefficient to 1 gives us bad efficiency as well as prediction which moves slowly towards under-fitting. Hence it is safe to conclude that regularization coefficient around 0.1 is a viable option.

(B) Number of hidden layers

Number of hidden layers is another way to achieve balance between under-fitting and over-fitting. Hidden layers determine the level of complexity of the curve. More the number of hidden layers, more is the complexity and vice versa [125]. Prediction distribution of modes for different number of hidden layers is shown in Fig. 4.10. For 25 and 35 hidden layers the predicted modes are 6. Whereas for 45 number of hidden layers neural network has predicted 6 to 9 modes with equal probability. Hence 25 number of hidden layers is optimized value. Decreasing the number of hidden layers further will lead to under-fitting which is not desirable.

(C) Number of image samples for training set

In the theory of neural networks, the most important feature for determining the learning of the network is the number of training examples. The training set should be such that it covers all possible outcomes and that too in proportion.

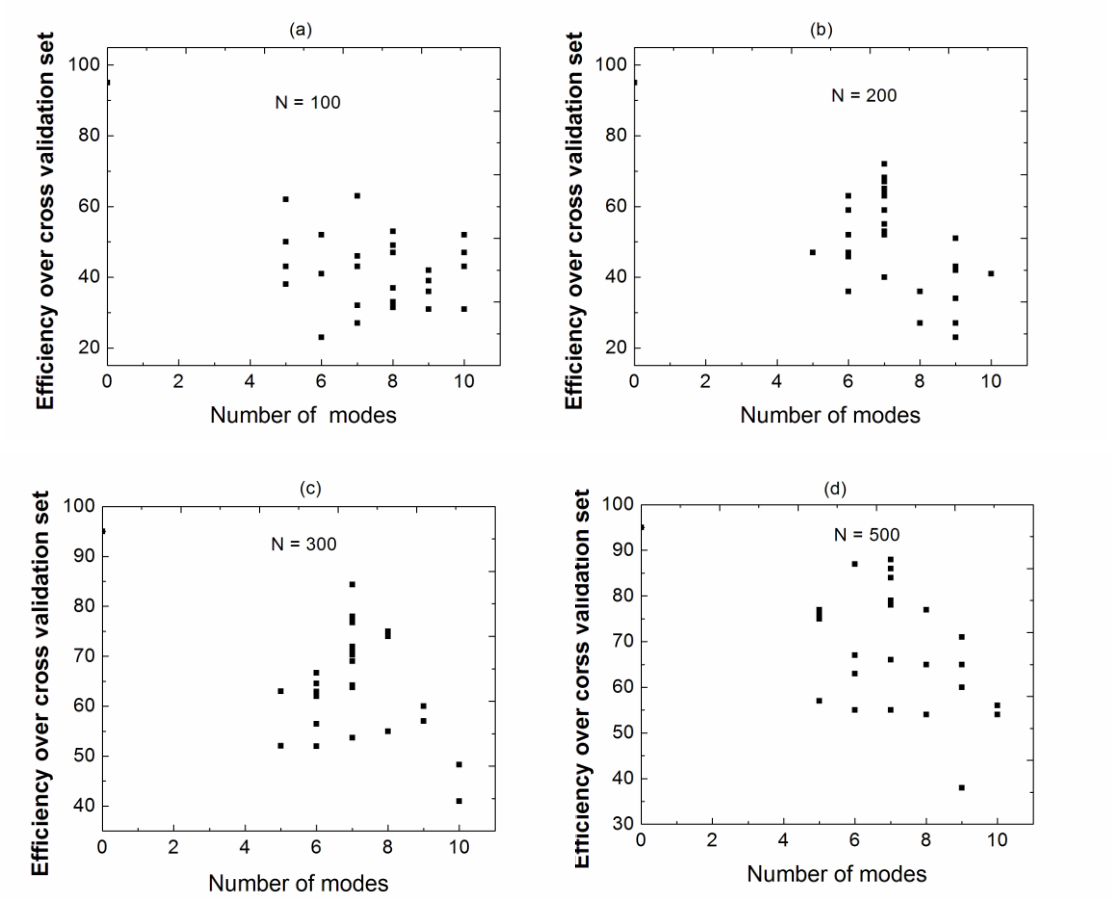

Figure 4.11 *Variation in prediction distribution of modes for (a) N = 100, (b) N = 200, (c) N=300, (d) 500.*

If number of images is too less than the neural network fails to learn the patterns. More number of images are always favorable for learning. Sometimes too many images may lead to two outcomes. If the variance is less then it may lead the neural network to learn as it would have learned with lesser number of images i.e. the outcome would be same with 500 image samples as oppose to 1000 samples. This may lead to slow execution of program by making the long learning process. If variance is more then there are chances of over-fitting [125]. In Fig. 4.11 prediction of modes for different number of image

samples has been plotted. It is observed that outcomes or the prediction for 500 images is just enough for our application. The outcomes of 300 images are similar, only with a low variance in efficiency and neural network predicts 6-7 number of modes. Increasing number of image samples above 500 may lead to either over-fitting or the network would learn nothing new. Thus we conclude that experimentally captured image consists of 6 or 7 modes at the exit end of the fiber and all other modes leaks out. If the fiber is having step index cladding instead of segmented cladding then fiber supports 20 modes. Segmented cladding of the fiber therefore helps in filtering out approximately 15 modes.

4.5 Conclusions

Development of technology for SCF fabrication in silica based glass has been reported. Three fiber samples having 4 segments and 0.43% relative index difference, with core/cladding diameters 45/125μm (without jacket), 30/80 μm (without jacket), and 30/80 μm with jacket have been fabricated. Fibers have been fabricated using Stack-and-Draw technique from a stacked preform with central silica core surrounded by eight alternatively arranged F-doped and undoped silica rods. Fabricated fibers were then characterized by launching He-Ne laser light and by measuring the output intensity patterns to check the beam quality at the exit end of the fiber. Neural network analysis has been done for prediction of number of modes at the exit end of the fiber and shows mode filtering effect**.** Segmented cladding of the fiber with jacket helps in filtering out of approximately 15 modes.

CHAPTER–5

Depressed Index Clad Fiber as a Highly Sensitive Low-Cost Refractive Index Sensor *

5.1 Introduction

Measurement of refractive index of various biological and chemical samples is important for detecting several physical and biological parameters. Optical techniques have several applications in biomedical fields, such as photodynamic therapy [126], functional imaging [127], optical biopsy [128] and laser-induced thermotherapy [129]. Light or laser beams are transported and distributed in biological tissues in all of these applications. When light enters a biological tissue or a chemical liquid, the optical properties of material like absorption coefficients, reflection, irradiance levels, and the scattering phase functions determine the light transmission and distribution. These properties strongly depend on the refractive indices of tissues or liquids. Also, the

* A part of the results presented in this chapter have been reported in a research publication:
Babita and Vipul Rastogi "Depressed Index Clad Fiber as a Highly-sensitive Low-cost Refractive Index Sensor", International Conference on Fiber Optics and Photonics, IIT Guwahati, Dec. 2010.

refractive properties of tissues reflect their structural organization, which can be used as an intrinsic marker for a disease. Therefore, to understand the light behavior in biological tissues and in chemical liquids, it has become imperative to have accurate data of the refractive indices of the tissues or liquids. The sensor community has**,** therefore**,** paid considerable attention towards the refractive index sensors. Optical waveguide sensors, based on optical fibers or planar waveguides, are widely used for this purpose. Several methods have already been reported for measurement of refractive index of various types of materials including bio-logical samples. Light refraction from turbid liquids is of great interest for many applications of science and technology specifically in area of physical chemistry [130]. However, only a few techniques have been reported on the measurement of refractive index of colloidal solutions. The conventional methods of measuring refractive index using Brewster angle and critical angle are not suitable for absorbing and turbid liquids [131]. For sensing the refractive index of a biological sample it is required to measure small variations in refractive index of liquid. Conventional bulk refractometers are inconvenient for such measurements. In view of the above there is a need for development of alternative refractive index sensors. An optical fiber refractive index sensor provides a good alternative for a compact lightweight and highly sensitive refractive index sensor. An optical fiber refractometer is also suitable for remote sensing and in otherwise inaccessible places. In addition, it can be used for sensing liquids or polymer composites. The amount of sample needed to carry out the measurement can also be very small. Currently, metal-fibers with metal coating employing surface plasmon resonances [25] and FBG are being widely studied as highly sensitive refractive index sensing devices for biological and chemical fields [30,31]. Tapering of fiber and stripping of the fiber cladding have also been used as another alternative for refractive index sensors [32, 34]. Long period grating (LPG) [37] and untapered fibers having thin film coating over full cladding [42] have also been used as refractive index sensors. Villatoro et al. have proposed a low cost optical fiber refractive index sensor based on core diameter mismatch [44]. The sensor has been formed by splicing a short section of single mode fiber (SMF) to a multimode fiber. Recently a low cost core diameter mismatch based sensor in a single-mode fiber has been reported [45]. The choice of technique employed is a tradeoff between fabrication cost, practicality, robustness, simple manufacturing processes, sensitivity, and sensing range.

Here we present an optical fiber sensor that combines simplicity, compactness, high resolution, low cost and competitive sensing range. The sensor is based on a depressed index cladding (DIC) type leaky fiber. Leakage loss in such fibers can be

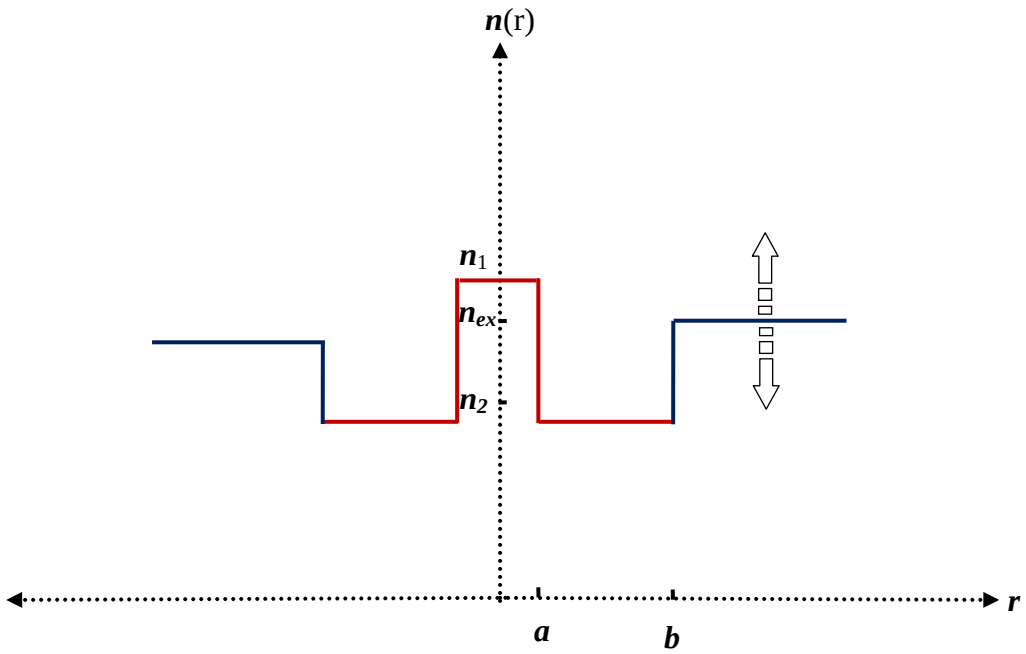

Figure 5.1. *The refractive index profile of the proposed DIC leaky fiber structure*.

highly sensitive to the variations in refractive index of the outermost leaky layer. We show that for a particular value of refractive index of the leaky layer there can be resonant leakage of power and one obtains a peak in a leakage loss curve as a function of refractive index. The regions near the peak can be utilized in designing a highly sensitive small-range refractive index sensor. The regions away from the peak are less sensitive to the variations in refractive index and can be utilized as larger range refractive index sensors.

5.2. Fiber Structure

The fiber which we have considered is SM-600 fiber but when we etch out some portion of the cladding of the fiber and put another medium having refractive index equal to or greater than the refractive index of core of the fiber, refractive index profile changes to refractive index profile of DIC type fiber as shown in Fig. 5.1 Where *a* is the core radius

and b defines the radius of the inner cladding of the fiber. n_1 and n_2 are the refractive

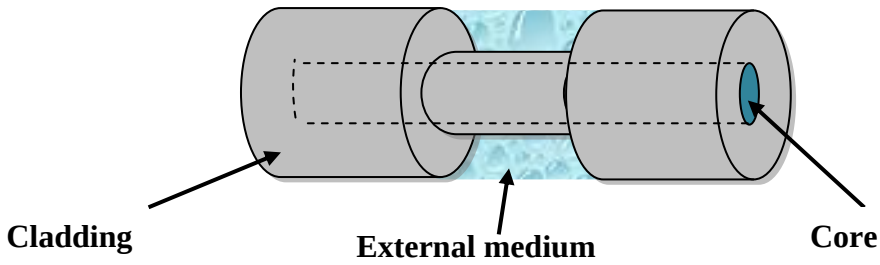

Figure 5.2. *Schematic representation of fiber sensor*.

indices of the core and the inner cladding of the fiber respectively. n_{ex} is the refractive index of the external medium and corresponds to the refractive index of the material to be sensed. The width of the outermost layer is assumed to be infinitely extended. Schematic representation of the sensor is shown in Fig. 5.2. In such a DIC fiber refractive index of outer cladding is equal to or higher than refractive index of core therefore modes of the fiber will not be perfectly guiding and will suffer from finite leakage loss. This leakage loss of the fiber can be calculated using transfer matrix method which is described in chapter 2 [86]. The sensing mechanism of the sensor is described in the next section.

5.3. Sensing Mechanism

In a single mode fiber power is confined in fundamental mode of the waveguide as

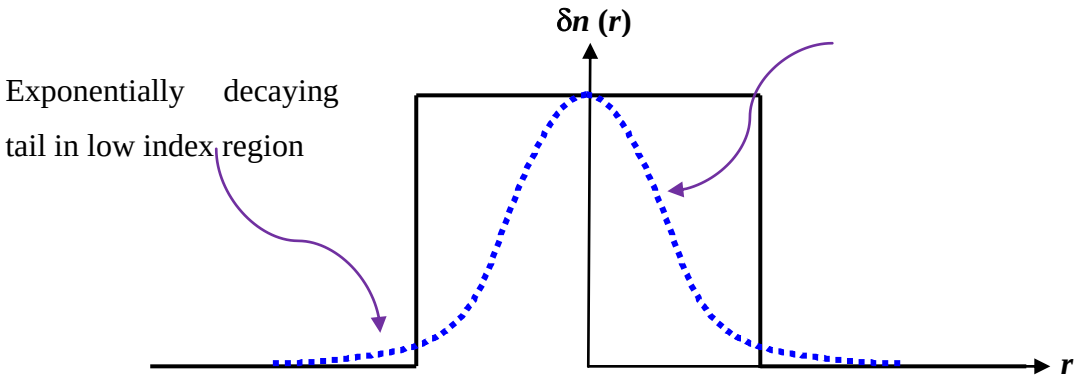

Figure 5.3. *Guided mode in waveguide.*

shown in Fig. 5.3 and mode is perfectly guiding. When some portion of cladding is removed and replaced by other medium the guided mode may become leaky if the

refractive index of the external medium is equal to or greater than that of the refractive index of the core of the fiber as shown in Fig. 5.4.

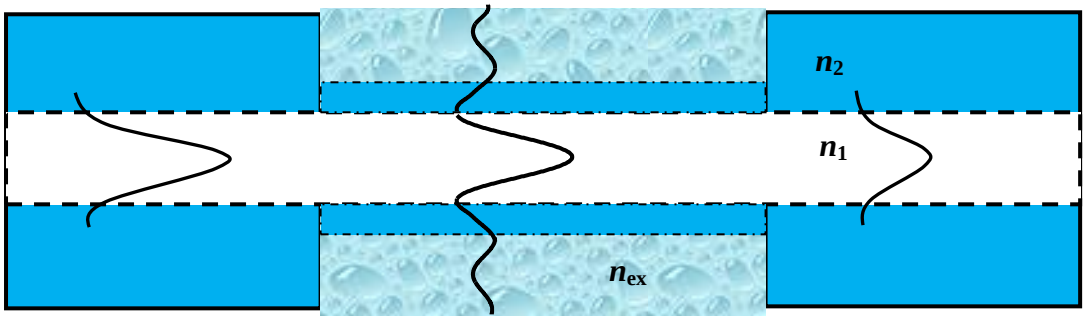

Figure 5.4. *Schematic representation of fundamental mode when an external medium having refractive index greater than or equal to core of the waveguide is placed.*

So when we remove the cladding portion of the optical fiber and put a high index material on it then its index profile will change and structure becomes leaky. Leakage of the power is highly sensitive to refractive index of external medium. This phenomenon can be used to sense the refractive index of the external medium. The guiding of the leaky modes only occurs over a fraction of a degree for in-coupling angle of the light for a given refractive index. This occurs when the angle of incidence is greater than the critical angle. At the same time, an evanescent wave is produced in the cladding of the fiber. The evanescent wave propagates parallel to the core-cladding interface, and decays exponentially from the interface. If the thickness of the inner cladding layer is comparable to the penetration depth of the evanescent field of the mode, tunneling of the power in the outer cladding of the fiber takes place. Any variation in the refractive index of the outer medium (n_{ex}) changes the amount of power it can trap and thus, changes the transmittance of the fiber. The structure can, therefore, work as a refractive index sensor. This tunneling of energy into the outermost region can be very strong for a particular value of n_{ex} due to resonance effect and the variation of transmittance of the fiber with n_{ex} near this value can be very strong. In this region the fiber can work as a highly sensitive refractive index sensor. As refractive index of the external medium increases, leaky modes are more confined and the leakage loss decreases. This region of higher refractive index can also be used for designing a refractive index sensor.

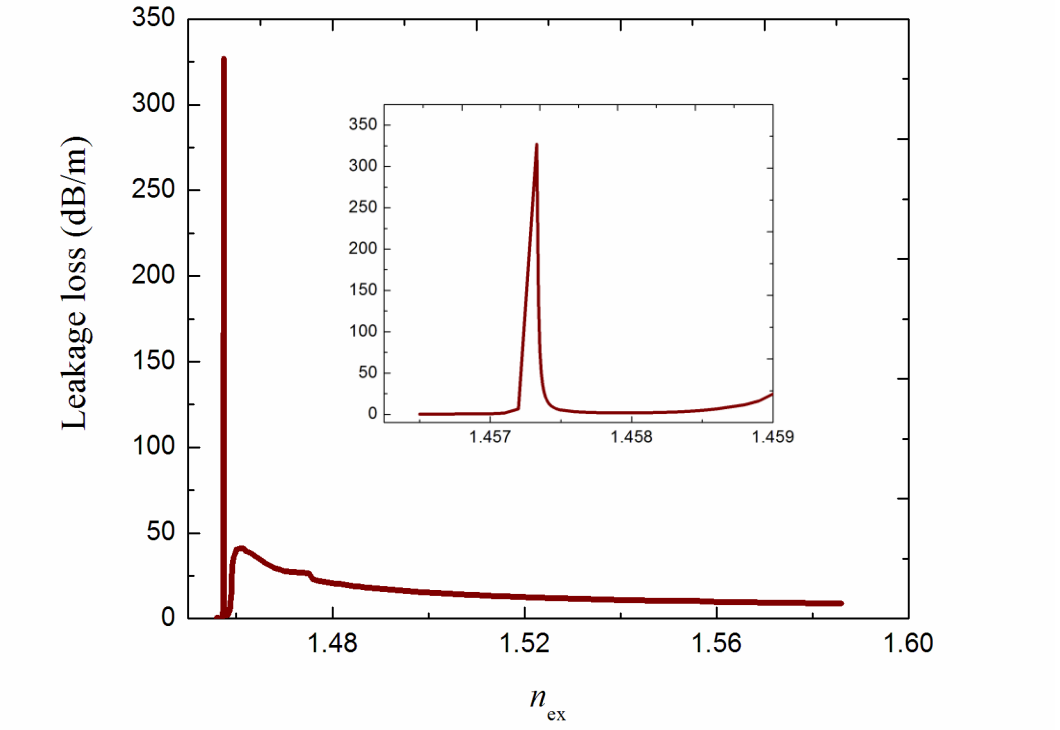

Figure 5.5. *Variation of leakage loss with the refractive index of the outermost layer*.

However, the sensitivity in the region is smaller. Sensitivity of the sensor is defined as $\Delta T/\Delta n_{ex}$ in units of dB/RIU and resolution of sensor is defined as value of Δn_{ex} that causes 1% change in transmitted power.

5.4. Results and Discussion

For numerical calculations we have considered a = 1.7 μm and cladding is etched down to b = 8 μm. The fiber is single-moded at 0.633 μm wavelength. To investigate the refractive index sensing characteristics of the fiber we have calculated the leakage loss of the fiber for different values of n_{ex} at 0.633 μm wavelength. The results are shown in figure 5.5. One can clearly see two resonance peaks. On zooming in the curve in relatively smaller range of n_{ex} shown in the inset we can see a clear strong resonance peak in the leakage loss curve. We have used different regions of this curve to exploit refractive index sensing potential of the structure for various applications. In this range the fiber works as a highly sensitive refractive index sensor. We have used different regions of the leakage loss curve to design high sensitive as well as low sensitive refractive index sensor. First we pick up the range 1.45735–1.45737.

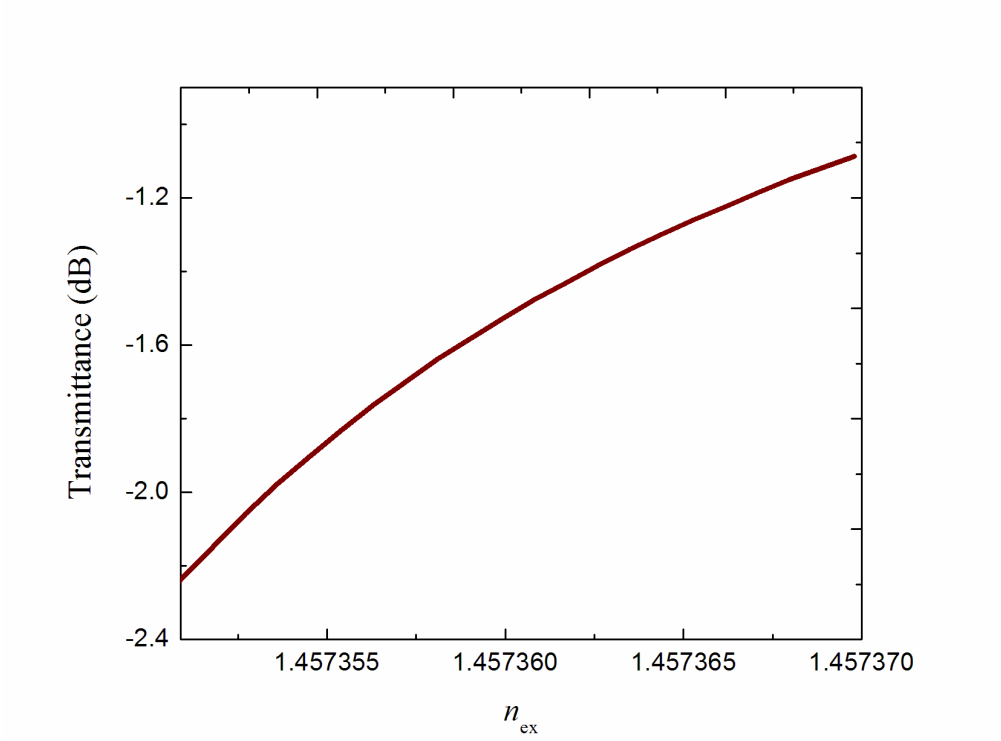

Figure 5.6 *Transmittance of the fiber as a function of* n_{ex} *in the range 1.45735-1.45737.*

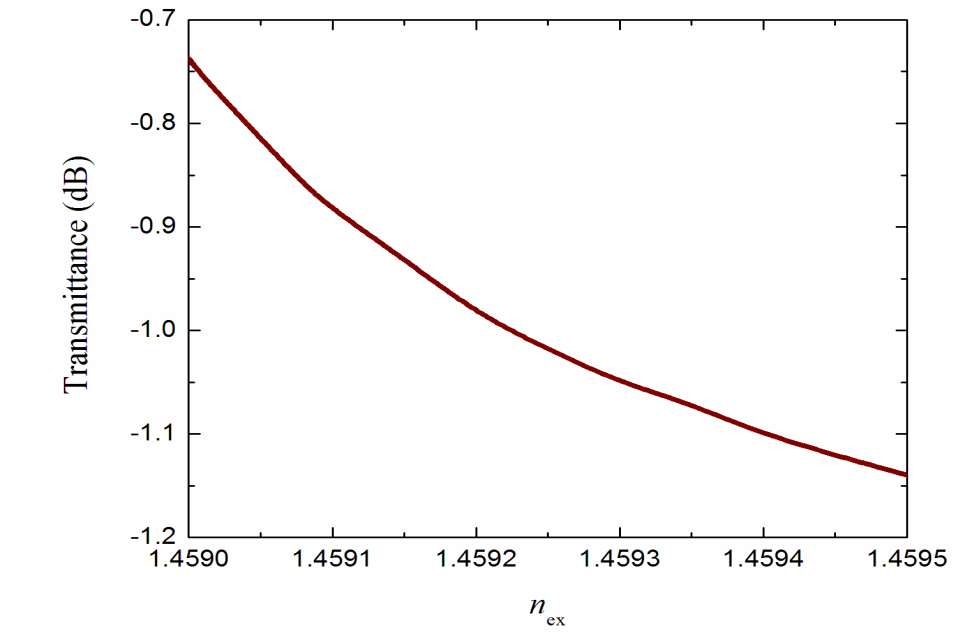

Figure 5.7 *Transmittance of the fiber as a function* n_{ex} *in the range 1.4590-1.45950.*

Variation of transmittance with n_{ex} for this range is shown in figure 5.6. and is almost linear therefore sensitivity will not vary much in this range. The sensitivity of the sensor in this range is 6.2 × 10^4 dB/RIU around 1.45736. This can be exploited to construct a refractive index sensor for jojoba oil in this range [132]. Ozone of liquid wax jojoba oil is used to control certain strains of diarrheas. A jojaba oil refractive index sensor can be

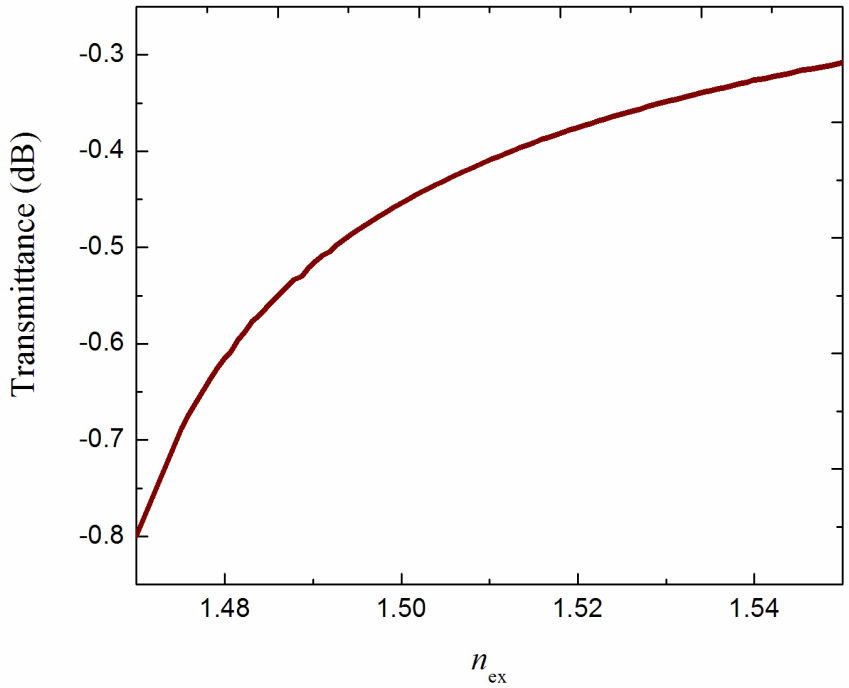

Figure 5.8 *Transmittance of the fiber as a function of* n_{ex} *in the range 1.47-1.55.*

useful in detecting any adulteration in the oil. This can also be used to sense refractive index of carbon tetrachloride [133]. Figure 5.7 shows the refractive index sensing characteristics of the fiber in the range 1.4590-1.45950. This range corresponds to the refractive index of mentha oil and the sensitivity within this range is 1.0 × 10^3 dB/RIU around 1.4592. The transmittance of the fiber decreases with n_{ex} in this range and the variation is also relatively small. The same fiber can also work for large-refractive index-range but with decreased sensitivity. Figure 5.8 shows the variation of transmittance of the fiber in the range 1.47–1.55. One can easily calculate from Fig. 5.8 that sensitivity within this range is 4.5 dB/RIU around 1.4590 and varies from 1.9 to 8.8 dB/RIU. This range can be utilized for sensing the refractive index of soybean oil, lipid membrane having cholesterol and lecithin mixture and glycerol [134].

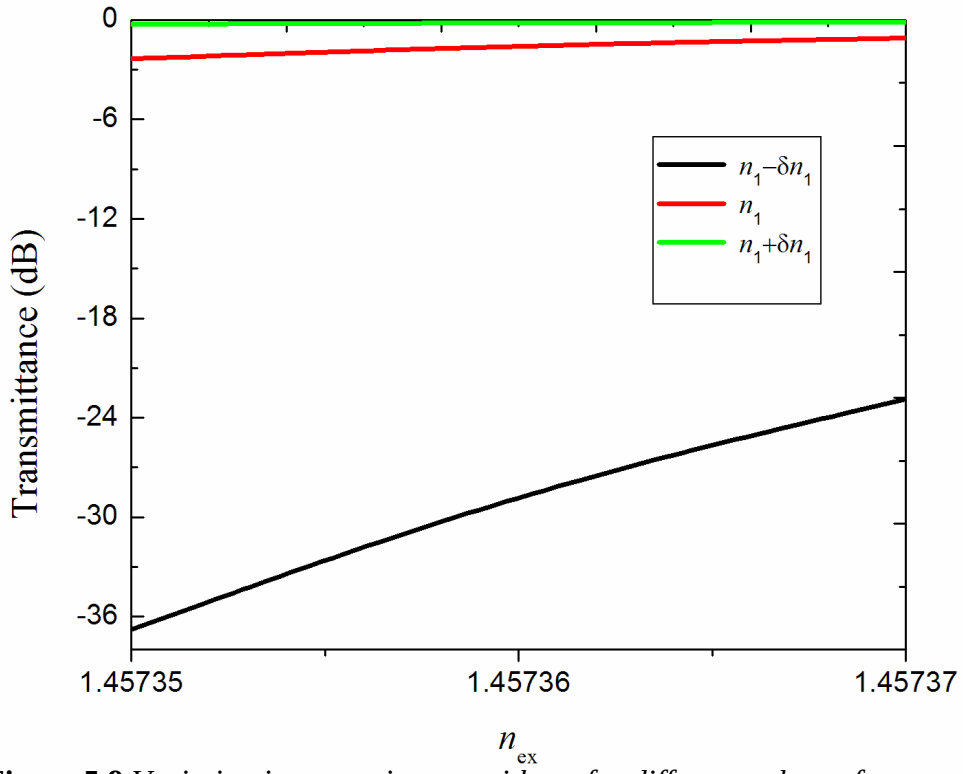

Figure 5.9 *Variation in transmittance with n_{ex} for different values of n_1.*

5.5. Sensitivity Analysis of the Structural Disorders on the Performance of the Fiber:

In previous sections we have studied that the proposed fiber structure acts a refractive index sensor with high sensitivity. To study how the imperfections introduced during fabrication of the fiber will affect performance of the fiber, we have carried out a study on the performance of the fiber with variation in fiber parameters. Performance of the fiber will be affected much by variation in core parameters of the fiber due to small core. Refractive index can be precisely controlled with precision 4×10^{-4} by MCVD (modified chemical vapor deposition technique) *b* of the fiber can be controlled very precisely by etching out the cladding carefully.

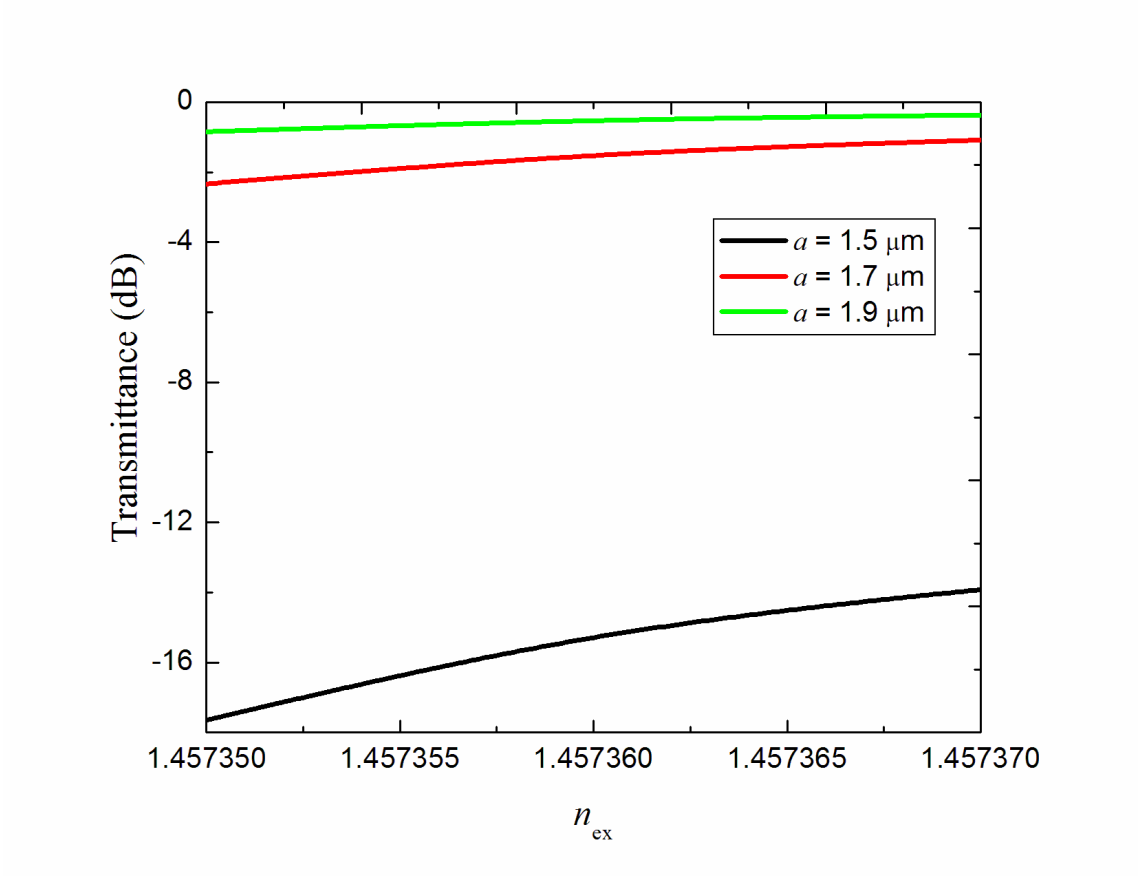

Figure 5.10. *Variation in transmittance with n_{ex} for different values of a.*

Therefore, we have studied impact of core parameters within the most sensitive range. To study effect of variation in n_1 we have calculated variation in transmittance with n_{ex} by varying n_1 by $\delta n_1 = 8\times10^{-4}$. We see from Fig. 5.9 that decreasing n_1 by δn_1 increases variation in transmittance where as increasing n_1 by δn_1 decreases variation in transmittance. Therefore increase in value of n_1 by δn_1 decreases sensitivity and decrease in value of n_1 by δn_1 increases sensitivity of the sensor. Maximum variation in sensitivity by increase in value of n_1 is -5.4×10^4 dB/RIU. Maximum variation in sensitivity by decrease in value of n_1 is $+6.3\times10^5$ dB/RIU. However the transmittance of the fiber decreases substantially. One would therefore require a highly sensitive detector and/or a powerful light source to operate the sensor. Variation in transmittance for different values of a is shown in Fig. 5.10. We see from Fig. 5.10 that decreasing a by 0.2 μm results in 1.2×10^5 dB/RIU increase in sensitivity whereas increase in value of a by 0.2 μm results in decrease in sensitivity by 3.8×10^4 dB/RIU.

5.6. Conclusions

The light transmittance characteristics of the DIC leaky fiber show that the fiber has good potential of refractive index sensing. The fiber can be fabricated by etching the cladding of an SM 600 fiber. We have investigated the transmission characteristics of the fiber by using the TMM and have shown that the leakage loss of the structure is highly sensitive to variations in refractive index of outer most region. As a result of these investigations we conclude that the fiber can be designed to sense the refractive index of various materials including jojoba oil, peppermint oil, mentha oil, soybean oil, cholesterol, lecithin mixture and glycerol. The proposed sensor is low-cost, highly sensitive, easy to handle and fabricate, and can be used with a small liquid volume. These features make the sensor useful for sensing refractive index of biological materials and chemical liquids.

CHAPTER–6

Planar waveguide based refractive index sensor*

6.1 Introduction

In the previous chapter we have studied optical fiber based refractive index sensor. But optical fiber based refractive index sensors are sometimes fragile in nature and are very difficult to handle. The fibers specially designed for this purpose are not cost effective because manufacturing process of an optical fiber is expensive. Integrated-optic sensors, therefore, have attracted rapidly growing interest. Various types of integrated-optic sensors have been reported in literature including interferometric [135-137], refractrometric [138], evanescent field [139], fluorescent or absorbance [140] based, and surface-plasmon resonance based sensors [141]. The choice of technique employed is a tradeoff between fabrication cost, practicality, robustness and simplicity of manufacturing process. Although some of the refractometric biosensing systems or sensors have been commercially successful but their use has been mostly limited to research laboratories due to their cost and complexity.

* A part of the results presented in this chapter have been reported in following publication:

Babita and Vipul rastogi, "Design and analysis of a low cost highly sensitive refractive index sensor", The XXIth International Workshop on Optical Wave & Waveguide Theory and Numerical Modelling, Enschede, The Netherlands, April 19-20, 2013.

In this chapter, we present a leaky planar waveguide based refractive index sensor. The sensing structure is a Teflon-Cytop-Teflon waveguide formed on a glass substrate. Any change in the refractive index of the external medium affects light guidance in the cytop layer and this forms the working principle of the sensor. We observe resonant coupling of power from cytop layer to the external medium (analyte) for a particular value of refractive index of the analyte. The sensor has high sensitivity around this value of refractive index. We have designed refractive index sensors for biochemical applications and have studied tolerance with respect to various design parameters.

6.2 Waveguide structure and method of analysis:

We have considered the waveguide structure as shown in Fig. 6.1. The waveguide structure has been formed on SiO_2 glass substrate of refractive index n_s. The width of the core of the waveguide having refractive index n_c is d. The core of the waveguide is surrounded by upper cladding and lower cladding having widths d_{uc} and d_{lc} respectively. The refractive index of upper cladding and lower cladding is n_2. The analyte is put on the top of the waveguide structure and is treated as external medium of refractive index n_{ex}. For the values of n_{ex} close to or greater than n_c, the structure becomes leaky. Hence some portion of the light propagating through waveguide is trapped by high refractive index material. So, we get a modulated output and by measuring the fraction of input power that comes out of the output end, we can find out the refractive index of the liquid. Transfer matrix method (TMM) has been used to analyze the structure [67]. Multilayer representation of planar leaky waveguide is shown in Fig. 6.2. To implement TMM, electric field in the p^{th} layer having refractive index n_p can be expressed as:

$$E_p = \begin{cases} A_p \cos k_p[x - d_{p+1}] + B_p \sin k_p[x - d_{p+1}]; & k_p^2 > 0 \\ A_p \cosh k_p[x - d_{p+1}] + B_p \sinh k_p[x - d_{p+1}]; & k_p^2 < 0 \end{cases} \quad (6.1)$$

Where $k_i = |\kappa_i|$, $\kappa_i^2 = k_0^2(n_i^2 - n_{eff}^2)$, and $k_0 = 2\pi/\lambda$ is free space wave number. $n_{eff} = \beta/k_0$ represents effective index of mode and β is propagation constant. A_p and B_p are arbitrary coefficients. A_p, B_p, A_{p+1}, and B_{p+1} are correlated by a 2×2 matrix:

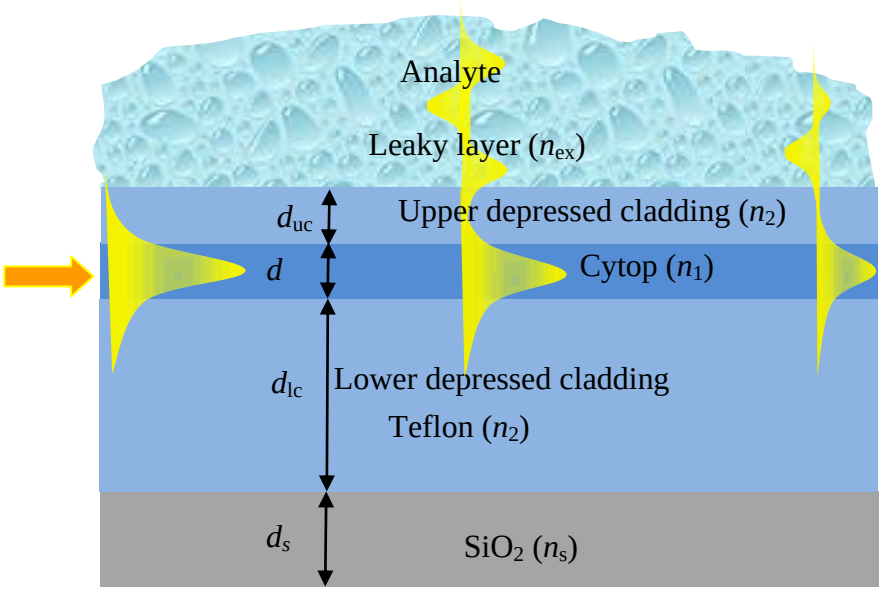

Figure 6.1 (a) *Schematic representation of proposed refractive index sensor.*

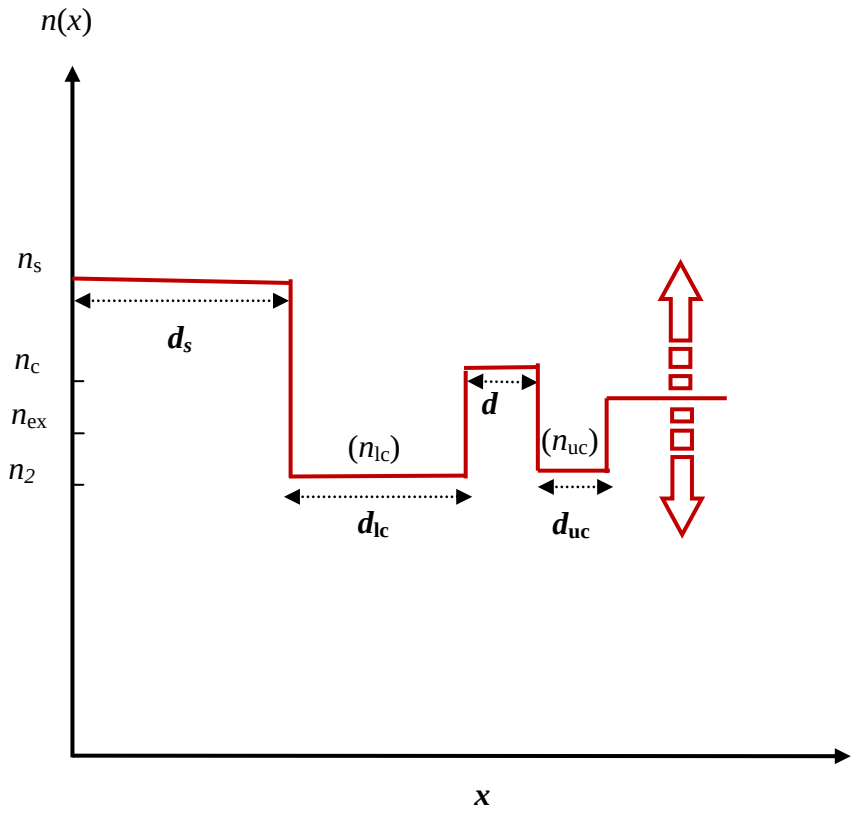

Figure 6.1(b) *Corresponding refractive index profile of waveguide employing variation in* n_{ex}.

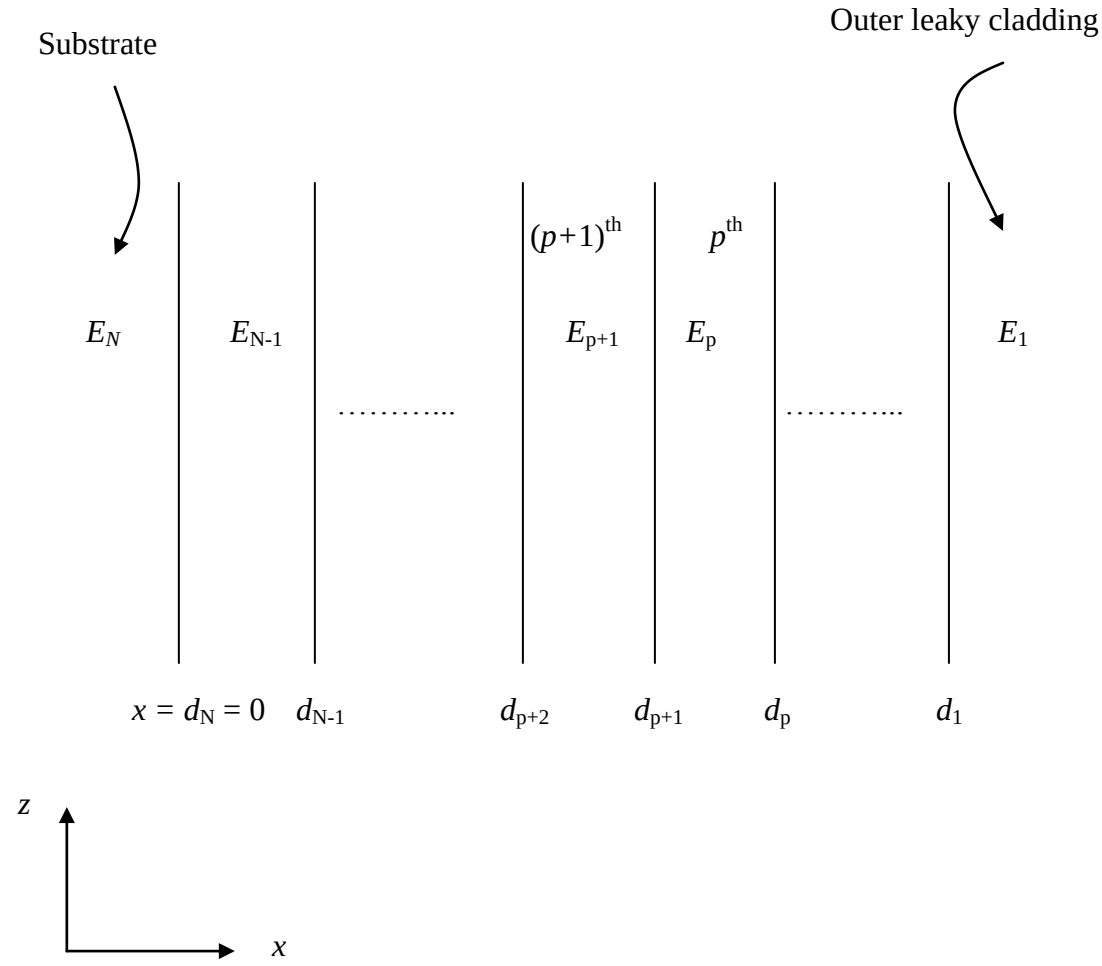

Figure 6.2 *Multilayer representation of the planar leaky waveguide.*

S_p for TE mode can be written as:

$$\begin{bmatrix} A_{p+1} \\ B_{p+1} \end{bmatrix} = S_p \begin{bmatrix} A_p \\ B_p \end{bmatrix} \tag{6.2}$$

$$S_p = \begin{pmatrix} \cos\Delta_{p+1} & -(\frac{k_p}{k_{p+1}})\sin\Delta_{p+1} \\ \sin\Delta_{p+1} & (\frac{k_p}{k_{p+1}})\cos\Delta_{p+1} \end{pmatrix}, \quad for\, k_p^2 > 0$$

$$= \begin{pmatrix} \cosh\Delta_{p+1} & (\frac{k_p}{k_{p+1}})\sinh\Delta_{p+1} \\ \sinh\Delta_{p+1} & (\frac{k_p}{k_{p+1}})\cosh\Delta_{p+1} \end{pmatrix}, \quad for\, k_p^2 < 0 \qquad (6.3)$$

Where $\Delta_p = k_p(d_p - d_{p+1})$. A_1, B_1, A_N, and B_N are interrelated by an appropriate matrix g which can be obtained by multiplying transfer matrices of all intervening layers:

$$\begin{bmatrix} A_N \\ B_N \end{bmatrix} = g \begin{bmatrix} A_1 \\ B_1 \end{bmatrix} \qquad (6.4)$$

Where $g = S_{N-1}S_{N-2}.....S_1$ and g is given as:

$$g = \begin{pmatrix} g_{11} & g_{12} \\ g_{21} & g_{22} \end{pmatrix} \qquad (6.5)$$

For leaky waveguide, in the high-index outermost region only the outgoing wave exists and in the low index region no amplifying term is allowed. These conditions lead to $A_1 = iB_1$ and $A_N = -B_N$. From Eq.(6.4) and Eq.(6.5), one can get:

$$A_N = [g_{12} + ig_{11}]B_1 \text{ and } B_N = [g_{22} + ig_{21}]B_1 \qquad (6.6)$$

Equating A_N and $-B_N$ from Eq. (6.6), gives an eigenvalue equation in terms of β, i.e. $G(\beta) = 0$. In general, β consists of real part as well as imaginary part and can be represented as: $\beta = \beta_r + i\beta_I$ where β_r is real part and β_I represents imaginary part. β_r and β_I can be calculated by drawing a plot between $1/|G|^2$ and β, which consist of resonance peaks in lorentzian shape. Each resonance peak corresponds to propagation constant of a mode. β_r can be calculated by the value of β corresponding to resonance peak and β_I can be calculated by FWHM of the resonance peak. β_r gives effective index of the mode and β_I leakage loss of the mode. Variations in values of n_{ex} results in change in leakage loss which corresponds to change in output power.

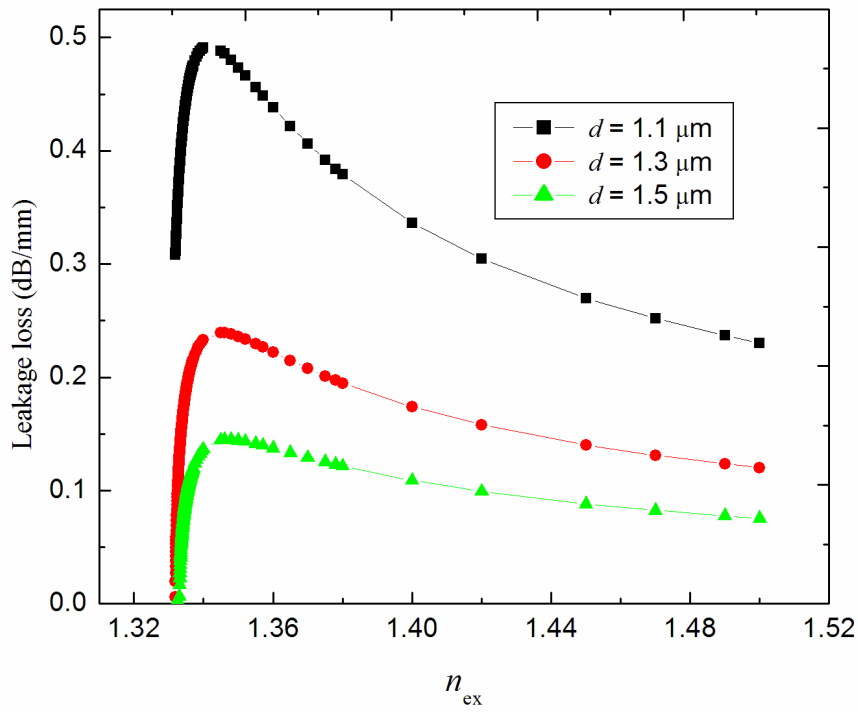

Figure 6.3 (a) *Variation in leakage loss of the TE_0 mode with n_{ex}* for *different values of guiding film thickness d.*

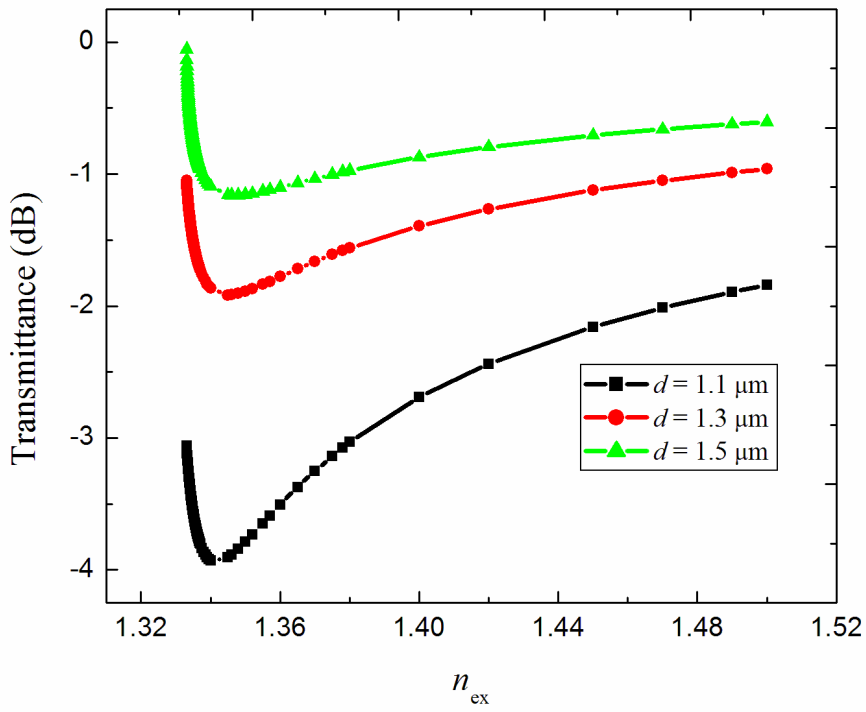

Figure 6.3(b) *Corresponding transmittance for 8 mm length of the sample.*

The sensitivity of the sensor is defined as $\Delta T/\Delta n_{ex}$ in the units of dB/RIU and the resolution of the sensor is defined as the value of Δn_{ex} that causes 1% change in transmitted power.

6.3 Numerical results and discussion:

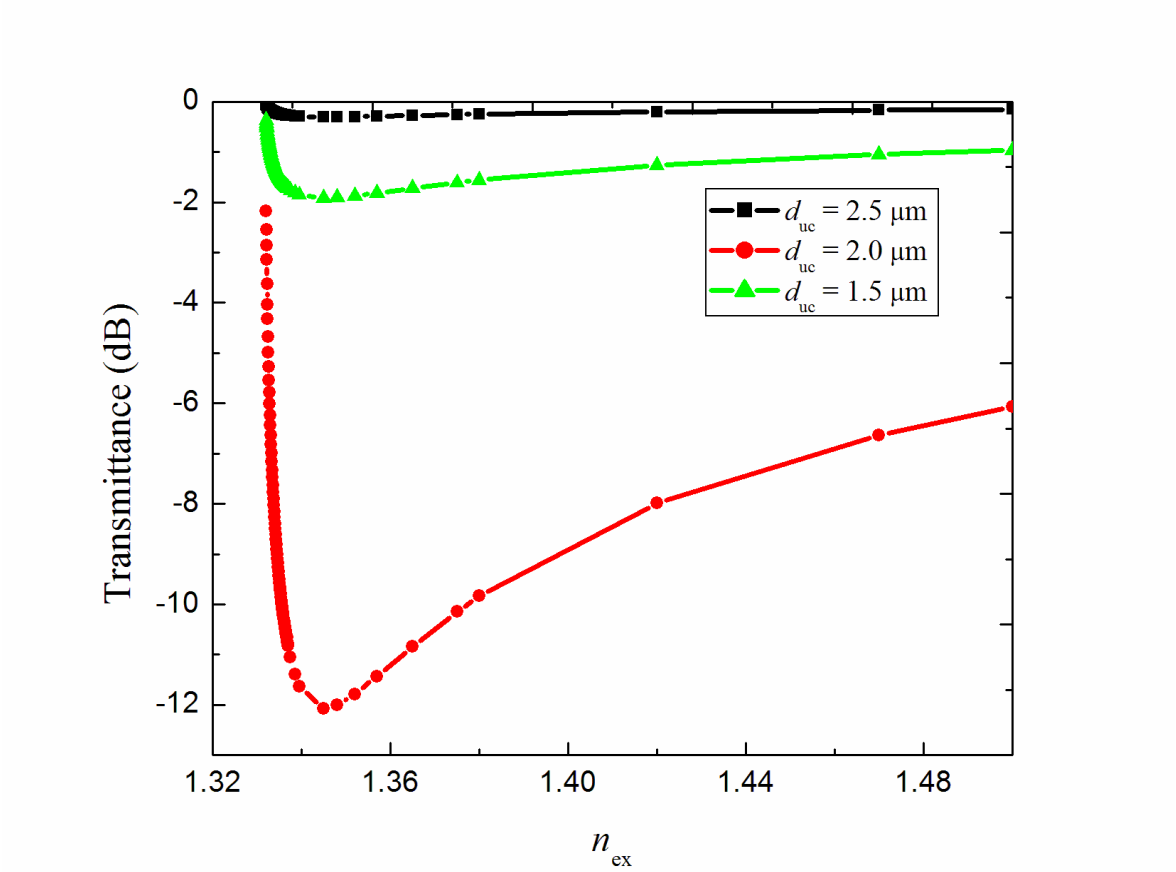

Figure 6.4 *Variation in transmittance as a function of* n_{ex} for different values of d_{uc}.

We have carried out numerical simulation for the following parameters:
n_s= 1.45, n_c = 1.3395, n_2 = 1.319, d_{lc} = 20 μm, d =2.0 μm, d_{uc} = 1.3 μm, wavelength = 0.633 μm. Refractive index of external medium is n_{ex}. The structure can be easily fabricated by using the cost-effective spin coating technique. We have taken glass as a substrate, on which polymers can be deposited. The refractive index of lower cladding having refractive index n_2 can be realized by spin coating teflon and core of the waveguide can be realized by depositing cytop. Cytop has high chemical resistance therefore it can be spin-coated with a large variety of optical polymers for realizing high-index-contrast planar waveguide. Cytop and teflon are suitable materials for optical waveguide because they can be made into well controlled submicron structures

and have low optical absorption loss; in addition these are easily available cost effective polymers. Sensing can be realized by putting analyte on the waveguide as the external medium and by measuring corresponding change in output power. This change in output power will indicate the change in refractive index of the external medium, n_{ex}. In Fig. 6.3 (a), we show the dependence of leakage of the power on n_{ex}. The guiding of leaky modes occurs over a fraction of a degree for in-coupling angle of the light for a given refractive index. This occurs when the angle of incidence is greater than the critical angle. The evanescent wave propagates parallel to the core-cladding interface, and decays exponentially from the interface. The penetration depth of evanescent wave into the sample increases with wavelength. Human tissue and cells have low absorption loss between 0.6 and 1.2 μm, the so called therapeutic zone for laser treatment. Therefore, while designing the sensor one should take into consideration the wavelength as well as availability of the source. We have designed this sensor at 0.633 μm wavelength. Fig. 6.3 (a) shows the variation in leakage loss of the TE_0 mode as a function of refractive index of the analyte for different thicknesses of core radius and Fig. 6.3 (b) shows the corresponding transmittance for 8 mm length of the sample. We can see from Fig. 6.3 (a) that the resonant coupling of power to the test sample occurs at $n_{ex} = 1.345$. The sensitivity also depends on the upper cladding width d_{uc}. Therefore, we have optimized width of upper cladding of the waveguide also. Variations in transmittance of the fundamental mode with n_{ex} for different values of d_{uc} is shown in Fig. 6.4. Resonant coupling of power from core of the waveguide to analyte takes place for a particular value of d_{uc} which is 2 μm. Therefore 2.0 μm is the optimal value of d_{uc}. We have exploited different portions of the transmittance curve to design the sensor with different resolutions and for different refractive index ranges.

6.4 Applications:

The sensor can be used for sensing the refractive index of various biological and chemical liquids. Fig. 6.5 shows that in the range $1.33195 < n_{ex} < 1.33469$ sensitivity of sensor varies from 1.1×10^3 to 1.74×10^4 dB/RIU. This range can be used to sense refractive index of the following biological and chemical test samples:

(a) **Monitoring Refractive index of Proteins:**

Protein is an essential nutrient made up of building- block chemicals called amino acids. A total serum test measures the total amount of protein in the blood and also measures the two main groups of proteins called albumin and globulin. Measurement of concentration of proteins may detect liver disease, nutritional state, kidney disease and others. Low total protein levels can suggest a liver disorder, a kidney disorder or disorder in which protein digestion does not take place. High level of total protein can be seen with infections such as viral hepatitis or HIV. Therefore detection of level of protein is important for diagnosing various diseases. Importance of rapid detection of concentration of serum proteins in emergency has long been recognized. Greatly increased amounts of bilirubin or fats in serum alter the refractive index values in relation to concentrations of proteins [142]. Therefore by measuring the change in refractive index of the proteins we can detect the level of proteins and can detect the disease. We can sense refractive index of above mentioned proteins within this range with sensitivity in the range 1.1×10^{3} to 1.74×10^{4} dB/RIU.The sensitivity of the sensor

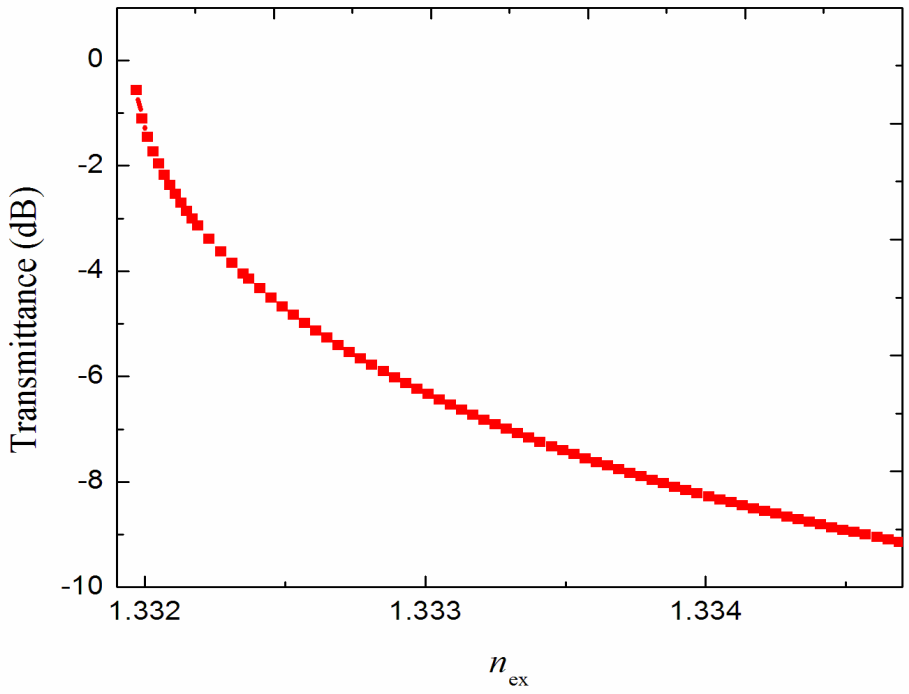

Figure 6.5 *Variation in transmittance as a function of n_{ex} in the range 1.33195-1.33469.*

around n_{ex} = 1.333 is 2.74×10^3. This sensitivity corresponds to 1% change in transmittance and can be increased by using more sensitive detectors. We can sense the refractive index of serum, globulin, albumin and edestine by preparing the solution having refractive index within the range 1.33195 to 1.33469 [143].

(b) **Monitoring Glucose concentration in blood**:

Millions of people in world are suffering from diabetes. A technique for monitoring blood sugar (d-glucose) will be of great interest. There are various techniques for estimating the glucose level in blood. One of the techniques is by measuring the change

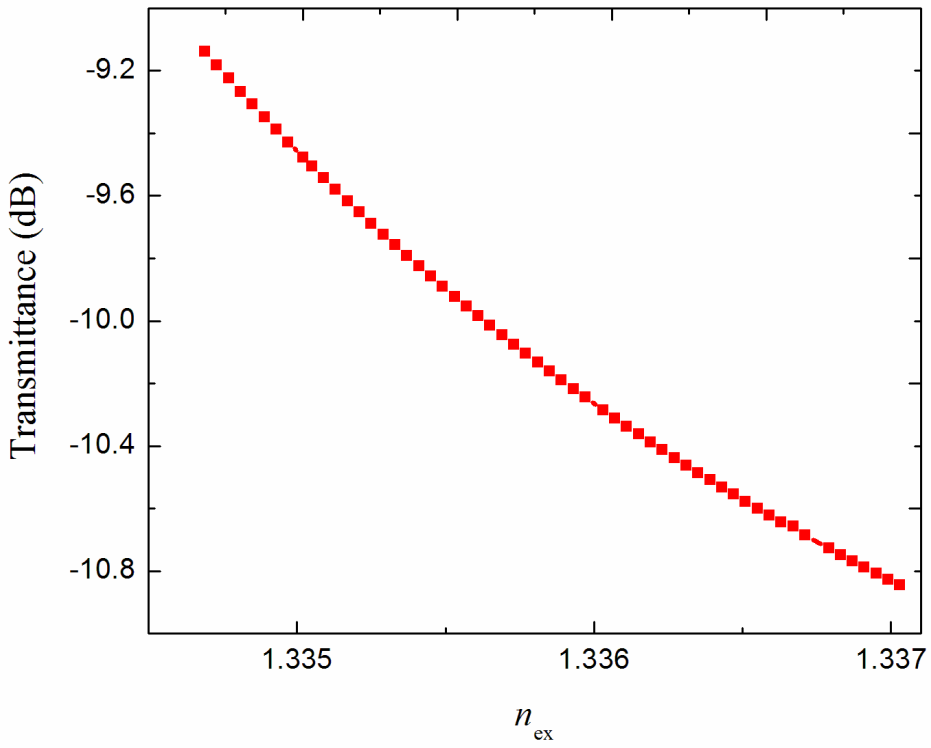

Figure 6.6 *Variation in transmittance as a function of n_{ex} in the range 1.33469-1.33703.*

in refractive index of blood. The refractive index of sugar solution changes with concentration of sugar. Sugar concentration changes from 0.1% to 0.3% (the range for diabetes) results in refractive index changes from 1.3334 to 1.3337. Proposed sensor can detect changes in the refractive index in the range 1.33195 to 1.33469 with sensitivity of 2.74 $\times10^3$ dB/RIU and hence can be used for monitoring glucose concentration in blood [144].

(c) **Testing water adulteration:**

Refractive index of water at 633 nm is 1.3321 at 20^{o}C [145]. Any impurity in water changes its refractive index. A refractive index sensor with right resolution can therefore be used for testing adulteration in water.

(d) **Monitoring salt concentration:**

Small concentration of salt in water can be sensed using this sensor. Addition of small quantity of NaCl increases the refractive index of solution. 1 gm/100 ml solution has refractive index 1.3310 and solution of 3 gm/100 ml concentration has refractive index 1.3340 [146]. Proposed sensor is suitable for monitoring low concentration of salt solution with sensitivity of 2.74 $\times 10^{3}$ dB/RIU.

(e) **Monitoring sucrose concentration:**

We can monitor very small concentration of sucrose solution in water. We can monitor solution of up to 3 gm/100 ml water. Refractive index of solution for concentration range 0-2 gm/100 ml varies from 1.3310 to 1.3346 [146]. This range is

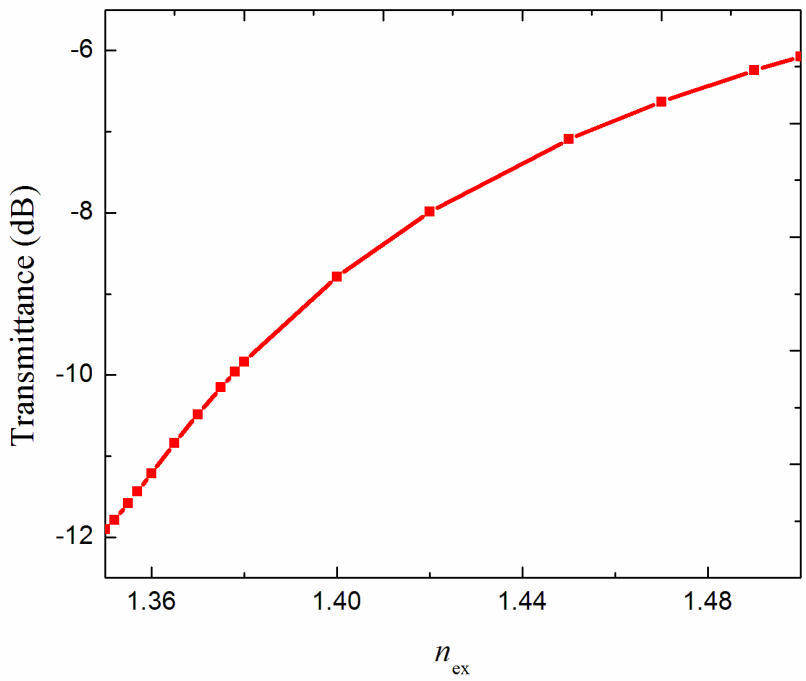

Figure 6.7 *Variation in transmittance as a function of n_{ex} in the range 1.35-1.50.*

good for sensing small concentration of sucrose in water but with high accuracy. The same sensor works in the range 1.33469 - 1.33703 also. The sensitivity of the sensor in

this range is 7.1×10^2 dB/RIU as can be seen from Fig. 6.6. High concentration of glucose in blood, high concentration of sucrose solution and NaCl solution can be sensed in this range [146]. This sensor can also work for large range of n_{ex} (1.35 to 1.5) with lower sensitivity. Variation in transmittance with n_{ex} in this range is shown in Fig. 6.7. The sensitivity of the sensor with in this range is from 6.9 to 39.9 dB/RIU. This region can be used for the applications where less sensitivity is required.

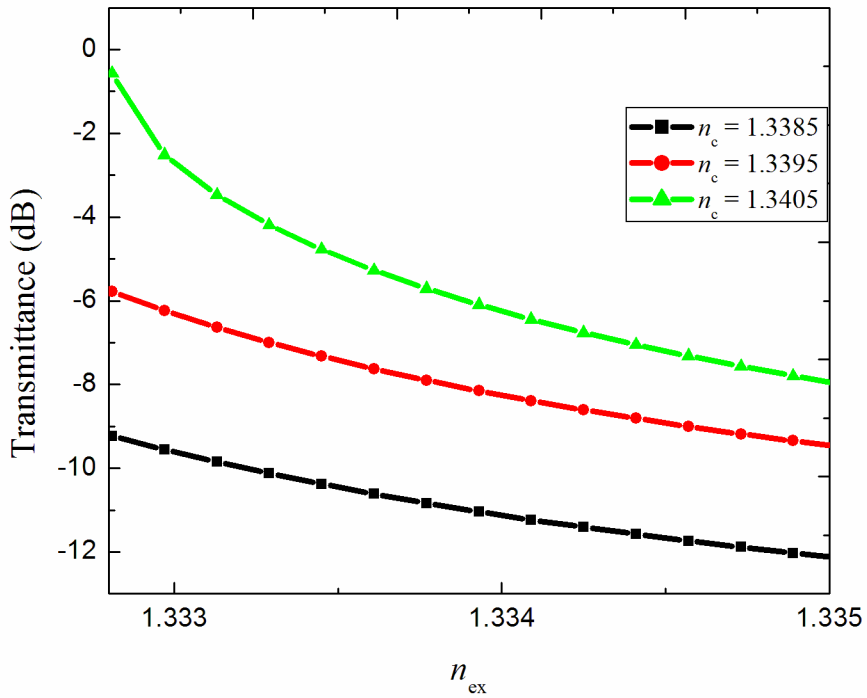

Figure 6.8 *Tolerance study of refractive index of core of the waveguide.*

6.5 Tolerance study

In previous sections we have numerically demonstrated that the proposed waveguide structure acts as a good refractive index sensor. To study how the imperfections introduced during the fabrication will affect the performance of the waveguide, we have carried out a study on the performance of the sensor with variations in the values of various waveguide parameters. Widths of different layers of the considered structure can be controlled at submicron level using standard fabrication technology.

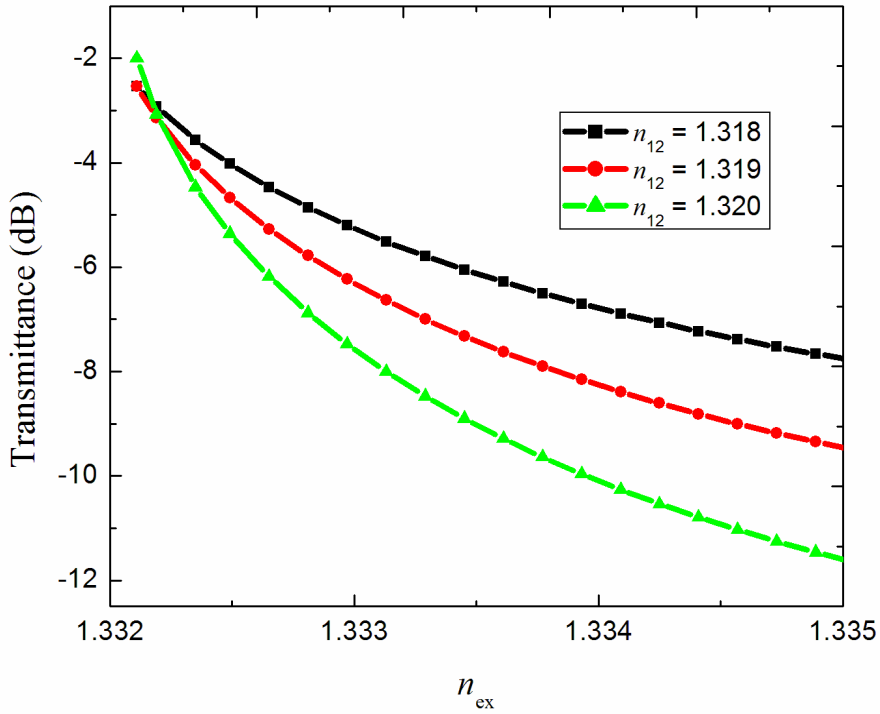

Figure 6.9 *Tolerance study of refractive index of upper cladding of the waveguide.*

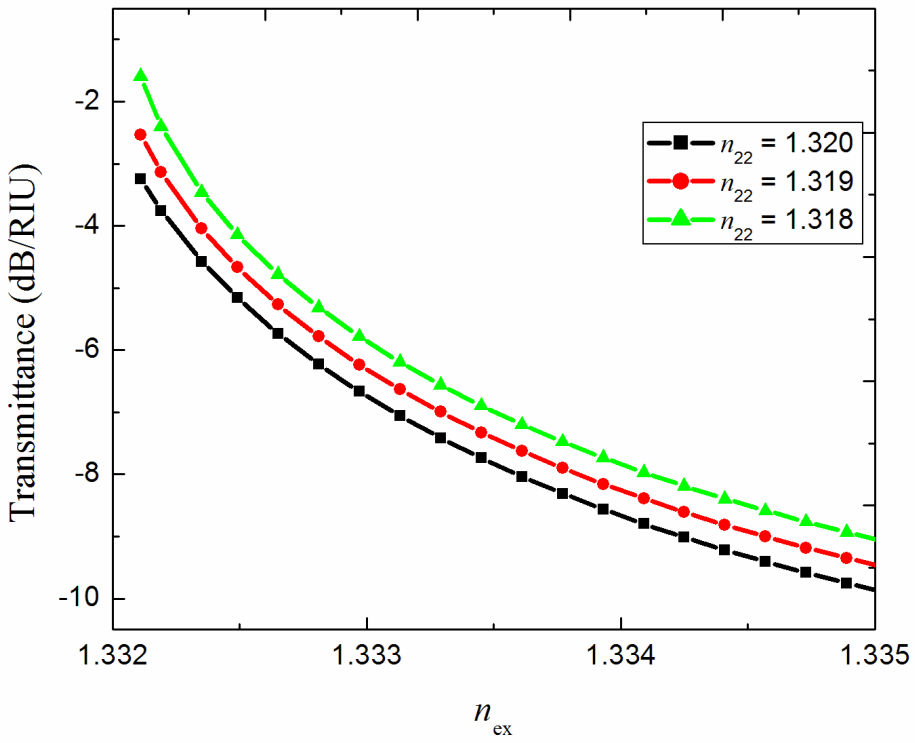

Figure 6.10 *Tolerance study of refractive index of lower cladding of the waveguide.*

However the control of refractive index is bit difficult. Therefore, we have studied the effect of variations of refractive index of the layers of the waveguide on the transmittance curves of the structure in the most sensitive range (1.332-1.335). Refractive index of the substrate of the waveguide does not affect the leakage loss of the waveguide as the width of the lower cladding is much larger than the penetration depth of evanescent field of the waveguide. Refractive index for polymers cytop and Teflon can be precisely controlled down to 10^{-3} to 10^{-4}. Firstly we have varied n_c by an amount $\delta n_c = \pm 1\times10^{-3}$ and results are shown in Fig. 6.8. One can observe that variation in n_c by $\delta n_c = +1\times10^{-3}$ results in maximum variation in sensitivity by $+2.1\times10^{3}$ dB/RIU and $\delta n_c = -1\times10^{-3}$ results in maximum variation in sensitivity by -9.6×10^{2} dB/RIU. To study effect of variation in refractive index of lower cladding and upper cladding we have represented refractive index of upper clad as n_{uc} and refractive index of lower clad as n_{lc}. The analogous study has also been carried out for variations in parameter n_{12} of the waveguide and results are depicted in Fig. 6.9. One can see from the Fig. that varying δn_{uc} by $+1\times10^{-3}$ results in maximum $+3.7\times10^{3}$ dB/RIU variation in sensitivity and variation in δn_{uc} by -1×10^{-3} results in maximum variation in sensitivity by -2.3×10^{3} dB/RIU . We have also studied the effect of deviations ($\delta n_{lc} = \pm1\times10^{-3}$) in n_{lc} also. One can observe from Fig. 6.10 that $\delta n_{lc} = \pm1\times10^{-3}$ results in negligible variation in sensitivity of the sensor. From the above discussion we can say that the imperfections created during fabrication of the waveguide will not affect the performance of the waveguide significantly.

6.6 Conclusions

A planar waveguide structure has been presented for realizing integrated optical sensor based on leakage loss of the waveguide. The output light of the single mode planar waveguide is shown to be a sensitive indicator of the refractive index of the chemical or biological sample which is put on the waveguide as an external medium. The most conspicuous advantages of this approach are: high sensitivity, low cost, robustness, simple manufacturing process, easy to handle, large sensing range, small volume of test sample, minimal space and power requirement. The same sensor can work for short as well as large refractive index sensing range with varying sensitivity. These features make the sensor attractive for sensing refractive index of various biological and chemical samples

CHAPTER–7

Multilayer Leaky Structure for Organic Light Emitting Diodes

7.1 Introduction

Opto-electronic devices made of organic materials have been of interest because such devices are relatively inexpensive in comparison to the devices made of inorganic materials. Organic materials are easy to fabricate on flexible substrate because of their inherent property. Organic opto-electronic devices include organic light emitting diode, organic solar cells, organic transistors, organic photovoltaic cells, organic photodetectors. In case of OLED, organic materials have advantage that the wavelength at which an organic emissive layer emits light can be easily tuned with appropriate dopants. Organic light emitting diodes (OLED) have been of interest recently because of their potential applications in flat panel displays, illumination, domestic solid state lighting etc. Radiative decay of molecular excited state is responsible for light generation mechanism in organic light emitting devices. But a large fraction of light is lost inside the device because of different mechanisms. A large fraction of generated light approximately 40% is coupled to surface Plasmon polaritons generated at metal/organic interface and is lost [53]. Due to total internal reflection at glass/ITO interface 15% of the light is lost in guided modes. Approximately 23% of generated photons are lost at substrate/air interface by total internal reflection. Roughly 20% of generated photon in organic layer is extracted out from the device. Many approaches

have been reported in literature to increase the performance of OLED. The ratio of total number of photons generated in organic layer to the number of injected electrons defines the internal quantum efficiency of OLED which is only 25%. However the internal quantum efficiency of OLEDs can be achieved near 100% by harvesting both singlet as well as triplet excitation states using electrophosphorescent materials. External quantum efficiency of the device is defined as the number of generated photons coming out of the device per number of photons generated in the device. Approximately 80% of the generated light has been lost in the wave-guided modes generated due to glass substrate/ITO, substrate/air interface and due to coupling to surface plasmons at metal/organic interface. To extract power from waveguide modes and to increase the extraction efficiency of OLED various approaches have been reported. Back texturing of the glass substrate can suppress propagation of light in substrate modes and can lead to increase in extraction efficiency [54]. High index substrate can also be used to increase extraction efficiency [55]. However, high index substrate can lead to high index contrast between substrate and air. Micro lenses and periodic micro structures can also be inserted to couple the guided modes to useful power radiations [53-59]. However the process to fabricate micro-lenses and periodic structures is not so simple and may not be practical. Another important technique to out couple the guided modes is grating coupler method where a grating is used to circumvent refractive index mismatch which prohibits the coupling of external to guided modes [60]. Patterned ITO electrode coated with PEDOT: PSS a low index polymer also results in increase in external quantum efficiency. The patterning of ITO has been done using photolithographic steps or micro-contact printing. To improve efficiency of OLED low index materials grids have been inserted at ITO/organic layer interface to redirect the light confined at this interface towards the substrate normal [61,62]. Standard photolithographic method has been used to embed these grids at ITO/organic layer interface. Insertion of aerogel layer between glass and ITO in conventional OLED structure can avoid coupling of power to substrate modes [63]. Significant enhancement in external quantum efficiency has been observed. But this method is accompanied by change in radiation pattern and exhibits an undesirable angle dependent emission spectrum and also involves complex processing methods. . The choice of technique employed is a tradeoff between fabrication cost, practicality, robustness, and simplicity of manufacturing processes. Here we numerically

demonstrate an enhancement of out coupling efficiency by using a uniform teflon layer inserted between glass and ITO. This layer helps in leakying out power into the glass substrate, which is eventually available for extraction.

7.2 Proposed Structure and Method of Analysis

If we consider the whole structure of OLED as a waveguide having refractive index profile as shown in Fig. 7.1 (a) and schematic representation is shown in Fig. 7.1 (b). In an optical waveguide guided modes are formed by sandwiching a high index layer between two low index layers. The modes are confined in the high index layer and very small power is extended into the low index regions. If one introduces a high index layer on the waveguide then waveguide light can be trapped by the high index region because of frustrated total internal reflection and in terms of ray theory and leaky modes in terms of wave theory. Leaky modes can carry large amount of energy into high index region and then radiate out as shown in Fig. 7.2. The amount of leakage of power into the high index region can be controlled by various waveguide parameters. In case of an OLED most of the power is confined into the guided mode of ITO layer. These modes travel in lateral direction and the light coupled in these modes comes out of the sides of the device and does not contribute to the emission of OLED. If we put an appropriate layer of low index material between glass and ITO then because of frustrated total internal reflection mode can be coupled to the glass substrate and can be radiated out by some special mechanism at glass surface. This low index polymer layer can be of Teflon polymer and can be deposited using spin coating technique. Teflon is a suitable material for optical waveguide because it can be made into well controlled sub micron structures and has low absorption loss. In addition it is easily available cost effective polymer. We have carried out numerical simulation for the OLED design shown in Fig. 7.1. Refractive index profile is shown in Fig. 7.1(a). There are many techniques to calculate characteristics of the structure and can mainly be divided into three main schemes: (1) The radiant molecule in emissive layer are considered as oscillating dipole antennas and classical approach can be used to calculate far field radiation of these dipoles. (2) Another one is quantum mechanical approach where sum of eigen modes represent the total electromagnetic field of OLED and Fermi golden rule is used to calculate the transition probability of these modes.

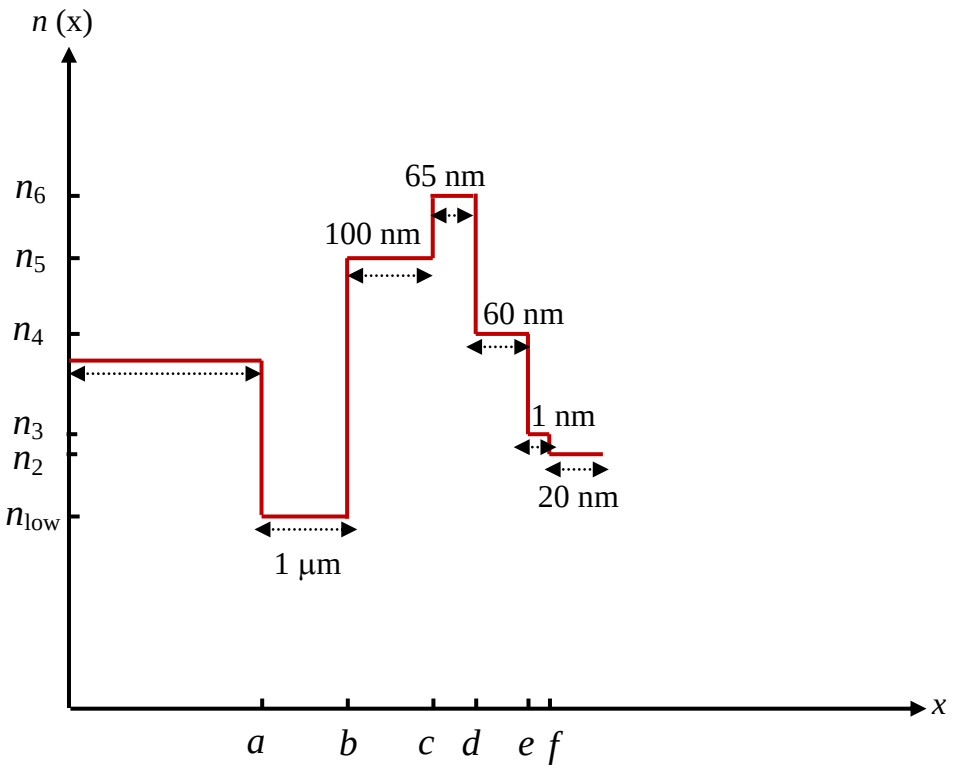

Figure 7.1 (a) *Refractive index profile of OLED stack structure*

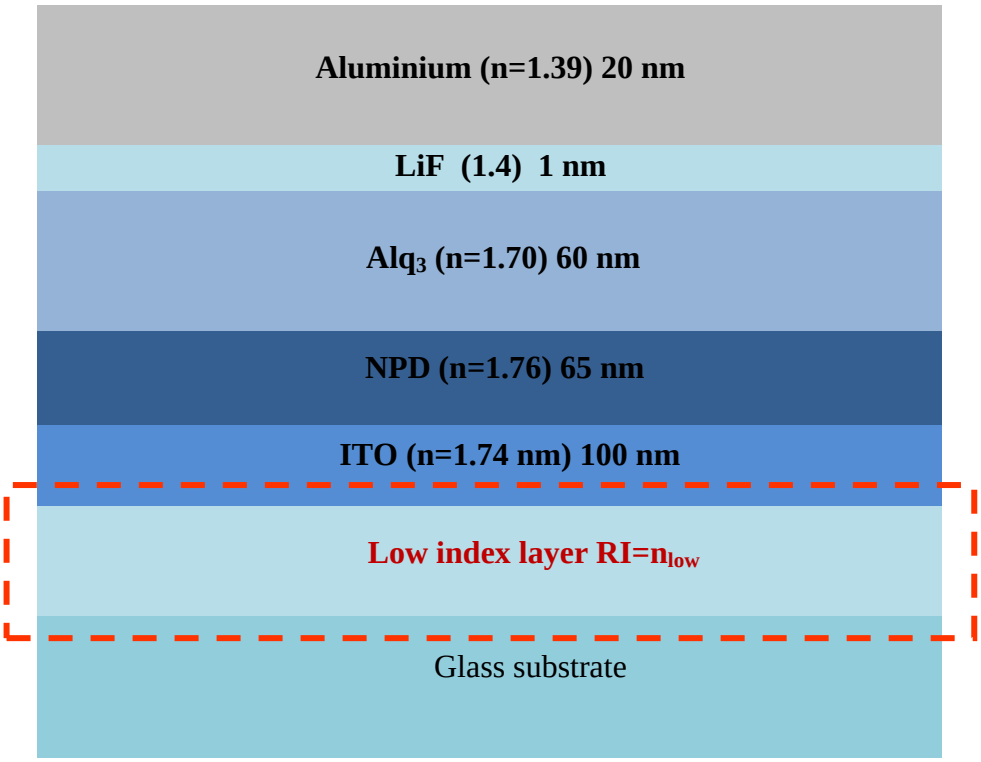

Figure 7.1(b) *Schematic design of OLED with low index layer*

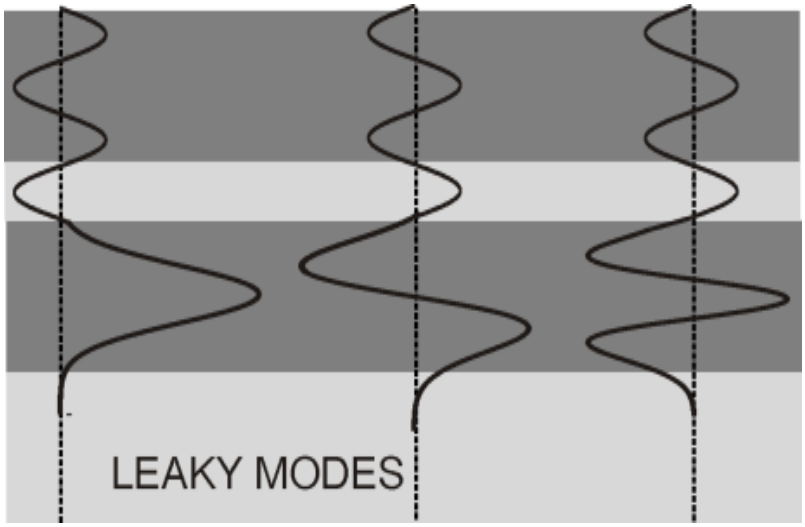

Figure 7.2 *Leaky modes in waveguide*

(3) In this technique interference effects caused due to refractive index discontinuities in a multilayer stack, are taken into account. Transfer matrix formalism is used to handle these interference effects. Here we have taken into account transfer matrix formalism to

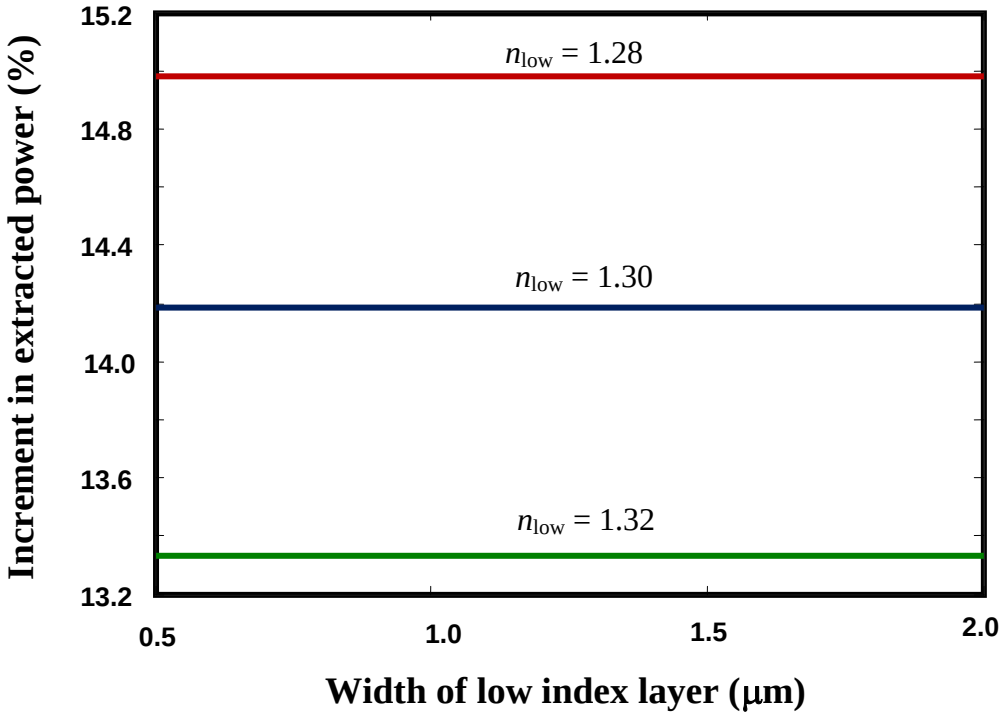

Figure 7.3 *Variation of increment in extracted power with low index layer inserted between glass and ITO at 442 nm wavelength.*

calculate power extraction in glass substrate. We have used transfer matrix method which is described in chapter 6, to analyze the structure [15]. Increment in optical power extraction has been calculated using the formula = $Ploss_{low} - Ploss_{conv}$ Where $Ploss_{conv}$ = power loss in the waveguide without any low index layer. $Ploss_{low}$ = power loss in the waveguide after insertion of low index layer.

7.3 Numerical Results and Discussion

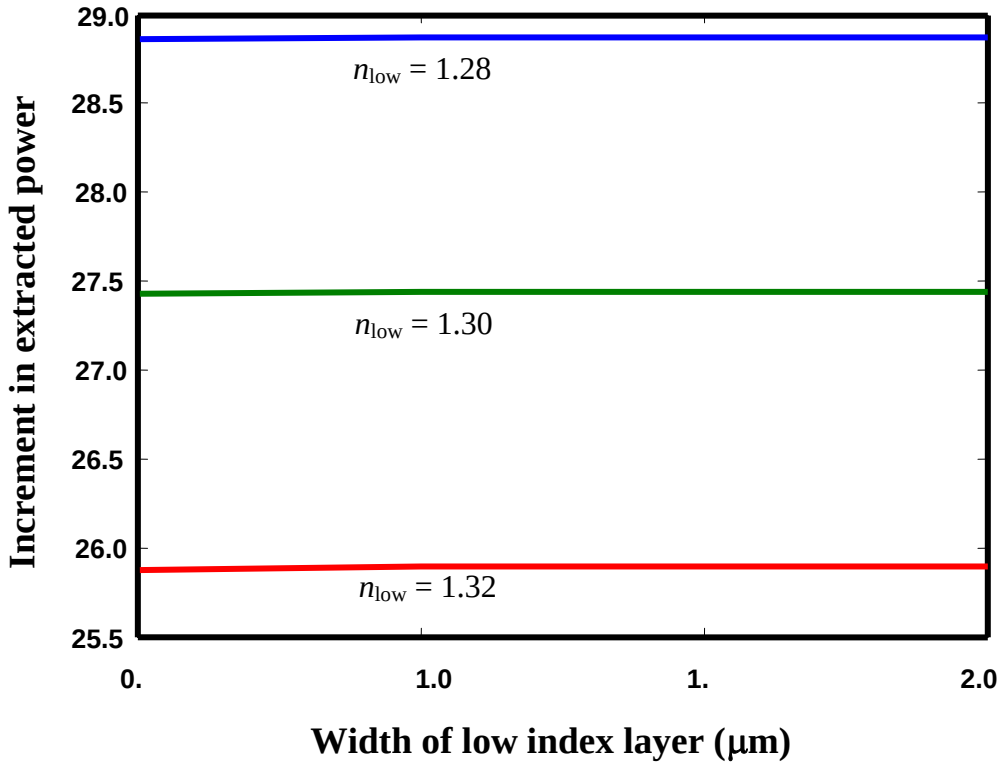

Figure 7.4 *Variation of increment in extracted power with low index layer inserted between glass and ITO at 539 nm wavelength.*

Most of the power in a waveguide is confined in the fundamental mode of the waveguide. Therefore, we have calculated increment in extracted power of fundamental mode after insertion of low index layer in conventional OLED design. Increment in power extraction at 420 nm wavelength is shown in Fig. 7.3. We observe from Fig.7.3 that at 420 nm wavelength, increment in power extraction is around 15 % for 1 μm width of low index layer after 1 μm propagation through the device after insertion of low index layer of n_{low} = 1.28 As lower is the refractive index of the low index layer higher is the power extraction. Because of the property of the waveguide we get resonance in leakage loss for a particular wavelength for particular waveguide design.

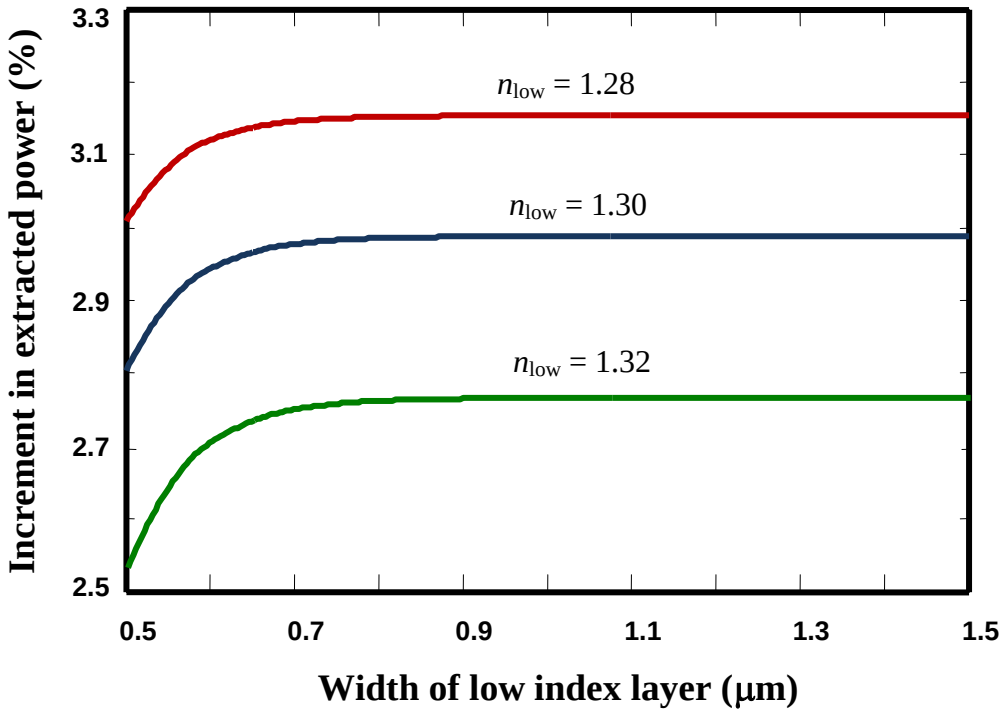

Figure 7.5 *Variation of increment in extracted power with low index layer inserted between glass and ITO at 620 nm wavelength.*

Therefore at 539 nm wavelength we get more increment in power extraction than that of 620 nm wavelength as 539 is the resonant wavelength for considered design. Increment in power extraction for 539 nm wavelength is shown in Fig. 7.4 and one can observe that it is approximately 29% for n_{low} = 1.28 for 1 μm propagation of power through the device. Fig. 7.5 shows that at 620 nm wavelength power extraction increases by approximately 3 % after insertion of low index layer. Experimentally, the device can be realized by depositing a teflon layer between glass and ITO by using spin coating deposition technique.

7.4 Conclusions

An OLED structure with improved light extraction efficiency has been presented. Insertion of low index layer results into more extraction of power from the device at all three wavelengths red, green and blue. However due to waveguide property there is resonant wavelength at which leakage of power from waveguide is maximum and that wavelength for the proposed structure is 539 nm wavelength. Therefore we get maximum extraction of power from the device at 539 nm wavelength.

CHAPTER–8

Concluding remarks and scope for future work

In the thesis we have presented novel multilayer designs in planar and fibre geometries for specific applications. In particular, we have presented segmented core, segmented cladding and three-layer W-fiber designs for optical fiber and multilayer designs for planar waveguides. With segmented core design assisted with a low-index trench in the cladding, dispersion of the fiber has been flattened and mode area has been increased as compared to conventional dispersion flattened fiber designs. Designed fiber also shows low bending lossand can offer small positive, small negative and near zero dispersion while maintaining efficient structural disorder performance. W-type fiber offers large mode area with low mode coupling between fundamental mode and first higher order mode. Designed fiber is able to achieve 1900 μm^2 mode area and is able to deliver 100-fs, 55.5–kW peak power sech pulses at 1550 nm wavelength. Segmented cladding design has also been presented for ultra-short laser pulse delivery with mode area and low susceptibility to intermodal coupling like W-fiber design. However, the interesting feature of SCF is that it is able to deliver USPs at more than one wavelengths. SCF has mode area of 1825 μm^2 at 1550-nm wavelength and 1793 μm^2 at 1064 nm wavelength. SCF can deliver 100-fs sech and Gaussian pulses at 1550-nm wavelength and 250 fs laser pulses at 1064 nm wavelength. Three layered W-fiber structure is easier to fabricate using conventional MCVD technique whereas fabrication technology for SCF in silica glass material is yet to be established. Development of

technology for fabrication of SCF has also been presented in the thesis. Three layer fiber design has also been presented for sensing refractive of various materials. Transmission characteristics of the fiber shows that the leakage loss of the fiber is highly sensitive to refractive index of analyte. Fiber is able to sense refractive index of various materials including peppermint oil, jojoba oil, menthe oil, soybean oil, cholesterol, lecithin mixture and glycerol. Multilayer planar waveguides have also been presented for sensing refractive index and to improve light extraction efficiency of organic light emitting diode. Multilayer planar waveguide presented for sensing refractive index is able to realize integrated optical sensor based on leakage loss of the waveguide. The output light of single mode planar waveguide is a sensitive indicator of refractive index of the biological or chemical analyte. A structure of OLED based on planar waveguide geometry has been presented to improve power extraction from the device. As the scope for future work, proposed waveguide and fiber designs can be implemented in active materials and their performance can be investigated. Fiber sensor and waveguide sensor designs can be tested experimentally to access the actual device performance. Performance of dispersion flattened fibers can be thoroughly investigated by implementing them in communication system. Potential of multi-layer fiber designs can be explored for gain flattening and fiber lasers. The gain flattening in thulium doped fibre amplifier (TDFA) and Raman amplifiers can also be explored using these designs. Performance of the OLED device can be experimentally tested after insertion of low index layer.

BIBLIOGRAPHY

[1]. H. Ma, A. K. Y. Jen, L. R. Dalton,"Polymer-based optical waveguides: materials, processing, and devices," *Adv. Mater*., vol. 14, 1339–1365, 2002.

[2]. A. Ishimaru,"Electromagnetic wave propagation, radiation, and scattering," Englewood Cliffs, NJ: Prentice Hall, 1991.

[3]. A. K. Ghatak, "Optical electronics," Cambridge University Press, 1989.

[4]. W. Sijun, L. Pei, R. Zhao, J. Yang, and Y. Wang. "Optical devices based on multilayer optical waveguide." *Front. Optoelectron.*, vol. 6, 146-152, 2013.

[5]. R. K. Varshney, A. K. Ghatak, I. C. Goyal, and C. S. Antony, "Design of flat field fiber with very small dispersion slope," *Opt. Fiber Technol.*, vol. 9, 189-198, 2003.

[6]. X. Tian, and X. Zhang,"Dispersion-flattened designs of the large effective area single-mode fibers with ring index profiles," *Optics Commun.*, vol. 230, 105-113, 2004.

[7]. T. Okuno, S. K. Hatayama, T. Sasaki, M. Onishi, and M. Shigematsu,"Negative dispersion flattened fiber suitable for 10 Gbits/s directly-modulated signal transmission in whole telecommunication band," *Electron. Lett.*, vol. 40, 1306-1308, 2004.

[8]. A. Rostami and S. Makouei, "Modified W-type single mode optical fiber design with ultra-low, flattened chromatic dispersion and ultra-high effective area for high bit rate long haul communications," *Prog. Electromag. Res. C*, vol. 12, 79-92, 2010.

[9]. N. Kumano, K. Mukasa, M. Sakano, H. Moridaira, T. Yagi, K. Kokura," Novel NZ-DSF with ultra low dispersion slope lower than 0.020 ps/km/nm^2," in: *Proceedings of ECOC*'2001, PDA, 1–5, 2001.

[10]. B. Zhu, L.E. Nelson, L. Leng, S. Stulz, S. Knudsen, D. Peckham,"1.6 Tbits/s (40 × 42.7 Gbit/s) WDM transmission over 2400 Km of fiber with 100 Km dispersion managed spans," *Electron. Lett.*, vol. 38, 647–648, 2002.

[11]. R. Lundin, "Dispersion flattening in W fiber," *Applied Optics*, vol. 33, 1011-1014, 1994.

[12]. M. Liu and K. S. Chiang,"Propagation of ultrashort pulses in a nonlinear two-core photonic crystal fiber," *Appl. Phys B*, vol. 98, 815-820, 2010.

[13]. K. Saitoh, N. J. Florous, T. Murao, and M. Koshiba," Design of photonic band gap fibers with suppressed higher-order modes: Towards the development of effectively single mode large hollow-core fiber platforms,"*Opt. Express*, vol. 14, 7342-7352, 2006.

[14]. X. Peng, M. Mielke, and T. Booth," High average power, high energy 1.55 μm ultra-short pulse laser beam delivery using large mode area hollow core photonic band-gap fiber," *Opt. Express*, vol. 19, 2011.

[15]. F. Luan, J. C. Knight, St. J. P. Russell, S. Campbell, D. Xiao, D. T. Reid, B. J. Mangan, D. P. Williams, and P. J. Roberts," Femtosecond soliton pulse delivery at 800 nm wavelength in hollow-core photonic bandgap fibers," *Opt. Express*, vol. 12, 835-840, 2004.

[16]. P. J. Mosley, W. C. Huang, M. G. Welch, B. J. Mangan, W. J. Wadsworth, and J. C. Knight,"Ultrashort pulse compression and delivery in a hollow-core photonic crystal fiber at 540 nm wavelength," *Opt. Lett.*, vol. 35, 3589-3591, 2010.

[17]. W. Göbel, A. Nimmerjahn, and F. Helmchen," Distortion-free delivery of nanojoule femtosecond pulses from a Ti:sapphire laser through a hollow-core photonic crystal fiber," *Opt. Lett.*, vol. 29, 1285-1287, 2004.

[18]. S. G. Johnson, M. Ibanescu, M. Skorobogatiy, O. Weisberg, T. D. Engeness, M. Soljačić, S. A. Jacobs, J. D. Joannopoulos, and Y. Fink, "Low-loss asymptotically single-mode propagation in large-core OmniGuide fibers," *Opt. Express*, vol. 9, 748–779, 2001.

[19]. S. Ramachandran, M. F. Yan, J. Jasapara, P. Wisk, S. Ghalmi, E. Monberg, and F. V. Dimarcello,"High-energy (nanojoule) femtosecond pulse delivery with record dispersion higher-order mode fiber,"*Opt. Lett.*, vol. 30, 3225-3227, 2005.

[20]. Y. Zaouter, D. N. Papadopoulos, M. Hanna, J. Boullet, L. Huang, C. Aguergaray, F. Druon, E. Mottay, P. Georges, and E. Cormier,"Stretcher-free high energy nonlinear amplification of femtosecond pulses in rod-type fibers," *Opt. Lett.*, vol. 33, 107-109, 2008.

[21]. J. W. Nicholson, S. Ramachandran, S. Ghalmi, M. F. Yan, P. Wisk, E. Monberg, F. V. Dimarcello,"Propagation of femtosecond pulses in large-mode-area, higher-order-mode fiber," *Opt. Lett.*, vol. 31, 3191-3193, 2006.

[22]. S. Ramachandran, J. W. Nicholson, S. Ghalmi, M. F., Yan, P. Wisk, E. Monberg, and F. V. Dimarcello," Light propagation with ultra large modal areas in optical fibers," O*pt. Lett.*, vol. 31, 1797-1799, 2006.

[23]. K. T. Grattan, and B. T. Meggitt,"Optical Fiber Sensor Technology: Fundamentals," Springer, 2000.

[24]. G.D. Peng, and P. L. Chu, "Polymer optical fiber sensing," *Proc. SPIE* 4929, Optical Information Processing Technology, 303, 2002.

[25]. X. Yu, Y. Zhang, S. Pan, P. Shum, M. Yan, Y. Leviatan, and C. Li,"A selectively coated photonic crystal fiber based plasmon resonance sensor," *J. Opt*., vol.12, 0150051-4, 2010.

[26]. B. Marcus, D. K. Dandge, K. Goswami, and S. M. Klainer, "Fiber optic refractive index sensor using metal cladding," U.S. Patent 5,026,139, 25, 1991.

[27]. A. Baliyan, P. Bhatia, B. D. Gupta, E. K. Sharma, A. Kumari, R. Gupta, "Surface plasmon resonance based fiber optic sensor for the detection of triacylglycerides using gel entrapment technique," *Sens Actuators B*, vol. 188, 917-922, 2013.

[28]. K. T. Grattan, T. Sun,"Fiber optic sensor technology: an overview," *Sens. Actuators A: Physical*, vol. 82, 40-61, 2000.

[29]. K. T. Grattan and B. T. Meggit,"Optical Fiber Sensor Technology: Advanced Applications - Bragg Gratings and distributed sensors," Kluwer Academic pub. Netherland, 2000.

[30]. M. Phan, G. Laffont, V. Dewynter, P. Ferdinand, L. Labonté, D. Pagnoux, P. Roy, W. Blanc, and B. Dussardier,"Tilted fiber Bragg grating photo written in microstructured optical fiber for improved refractive index measurement," *Opt. Express*, vol. 14, 10359-10370, 2006.

[31]. W. Liang, Y. Huang, Y. Xu, R. K. Lee, and A. Yariv,"Highly sensitive fiber Bragg grating refractive index sensors," *Appl. Phy. Lett*., vol. 86, 1511221-3, 2005.

[32]. J. Villatoro, D. Monzoon-Hernandez, D. Talavera,"High resolution refractive index sensing with cladded multimode tapered optical fiber," *Electron. Lett*., vol. 40,. 106-107, 2004.

[33]. A. Kumar, T.V.B. Subramanyam, A. D. Sharma, K. Thyagarajan, B. P. Pal and I. C. Goyal,"Novel refractometer using a tapered optical fiber," *Electron. Lett*., vol. 20, 534-535, 1984.

[34]. S. Kher, S. Chaubey, J. Kishore, and S. Oak,” Detection of fuel adulteration with high sensitivity using turnaround point long period fiber gratings in b/ge doped fibers,” *IEEE Sens. J.*, vol.13, 2013.

[35]. A. S. Lalasangi, J. F. Akki, K. G. Manohar, T. Srinivas, P. Raikar, S. Kher, and U. S. Raikar,”Highly sensitive cadmium concentration sensor using long period grating,” *Sens. Transducers*, vol. 134, 1726-5479, 2011.

[36]. Q. Liu and K. S. Chiang,"Refractive-index sensor based on long-range surface plasmon mode excitation with long period waveguide grating," *Opt. Express*, vol. 17, 7933-7942, 2009.

[37]. K. S. Chiang, Y. Liu, M. N. Ng, & X. Dong,”Analysis of etched long-period fibre grating and its response to external refractive index,” *Electron. Lett.*, vol. 36, 966-967, 2000.

[38]. A. Kapoor, and E. K. Sharma, "Long period grating refractive-index sensor: optimal design for single wavelength interrogation," *Appl. Opt.*, vol. 48, G88-G94, 2009.

[39]. R. Singh, H. Kumar, and E. K. Sharma,”Design of long-period gratings: necessity of a three-layer fiber geometry for cladding mode characteristics,” *Microwave and Opt. Technol. Lett.*, vol. 37, 45-49, 2003.

[40]. T. M. Libish, J. Linesh, M. C. Bobby, P. Biswas, S. Bandyopadhyay, K. Dasgupta, P. Radhakrishnan,”Detection and analysis of paraffin oil adulteration in coconut oil using fiber optic long period grating sensor,” *Optik*, vol. 122, 1939-1942, 2011.

[41]. T. S. N. George, P. Sureshkumar, P. Radhakrishnan, C. Vallabhan and V. Nampoori, "Chemical sensing with microbent optical fiber," *Opt. Lett.*, vol. 26, 1541-1543, 2001.

[42]. S. T. Lee, J. Gin, V. P. N. Nampoori, , C. P. G. Vallabhan, N. V. Unnikrishnan, and P. Radhakrishnan,” A sensitive fibre optic pH sensor using multiple sol-gel coatings,” *J. Opt. A: Pure and Applied Optics*, vol. *3*, 355, 2001.

[43]. C. C. C. Lam, R. Mandamparambil, T. Sun, K. T. Grattan, S. V. Nanukuttan, S. E. Taylor, and P. M. Basheer,” Optical fiber refractive index sensor for chloride ion monitoring,”*IEEE Sens. J.*, vol. *9*, 525-532, 2009.

[44]. J. Villatoro and D. Monzon-Hernandez, “Low cost optical fiber refractive index sensor based on core diameter mismatch,” *J. Lightwave Technol*., vol. 24, 1409-1413 2006.

[45]. Kamakshi, K., V. Rastogi, A. Kumar and J. Rai,"Design and fabrication of a single mode optical fibre based refractive-index sensor," *Microwave Opt. Technol. Lett*., vol. 52, 1408-1411, 2010.

[46]. B. D. Gupta, A. Sharma, C. D. Singh,"Fiber optic evanescent field absorption sensor: effect of launching condition and the geometry of the sensing region,"*Opt. Eng*., vol. 33, 1864-1868, and 1994.

[47]. A. Brandenburg, R. Krauter, C. Künzel, M. Stefan and H. Schulte," Interferometric sensor for detection of surface-bound bioreactions," *Appl. Opt,* vol. 39, 6396-6405, 2000.

[48]. D. Freiner, R. E. Kunz, D. Citterio, U. E. Spichiger, and M. T. Gale,," Integrated optics sensors based on refractometry of ion-selective membranes," *Sens Actuators B*, vol. 29, 277-285, 1995,.

[49]. K. Schmitt, K. Oehse, G. Sulz and C. Hoffmann,"Evanescent field sensors based on tantalum pentoxide waveguides – a review", *IEEE Sens J*, vol. 8, 711-738, 2008.

[50]. R. Bernini, N. Cennamo, A. Minardo and L. Zeni,"Planar waveguides for fluorescence based biosensing: optimization and analysis," *IEEE Sens J*, vol. 6, 1218-1226, 2006.

[51]. J. Homola, S.S. Yee and G. Gaulitz,"Surface Plasmon resonance sensors: review," *Sens Actuators B*, vol. 54, 3-15, 1999.

[52]. Shruti, R. K. Sinha and R. Bhattacharyya,"Photonic crystal slab waveguide-based infiltrated liquid sensors: design and analysis," *J. Nanophoton*. vol. 5, 053505, 2011.

[53]. K. Saxena, V.K. Jain, D.S. Mehta, "A review on light extraction techniques in organic electroluminescent devices," *Opt. Mater*., vol. 32, 221-233, 2009.

[54]. S. Chen and H. S. Kwok, "Light extraction from organic light emitting diodes for lighting applications by sand -blasting substrates,"*Opt. Express*, vol. 18, 37-42, 2010.

[55]. M. M. Lu, J. C. Sturm, C. F. Madigan, R. Kwong,"Increased emission efficiency in organic light-emitting devices on high-index substrates," *US7053547 B2*, May *30*, 2006.

[56]. K. Chari, C. W. Lander, J. Wang, D. R. Preuss, R. S. Cok, Y. Tyan, J. D. Shore,"Light emitting device with microlens array," *US20080117519 A1*, May 20, 2008.

[57]. J. Xue, E. P. Douglas, "Top-emission organic light emitting devices with microlens arrays," *US8373341 B2*, Feb. 12, 2013.

[58]. Z. Shuyu, G. A. Turnbull and D. W. Samuel,"Enhancing the emission directionality of organic light-emitting diodes by using photonic microstructures," *Appl. Phy. Lett*, vol. 103, 213302, 2013.

[59]. W. L. Barnes, J. R. Sambles, I. R Hooper, S. Wedge," Optoelectronic device with periodic grating microstructure," *US8129738 B2*, March 6, 2012.

[60]. M. S. Weaver, V. Bulovic, M. M. Lu,"OLEDs having increased external electroluminescence quantum efficiencies,**"** *US7012363 B2*, March 14, 2006.

[61]. S. Moller, and S. R. Forrest, "Improved light out-coupling in organic light emitting diodes employing ordered microlens arrays," *J. Appl. Phys*., vol. 91, 3324, 2002.

[62]. M.-K. Wei, I.-L. Su, "Method to evaluate the enhancement of luminance efficiency in planar OLED light emitting devices for microlens array," *Opt. Exp*ress, vol. 12, 5777, 2004.

[63]. A. Perschke, T. Fuhrmann, "Molecular Azo glasses as grating couplers and resonators for optical devices," *Adv. Mater*., vol. 14, 841, 2002.

[64]. Y. Sun, S. R. Forrest, Enhanced light out-coupling of organic light-emitting devices using embedded low-index grids," *Nat. Photonics*, vol. 2, 483, 2008.

[65]. S. Forrest, Y. Sun," Low index grids (LIG) to increase outcoupled light from top or transparent OLED", *US 20080265757 A1*, Oct. 30, 2008.

[66]. T. Tsuitsui, M. Yahiro, H. Yokogawa, K. Kawano, Y. Yokoyama, "Doubling coupling-out efficiency in organic light-emitting devices using a thin silica aerogel layer," *Adv. Mater*., vol. 13, 1149–1152, 2001.

[67]. M. R. Ramadas, E. Garmire, A. K. Ghatak, K. Thyagarajan, and M. R. Shenoy, "Analysis of absorbing and leaky planar waveguides: a novel method," *Opt. Lett*., vol. 14, 376–378, 1989.

[68]. S. Varshney, K. Saitoh, M. Koshiba, B. P. Pal, and R. Sinha,"Design of S-Band erbium-doped concentric dual-core photonic crystal fiber amplifiers with ase suppression," *J. Lightwave Technol*. 27, 1725-1733, 2009.

[69]. J. Anand, J. K. Anand, and E. K. Sharma,"Inherent gain flattening due to two mode interference in erbium doped coaxial fibers." *Opt. Fiber Technol.* 19, 298-303, 2013.

[70]. J. Yang, H. Ming, and K. S. Chiang,"Analysis of erbium-doped ultralarge-core segmented-cladding fibers for optical amplification,"*J. Lightwave Technol*., vol. 26, 3098-3103, 2008.

[71]. J. Anand, J. K. Anand, and E. K. Sharma, "Inherent gain flattening due to two mode interference in erbium doped coaxial fibers," *Opt. Fiber Technol.* 19, 298-303, 2013.

[72]. H. D. Kidorf and K. L. Walker,"Optical fiber communication system with a distributed Raman amplifier and a remotely pumped er-doped fiber amplifier," U.S. Patent 6,081,366, 27, 2000.

[73]. D. Silva, L. Valeria, and Y. Silberberg,"Optical fiber amplifier with flattened gain.," *U.S. Patent 5*, 239, 607, 1993.

[74]. R. J. Mears, L. Reekie, I. M. Juancey, and D. N. Payne, "Low-noise erbium-doped fiber amplifier operating at 1.54 μm," *Electron. Lett.*, vol. 23, 1026-1028, 1987.

[75]. L. Goldberg, J. P. Koplow, and D. A. V. Kliner, "Highly efficient 4-W Yb-doped fiber amplifier pumped by a broad-stripe laser diode," *Opt. Lett.*, vol. 24, 673–675, 1999.

[76]. N. G. R. Broderick, D. J. Richardson, D. Taverner, J. E. Caplen, L. Dong and M. Ibsen, "High power chirped-pulse all-fiber amplification system based on large-mode-area fiber gratings," *Opt. Lett*., vol. 24, 566-568, 1999.

[77]. J. Auguste, R. Jindal, J. M. Blondy, M. Clapeau, J. Marcou, B. Dussardier, and K. Thyagarajan,"−1800 ps/(nm. km) chromatic dispersion at 1.55 μm in dual concentric core fibre," *Electron. Lett.*, vol. *36*, 1689-1691, 2000.

[78]. K. Thyagarajan, R.K. Varshney, P. Palai, A.K. Ghatak, I. C. Goyal, "A novel design of a dispersion compensating fiber," *Photon. Technol. Lett., IEEE* , vol. 8, 1510-1512, 1996.

[79]. T. A. Birks, D. Mogilevtsev, J. C. Knight, P. S. J. Russell,"Dispersion compensation using single-material fibers," *Photon. Technol. Letters, IEEE*, vol.11, 674-676, 1999.

[80]. N. Yi, L. Zhang, L. An, J. Peng, C. Fan,"Dual-core photonic Crystal fiber for dispersion compensation," *Photon. Technol. Lett., IEEE* , vol. 16, 1516-1518, 2004.

[81]. S. Dasgupta, B.P. Pal, and M. R. Shenoy, "Design of dispersion-compensating Bragg fiber with an ultrahigh figure of merit," *Opt. Lett.*, vol. 30, 1917-1919, 2005.

[82]. J. Auguste, R. Jindal, J-M Blondy, M. Clapeau, J. Marcou, B. Dussardier, G. Monnom, D. B. Ostrowsky, B.P. Pal,, K. Thyagarajan,"−1800 ps/(nm.km) chromatic dispersion at 1.55 μm in dual concentric core fibre," *Electron. Lett.*, vol. 36, 1689-1691, 2000.

[83]. V. Rastogi, R. Kumar, A. Kumar,"Large effective area all-solid dispersion compensating fiber," *J. Opt.*, vol. 13, 125707, 2011.

[84]. A. Peer, G. Prabhakar, V. Rastogi, and A. Kumar,"A Microstructured dual-core dispersion compensating fiber design for large-mode-area and high-negative dispersion," *International Conference on Fibre Optics and Photonics*, paper WPo.24, 2012.

[85]. H. Hatayama, T. Kato, M. Onishi, E. Sasaoka, and M. Nishimura, "Dispersion flattened fiber with large-effective-core area more than 50 μm^2," *Proceedings of Optical Fiber Communication Conference*, vol. 2, paper ThK4, 1998.

[86]. K. Thyagarajan, S. Diggavi, A. Taneja, and A. K. Ghatak,"Simple numerical technique for the analysis of cylindrically symmetric refractive-index profile optical fibers," *Appl. Opt.*, vol. 30, 3877–3879, 1991.

[87]. K. Morishita,"Numerical analysis of pulse broadening in graded index optical fibers," *Microw. Theory and Tech., IEEE Transactions on*, vol. 29, 348-352, 1981.

[88]. G. P. Agrawal, "Nonlinear fiber optics," Academic Press, San Diego., 2001.

[89]. C. Pask, "Physical interpretation of Petermann's strange spot size for single-mode fibres," *Electron. Lett.*, vol. 20, 144-145, 1984.

[90]. A.W. Snyder and J. D. Love, "Optical waveguide theory," London, U.K.: Chapman and Hall, 1983.

[91]. E. G. Neumann, "Single-mode fibers: fundamentals," Springer-Verlag, Berlin, 1988.

[92]. M. J. Messerly, J. W. Dawson, R. J. Beach, C. P. J. Barty, "Optical fiber having wave-guiding rings," *U.S. Patent No. 7907810*, 2011.

[93]. S. H. Oh, and Y. S. Yoon, "Optical fiber with smooth core refractive index profile and method of fabrication," *U.S. Patent No. 5761366*, 1998.

[94]. J. H. Kim, M. H. Do, J. H. Lee, "Single mode optical fiber having multi-step core structure and method of fabricating the same," *U.S. Patent No. 6205279*, 2001.

[95]. B. Dussardier, V. Rastogi, A. Kumar and G. Monnom, "Large-mode-area leaky optical fiber fabricated by MCVD," *Appl. Opt.*, vol. 50, 3118-3122, 2011.

[96]. X. Liu, D. Du, and G. Mourou, "Laser ablation and micromachining with ultrashort laser pulses," IEEE J. *Quantum Electron*., vol. 33, 1706-1716, 1997.

[97]. M. D. Shirk, and P. A. Molian, "A review of ultrashort pulsed laser ablation of materials," *J. Laser Appl*., vol. 10, 18-28, 1998.

[98]. A. H. Zewail, "Laser femtochemistry," *Science*, vol. 242, 1645-1653, 1988.

[99]. C. Xu, W. Zipfel, J. B. Shear, R. M. Williams, and W. W. Webb, "Multiphoton fluorescence excitation: New spectral windows for biological nonlinear microscopy," *Proc. Natl. Acad. Sci. USA 93*, 10763-10768, 1996.

[100]. J. Takayanagi, S. Kanamori, K. Suizu, M. Yamashita, T. Ouchi, S. Kasai, H. Ohtake, H. Uchida, N. Nishizawa, and K. Kawase, "Generation and detection of broadband coherent terahertz radiation using 17-fs ultrashort pulse fiber laser," *Opt. Express*, vol. 16, 12859-12865, 2008.

[101]. B. R. Washburn, W. C. Swann, and N. R. Newbury, "Response dynamics of the frequency comb output from a femtosecond fiber laser," *Opt. Express*, vol. 13, 10622-10633, 2005.

[102]. J. Limpert, T. Schreiber, T. Clausnitzer, K. Zöllner, H. Fuchs, E. Kley, H. Zellmer, and A. Tünnermann, "High-power femtosecond Yb-doped fiber amplifier," *Opt. Express*, vol. 10, 628-638, 2002.

[103]. A. Malinowsky, A. Piper, J. H. V. Price, K. Furusawa, Y. Jeong, J. Nilsson, and D. J. Richardson, "Ultrashort Yb^{3+}-fiber-based laser and amplifier system producing > 25-W average power," *Opt. Lett*., vol. 29, 2073-2075, 2004.

[104]. T. Le, G. Tempea, Z. Cheng, M. Hofer, and A. Stingl, "Routes to fiber delivery of ultra-short laser pulses in the 25 fs regime," *Opt. Express*, vol. 17, 1240–1247, 2009.

[105]. S. O. Konorov, A. B. Fedotov, O. A. Kolevatova, V. I. Beloglazov, N. B. Skibina, A. V. Shcherbakov, E. Wintner, and A. M. Zheltikov, "Laser breakdown with millijoule trains of picosecond pulses transmitted through a hollow-core photonic-crystal fibre," *J. Phys. D*: *Appl. Phys.*, vol. 36, 1375–1381, 2003.

[106]. N. Bloembergen,"Nonlinear optics," Bnejamin reading, MA 1997.

[107]. Y. R. Shen, "Principles of nonlinear optics," Wiley New York, 1984.

[108]. P. N. Butcher and D. N. Cotter, "The elements of nonlinear optics," Cambridge University Press, Cambridge, UK, 1990.

[109]. R. W. Boyd, "Nonlinear optics," 2nd ed., Academic press, Boston, 2003.

[110]. R. G. Smith, " Optical power handling capacity of low loss optical fibers as determined by stimulated Raman and Brillouin scattering," *Appl. Opt.*, vol. 11, 2489-2494, 1972.

[111]. E. P. Lppen, in Laser applications to optics and spectroscopy," vol. 2, S. F. Jacobs, M. Sargent III, J. F. Scott, and M. O. Scully, Eds. (Addison-Wesley, Reading, MA), 1975.

[112]. S. Ramachandran, S. Ghalmi, M. F. Yan, P. Wisk, E. Monberg, F. V. Dimarcello, "Scaling to ultra-large-A_{eff} using higher-order-mode fibers," *Proceedings of Conference on Lasers and Electro-Optics* (CLEO), CThAA2, 2006.

[113]. T. Le, G. Tempea, Z. Cheng, M. Hofer, and A. Stingl," Routes to fiber delivery of ultra-short laser pulses in the 25 fs regime," *Opt. Express*, vol. 17, 1240–1247, 2009.

[114]. T. P. Tanaka, S. Onoda, and M. Sumi, "W-type optical fiber: relation between refractive index difference and transmission bandwidth," *Appl. Opt.*, vol. 15 1121-1122, 1976.

[115]. D. Marcuse, "Curvature loss formula for optical fibers," *J. Opt. Soc. Am.*, vol. 66 216–220, 1976.

[116]. K. S. Chiang," Radial effective index method for the analysis of optical fibers," *Appl. Opt.*, vol. 26, 2969-2973.

[117]. V. Rastogi and K. S. Chiang, “Analysis of segmented-cladding fiber by the radial-effective-index method,” *J. Opt. Soc. Am. B*, vol. 21, 258-265, 2004.

[118]. V. Rastogi and K. **S.** Chiang, “Propagation characteristics **of a** segmented cladding fiber,” *Opt. Lett.***,** vol. 16, 491-493, 2001.

[119]. K. S. Chiang and V. Rastogi, “Ultra-large-core single-mode fiber for optical communications: The segmented cladding fiber,” *in Tech. Dig. Opt. Fiber Commun. Conf.* (*OFC*), *Anaheim, CA, Mar., Paper ThGG6*, 2002.

[120]. A. Millo, I. Naeh, Y. Lavi, and A. Katzir, “Silver-halide segmented cladding fibers for the middle infrared,” *Appl. Phys. Lett.*, vol. 88, 251101, 2006.

[121]. J. Duan, C. Teng, K. Han, M. Yu, W. Wu, Q. Zhang, K. S. Chiang,"Fabrication of segmented cladding fiber by bicomponent spinning," *Polym. Eng. Sci.*, vol. 49 1865-1870, 2009.

[122]. A. Yeung, K. S. Chiang, V. Rastogi, P. L. Chu, and G. D. Peng, “Experimental demonstration of single-mode operation of large-core segmented cladding fiber,” *in Tech. Dig. Opt. Fiber Commun. Conf. (OFC 2004), Los Angeles, CA*, Paper ThI4, 2004,

[123]. A. Yeung, P. L. Chu, G. D. Peng, K. S. Chiang, and Q. Liu,"Design and fabrication of polymer cross fiber for large-core single-mode operation," *J. Lightwave. Technol.*, vol. 27, 101-107, 2009.

[124]. J. Kirchhof, J. Kobelke, K. Schuster, H. Bartelt, R. Iliew, C. Etrich, and F. Lederer, “Photonic crystal fibers in Photonic Crystals: Advances in Design, Fabrication, and Characterization,” Chapt.: 14, Wiley-VCH Verlag GmbH & Co. KGaA,266-288, 2004.

[125]. C.M. Bishop, “Neural networks for pattern recognition,” Newyork, USA, 1995.

[126]. T. J. Dougherty, C. J. Gomer, B. W. Henderson, G. Jori, D. Kessel, M. Korbelik, J. Moan, and Q. Peng, “Photodynamic therapy,” *J. Nat. Cancer Inst.*, vol. 90 889-905, 1998.

[127]. M. Ferrari, R. D. Blasi and G. Zaccanti, “Quantitative measurement of skeletal muscle oxygenation by combined near infrared time resolved and unsolved spectroscopy,” *Med. Opt. Tomogr. (SPIE IS11) ed GMuller (Bellingham,WA: SPIE),* 576–88, 1993.

[128]. J. Beuthan, C. Zur, F. Fink, and G. Muller, “Laser fluorescence spectroscopic experiments for metabolism monitoring,” *Laser Med. Surg.*, vol. 6, 72-76, 1990.

[129]. B. Gewiese, J. Beuthan, F. Fobbe, D. Stiller, G. Muller, J. Bose- Landgraf, K. Wolf, and M. Deimling, "Magnetic resonance imaging-controlled laser-induced interstitial thermograph," *Invest Radiol*., vol. 29, 345-351, 1994.

[130]. B. H. Zimm, W. B. Dandleker, "Theory of light scattering and refractive index of solutions of large colloidal particles," *J. Phys. Chem*., vol. 58, 644-648, 1954.

[131]. G. H. Meeten, "Refractive index errors in the critical-angle and the Brewster-angle method applied to absorbing and heterogeneous materials," *Meas. Sci. Technol.*, vol. 8, 728-733, 1997.

[132]. W. F. Sunderman, "A rapid method for estimating serum proteins," *J. Biol. Chem*., vol. 153, 139–142, 1944.

[133]. D. B. Hand, "The refractivity of protein solutions," *J. Biol. Chem*., vol. 108 703-707, 1934.

[134]. W. M. Yunus, and A. Rahman, "Refractive index of solutions at high concentrations," *Appl. Opt*., vol. 27, 3341-3343, 1988.

[135]. M. Weisser, G. Tovar, S. Mittler-Neher, W. Knoll, F. Brosinger, H. Freimuth, M. Lacher, and W. Ehrfeld, "Specific bio-recognition reactions observed with an integrated Mach-Zehnder interferometer, *Biosens. Bioelectron*., vol. 14, 405-41, 1999.

[136]. A. Brandenburg, R. Krauter, C. Künzel, M. Stefan, and H. Schulte, "Interferometric sensor for detection of surface-bound bioreactions," *Appl. Opt*., vol. 39, 6396-6405, 2000.

[137]. F. Prieto, L. Lechugo, A. Calle, A. Llobera, and C. Dominguez, "Optimized silicon antiresonant reflecting optical waveguides for sensing applications," *J. Lightwave Technol*., vol 19, 2001, 75-83, 2001.

[138]. D. Freiner, R.E. Kunz, D. Citterio, U.E. Spichiger, and M.T. Gale, "Integrated optics sensors based on refractometry of ion-selective membranes," *Sens. Actuators B* 29, 277-285, 1995.

[139]. K. Schmitt, K. Oehse, G. Sulz, and C. Hoffmann, "Evanescent field sensors based on tantalum pentoxide waveguides – a review," *Sensors*, vol 8, 711-738, 2008.

[140]. R. Bernini, N. Cennamo, A. Minardo, and L. Zeni, "Planar waveguides for fluorescence based biosensing: optimization and analysis," *IEEE Sens. J*., vol. 6 1218-1226, 2006.

[141]. Homola, S.S. Yee, and G. Gaulitz, “Surface plasmon resonance sensors: review, *Sens. Actuators B*, vol. 54, 3-15, 1999.

[142]. W. F. Sunderman, “A rapid method for estimating serum proteins,” *J. Biol. Chem.*, vol. 153, 139–142, 1944.

[143]. D.B. Hand, “The refractivity of protein solutions,” *J. Biol. Chem.*, vol. 108, 703-707, 1934.

[144]. Y. Liu, P. Hering, and M. O. Scully. "An integrated optical sensor for measuring glucose concentration." *Appl. Phys. B*, vol. 54, 18-23, 1992.

[145]. I. Thormählen, J. Straub, and U. Grigull. "Refractive index of water and its dependence on wavelength, temperature, and density" *J. Phys. and chem.Ref. Data*, vol. 14, 933-945, 1985.

[146]. W. M. Yunus, and A. Rahman, “Refractive index of solutions at high concentrations,” *Appl. Opt.*, vol. 27, 3341-3343, 1988.